# A protein complex formed by *Ustilago maydis* effectors is essential for virulence


**DISSERTATION**
**zur**
**Erlangung des Doktorgrades**
**der Naturwissenschaften**
**(Dr. rer. nat.)**

dem Fachbereich Biologie
der Philipps-Universität Marburg
vorgelegt von

Nicole Ludwig
geboren in Bonn

Marburg/Lahn im November 2018

Die Untersuchungen zur vorliegenden Arbeit wurden von Oktober 2014 bis Oktober 2018 am Max-Planck-Institut für terrestrische Mikrobiologie unter der Leitung von Frau Prof. Dr. Regine Kahmann in der Abteilung Organismische Interaktionen durchgeführt.

Vom Fachbereich Biologie der Philipps-Universität Marburg
als Dissertation angenommen am: .....

Erstgutachter/in: Frau Prof. Dr. Regine Kahmann
Zweitgutachter/in: Herr Prof. Dr. Stefan A. Rensing

Tag der mündlichen Prüfung am: .....

# Erklärung

Ich erkläre, dass ich meine Dissertation “A protein complex formed by *Ustilago maydis* effectors is essential for virulence” selbstständig, ohne unerlaubte Hilfe angefertigt und mich dabei keiner anderen als der von mir ausdrücklich gekennzeichneten Quellen und Hilfsmittel bedient habe. Die Dissertation wurde in der jetzigen oder einer ähnlichen Form noch bei keiner anderen Hochschule eingereicht und hat noch keinen sonstigen Prüfungszwecken gedient.

..... .....

(Ort, Datum) (Nicole Ludwig)

# Zusammenfassung

*Ustilago maydis* ist ein biotropher Brandpilz, der Maisbeulenbrand in Mais verursacht. Bei der Ausbreitung innerhalb einer Pflanze sekretiert *U. maydis* Effektorproteine um pflanzliche Abwehrreaktionen zu unterdrücken und die Physiologie der Wirtspflanze zu seinem eigenen Vorteil zu manipulieren. Die Funktion der Mehrheit dieser Proteine konnte noch nicht beschrieben werden und deren Wirkung beim Befall bleibt somit bislang ungeklärt.

Mittels einer Genexpressionsanalyse konnte eine Reihe von Effektoren bestimmt werden, deren Expression an die biotrophe Phase gekoppelt ist. Eine systematische Deletion dieser Effektoren führte zur Entdeckung dreier Mutanten, die nicht mehr in der Lage waren eine Erkrankung hervorzurufen. Die Mutanten dieser drei Effektoren, namentlich *stp2*, *stp3* und *stp4* (Stop nach Penetration), konnten immer noch Appressorien ausbilden und die Pflanzenzelle penetrieren, arretierten dann jedoch in der Maisepidermis. Dieser Stillstand wurde von Abwehrreaktionen der Pflanze begleitet, einschließlich des Absterbens der infizierten Zellen. Ein ähnlicher Phenotyp wurde bereits bei den früher beschriebenen Effektoren *stp1* und *pep1* beobachtet. Alle fünf Effektoren sind hochkonserviert innerhalb der Brandpilze, was auf eine wesentliche Funktion dieser hindeutet.

Mittels konfokaler Mikroskopie, *in vivo* Studien und *in vitro* Studien konnte nachgewiesen werden, dass Stp2, Stp3, und Stp4 vom Pilz sekretiert werden, jedoch nicht in das Zytoplasma der Wirtszelle translozieren. Konfokale Mikroskopie mit mCherry-Fusionsstämmen der fünf essentiellen Effektoren zeigte, dass diese ein gesprenkeltes Muster auf der Oberfläche der biotrophen Hyphe bilden. Durch Immunopräzipitation und anschließender massenspektroskopischer Analyse mit jedem der essentiellen Effektoren zeigte sich, dass Stp1, Stp3, Stp4 und Pep1 einen Effektorkomplex bilden. Diese vier Komplexeffektoren zeigten weder eine spezifische Interaktion mit Stp2 noch mit Pflanzenproteinen. Jüngste Experimente legen nahe, dass Stp2 mit mindestens zwei anderen *U. maydis* Effektoren interagiert, die einen vergleichbaren Deletionsphänotyp wie *stp2* haben. Versuche den *stp1*, *stp3*, *stp4* und *pep1* Effektorkomplex mittels einer bimolekularen Fluoreszenzkomplementation (BiFC) sichtbar zu machen, wirkte störend auf die Bildung des Komplexes und führte zu einem kompletten Verlust der Virulenz. Die folgende Überexpression von zwei BiFC Fragment getaggten Komplexmitgliedern im Wildtypallel führte zu einem dominant negativen Phenotyp. Hierdurch konnte bewiesen werden, dass nicht nur das Vorhandensein der einzelnen Komplexmitglieder, sondern auch die Komplexbildung selbst für eine erfolgreiche Kolonisierung der Pflanze notwendig ist. Indessen ermöglichte die Nutzung der intakten fluoreszierenden Proteine eine Co-Lokalisation der Komplexmitglieder innerhalb der Sprenkel. Schließlich bestätigten Interaktionsstudien in *Saccharomyces cerevisiae* die Bildung des Komplexes und demostrierten sogar paarweise Interaktionen und Subkomplexbildungen zwischen den Komplexmitgliedern. Basierend auf diesen Ergebnissen wird vorgeschlagen, dass der Effektorkomplex eine Struktur bildet, dessen Funktion unabdingbar für die Virulenz von *U. maydis* ist und sich potenziell auch als Ziel für zukünftige Pflanzenschutzmittelentwicklungen eignet.

# Summary

*Ustilago maydis* is a biotrophic fungal pathogen that causes smut disease in its host plant maize. During colonization, *U. maydis* secretes effector proteins to suppress plant defense responses and manipulate the host physiology for its own benefit. The majority of these proteins lack functional annotations and their role in virulence remains to be determined.

Transcriptional profiling defined a set of effectors whose expression is linked to the developmental stage in which biotrophy is established. Systematic deletion of these effectors identified three mutants that were no longer able to cause disease. Mutants of these three effectors, named *stp2*, *stp3* and *stp4* (stop after penetration), were still able to form appressoria and penetrate the plant, but arrested in the epidermal cell layer. The arrest was accompanied by plant defense responses, including a disruption of the plant plasma membrane surrounding the fungal hyphae. A similar phenotype was observed for the previously described effectors *stp1* and *pep1*. All five effectors are highly conserved among related smut fungi infecting different hosts, suggesting a essential function.

Using live cell confocal microscopy, *in vitro* and *in vivo* assays, it could be demonstrated that Stp2, Stp3, and Stp4 are secreted by the fungal hyphae, but are not translocated into the plant cell. Confocal microscopy of mCherry fusion strains revealed that all five essential effectors form a speckled pattern on the surface of the biotrophic hyphae. Co-immunoprecipitation/mass spectrometry experiments using each of these essential effectors revealed that Stp1, Stp3, Stp4 and Pep1 form an effector complex. The four complex members did not interact with Stp2 or plant proteins. Recent experiments suggest that Stp2 interacts with at least two other *U. maydis* effectors, which have a virulence phenotype comparable to *stp2* deletion strains. Attempts to visualize the Stp1, Stp3, Stp4 and Pep1 effector complex through bimolecular fluorescence complementation (BiFC) interfered with the complex formation and caused a complete loss of virulence. The subsequent overexpression of two BiFC-fragment tagged complex members in the wild type allele resulted in a dominant negative phenotype. This provides evidence that not only the presence of the individual complex members, but the formation of the complex itself is necessary for a successful colonization. However, using full-length versions of fluorescent proteins enabled the co-localization of complex members and located them in the speckles. Finally, interaction studies in *Saccharomyces cerevisiae* confirmed the formation of the complex and demonstrated pairwise interactions and subcomplex formations among the complex members. Based on these results, it is proposed that the effector complex forms a structure, whose function is essential for the virulence of *U. maydis* and could be used as a potential drug target in the future.

# Contents

# List of figures

# List of tables

# List of abbreviations

| | |
|---|---|
| Abbr | Abbreviation |
| Ade | Adenine |
| Apo | Apoplast |
| Avr | Avirulence |
| bE | bEast |
| BIC | Biotrophic interfacial complex |
| BiFC | Bimolecular fluorescent complimentation |
| bW | bWest |
| C-terminal | Carboxy-terminal |
| cbx/C | Carboxin |
| cDNA | Complementary DNA |
| CDPKs | Calcium-dependent protein kinases |
| CO-IP/MS | Co-immunoprecipitation and mass spectroscopy |
| CM | Complete medium |
| CWDE | Cell-wall-degrading enzymes |
| Cyto | Cytoplasm |
| $\Delta$ | Deletion/delta |
| DAMPs | Damage-associated molecular patterns |
| DIC | Differential interface contrast |
| DNA | Deoxyribonucleic acid |
| dpi | Days post infection |
| EGB | Early golden bantam |
| EHM | Extrahaustorial membrane |
| EHMx | Extrahaustorial matrix |
| ETI | Effector-triggered immunity |
| ETS | Effector-triggered susceptibility |
| f.c. | Finale concentration |
| g | Geneticin |
| glc | Glucose |
| GFP | Green fluorescent protein |
| H | Hygromycin |

| | |
|---|---|
| $H_2O_{bid}$ | Double distilled water |
| His | Histidine |
| hpi | Hours post infection |
| HR | Hypersensitive response |
| $Hyg^R$ | Hygromycin resistance cassette |
| Immuno-TEM | Immuno-transmission electron microscopy |
| *ip* | Gene encoding an ironsulphur protein |
| IP | Immunoprecipitation |
| kb | kilobase pair(s) |
| kDa | kilodalton(s) |
| LC-MS/MS | Liquid chromatography tandem mass spectrometry |
| Leu | leucine |
| LRR | Leucine-rich repeat |
| LysM | Lysine motifs |
| M | Molar |
| MAMPs | Microbe-associated molecular patterns |
| MAPK | Mitogen-activated protein kinase |
| MAPKK | Mitogen-activated protein kinase kinase |
| MAPKKK | Mitogen-activated protein kinase kinase kinase |
| N-terminal | Amino terminal |
| NLR | Nucleotide-binding domain and leucine-rich repeats |
| $OD_{600}$ | Optical density at 600 nm |
| P | Phleomycin |
| PAMPs | Pathogen-associated molecular patterns |
| PCA | Principal component analysis |
| PCD | Programmed cell death |
| PCR | Polymerase chain reaction |
| PD | Potato dextrose |
| PR | Pathogenesis-related |
| PRRs | Pattern recognition receptors |
| PTEX | Plasmodium translocon of exported proteins |
| PTI | PAMP-triggered immunity |
| R proteins | Resistance proteins |
| RLCKs | Receptor-like cytoplasmic kinases |
| RLKs | Receptor-like kinases |
| RLPs | Receptor-like proteins |
| RNA | Ribonucleic acid |
| RNAseq | RNA sequencing |

| | |
|---|---|
| rpm | Revolutions per minute |
| ROS | Reactive oxygen species |
| SA | Salicylic acid |
| SAR | Systemic acquired resistance |
| SD | Selection dropout |
| SDS | Sodium dodecyl sulfate |
| SP | Signal peptide |
| Strp | Streptavidin |
| T3SS | Type III secretion system |
| TCA | Trichloroacetic acid |
| Trp | Tryptophane |
| U | Unit (enzyme activity) |
| UTR | Untranslated region |
| UV | Ultraviolet radiation |
| WGA | Wheat germ agglutinin |
| Y2H | Yeast two-hybrid |

# 1 Introduction

In nature, plants are constantly attacked by a multitude of pathogens and pests. Among these disease-causing microorganisms are fungi, oomycetes, bacteria and viruses. Plant pathogens have a major economic impact as they cause harvest losses of agricultural crops worldwide. Current efforts to manage plant disease mostly rely on resistant cultivars or chemical agents, as alternative approaches are often uneconomical, not applicable in practice or ineffective. However, the use of extensive, unspecific pesticides can negatively impact the environment (Strange and Scott, 2005). When growing resistant plant varieties, new diseases and changes in existing pathogen populations remain a constant threat. As modern agriculture relies on large-scale cultivation of homogeneous host plants, pathogens are able to rapidly overcome the genetic resistance or to mutate, rendering once effective agrochemicals useless (Möller and Stukenbrock, 2017).

In a world with growing demand for food, the study of plant pathology is key to developing new ways to protect crops and improve the efficiency of existing ones. This includes understanding the pathogens' lifestyle, mechanisms of disease and strategies to fight it. In molecular plant pathology, this involves the analysis of processes at the level of the involved genes, proteins and metabolites.

## 1.1 Pathogenic strategies of filamentous plant pathogens

Plant pathogens have developed diverse lifestyles and strategies of plant pathogenesis. Based upon their deployed strategy, they can be classified as necrotrophs, biotrophs or hemibiotrophs. Necrotrophic pathogens kill their host plant or parts of it in order to obtain nutrients from the dead tissue. This lifestyle contrasts with the one of biotrophic pathogens, which derive nutrients from living cells by manipulating their host's metabolism to suit their own needs. In this form of pathogenesis, the pathogen has to maintain host viability and a constant balance between virulence and evasion of host defense mechanisms. Biotrophs establish this balance by utilizing a large set of secreted effector proteins (Glazebrook, 2005). Biotrophic pathogens include both obligate biotrophic pathogens, which can only grow on living plant tissue, and facultative biotrophs

that can be cultured *in vitro* (Barnett and Binder, 1973). The third group, hemibiotrophs, initially establish a biotrophic phase and switch to necrotrophy at later stages of disease. The duration of the respective phases strongly varies among hemibiotrophic pathogens. Necrotrophic and biotrophic pathogens differ substantially in their nutrient acquisition strategies, the infection process and infection-related morphogenesis. (Glazebrook, 2005).

There are only few plant-pathogenic fungi, whose pathogenic strategy and development can be studied on a functional, genome-wide level (Dean *et al.*, 2012). One of these well-suited models is the biotrophic fungus *Ustilago maydis*.

## 1.2 *Ustilago maydis* – the causative agent of corn smut

### 1.2.1 The *U. maydis* - maize pathosystem

*Zea mays*, known as maize or corn, is a member of the grass family *Poaceae*. Its seeds are used for human food, animal feed and industrial products such as biofuels (Scott and Emery, 2016). The basidiomycete *U. maydis* is a facultative biotrophic maize pathogen, belonging to the family of smut fungi (Ustilaginaceae) (Kahmann *et al.*, 2000). It causes corn smut disease on maize and its wild ancestor teosinte (*Zea mays* subsp. *mexicana*) (Christensen, 1963). Members of the large family of smut fungi are host-specific and mostly infect plants from the *Poaceae* family. Among their host plants are important cereal crops such as maize, sorghum, sugar cane, wheat and barley.

After infection, most smut fungi spread systemically throughout the plant, but induce disease symptoms only in the reproductive organs (Martinez-Espinoza *et al.*, 2002). *U. maydis* is an exception as it can cause symptoms in all aerial organs of the plant. Disease symptoms are chlorosis and anthocyanin development, followed by the formation of tumors. In the field, the most pronounced tumors develop in cobs. Within the tumors, black pigmented teliospores are produced, giving them a smut-like appearance. The reallocation of plant nutrients to the fungus leads to stunted growth of the infected plant and a substantial reduction in crop yield (Basse and Steinberg, 2004).

Even though corn smut disease is not as economically impactful as other fungal diseases, the *U. maydis* - *Z. mays* interaction constitutes a useful model system to study the molecular tools deployed by biotrophic fungi to cause disease (Brefort *et al.*, 2009; Dean *et al.*, 2012). The advantages of this model include a short generation time and simple cultivation in a laboratory setting. Furthermore, many versatile molecular tools for forward and reverse genetics, as well as for various biological approaches have been developed due to its sequenced and annotated genome (Brachmann *et al.*, 2004; Kämper *et al.*, 2006; Steinberg and Perez-Martin, 2008; Schuster *et al.*, 2016; Schuster *et al.*, 2018).

### 1.2.2 The life cycle of *U. maydis*

The life cycle of *U. maydis* is biphasic and includes a saprophytic phase and a biotrophic phase (Figure 1.1A). During the saprophytic phase, the fungus grows as a haploid yeast by budding. When two haploid cells with compatible mating loci recognize each other, budding ceases and conjugation hyphae are formed. These grow towards each other, fuse and form the infectious dikaryon (Figure 1.1B and C) (Snetselaar *et al.*, 1996). The recognition and fusion of compatible haploid sporidia is controlled by a pheromone-pheromone receptor system, which is encoded by the biallelic *a*-mating-type locus (Bölker *et al.*, 1992). The subsequent switch to filamentous growth is mediated by the *b*-mating-type locus. The multiallelic *b*-locus encodes two homeodomain transcription factors bEast (bE) and bWest (bW). When bE and bW originate from different alleles they dimerize and form an active heterodimeric bE/bW complex. The bE/bW heterodimer acts as a master regulator and is crucial for pathogenic development (Kämper *et al.*, 1995; Brachmann *et al.*, 2001).

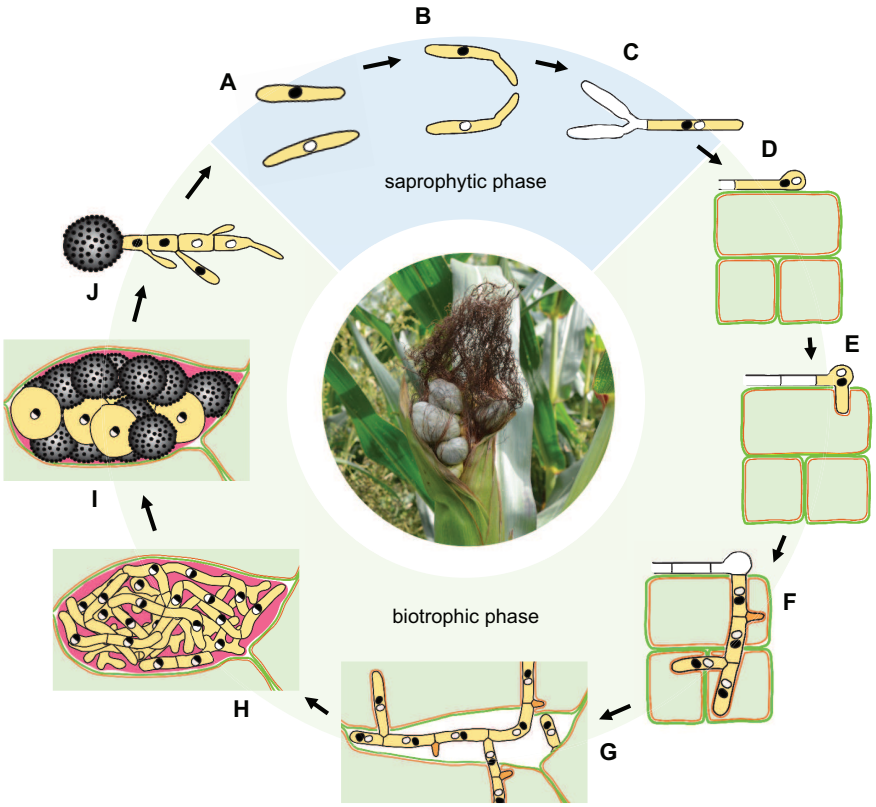


**Figure 1.1: Schematic representation of the *U. maydis* life cycle.** The life cycle of *U. maydis* is biphasic and includes a saprophytic (A-C) and biotrophic phase (D-J). The centered picture shows an infected maize cop. Figure modified from Lanver *et al.* (2017).

The dikaryotic filament extends by polarized growth with the cytoplasm being at the growing tip. The older parts of the filaments are vacuolated and separated by regularly inserted septa. At this developmental stage, the cell cycle is arrested at stage G2 (Banuett

and Herskowitz, 1994; Steinberg *et al.*, 1998; Garcia-Muse *et al.*, 2003; Castanheira and Perez-Martin, 2015). Upon sensing the right hydrophobicity of the plant surface and the presence of fatty acids, the polar growth terminates and the dikaryotic filaments form appressoria (Figure 1.1D) (Snetselaar and Mims, 1992; Mendoza-Mendoza *et al.*, 2009; Lanver *et al.*, 2014).

Among fungi the morphology of appressoria varies greatly in shape and size, but is always characterized by a swollen filament tip. Appressoria can be rather large and melanized, like the ones of the rice blast fungus *Magnaporthe oryzae* (Mendgen *et al.*, 1996). These appresoria accumulate intracellular glycerol, which builds up an enormous cell turgor pressure that is strong enough to allow invasive hyphae to mechanically penetrate the plant surface (Jong *et al.*, 1997; Foster *et al.*, 2017). In contrast, the appressoria of *U. maydis* are rather inconspicuous and non-melanized. They most likely use a combination of melanin-independent turgor pressure and highly local release of specific cell-wall-degrading enzymes (CWDEs) to breach the cell wall without triggering immune responses by the released fragments (Pryce-Jones *et al.*, 1999; Horbach *et al.*, 2011; Chang *et al.*, 2014).

During penetration, the host plasma membrane invaginates and tightly surrounds the intracellular hyphae, forming the biotrophic interaction zone (Figure 1.1E) (Doehlemann *et al.*, 2008). Inside the host, the cell cycle arrest is released and clamp structures involved in the distribution of nuclei are formed. The fungal hyphae branch and proliferate intracellularly in the plant tissue, always being tightly encased by the host plasma membrane (Figure 1.1F) (Snetselaar and Mims, 1994; Scherer *et al.*, 2006). With the ongoing infection process, hyphae reach the mesophilic cells. Here, the fungus starts to grow intra- and intercellularly and the formation of tumors is induced (Figure 1.1G) (Snetselaar and Mims, 1994). Tumors form due to enlarged plant cells that resume mitotic division. Subsequently, the two nuclei undergo karyogamie, followed by a massive proliferation of diploid cells that form huge fungal aggregates in apoplastic cavities (Figure 1.1H). Aggregated hyphae become embedded in a gelatinous polysaccharide matrix and finally undergo fragmentation and sporogenesis (Figure 1.1I) (Banuett and Herskowitz, 1996; Tollot *et al.*, 2016). Mature tumors break open and round, darkly pigmented diploid teliospores are released. These can be spread by wind, rain, insects or others animals and remain germinative for years. Under favorable conditions, the spores germinate and undergo meiosis. The resulting haploid nuclei migrate into a promycelium, from which they bud off (Figure 1.1J). The formation of haploid sporidia restarts the life cycle (Christensen, 1963; Kahmann *et al.*, 2000).

### 1.2.3 The biotrophic interaction zone

The invading hyphae of *U. maydis* are fully encased by the plant plasma membrane, establishing an intimate and extended interaction zone. This biotrophic interface is used by the pathogen to obtain nutrition and traffic effectors into the host cells (Djamei and Kahmann, 2012). In the broadest sense, effectors can be defined as any secreted molecule that modulates the interaction between the pathogen and its host. Effectors are often associated with exclusive expression during the colonization stage and the lack of any defined functional domain (Lo Presti *et al.*, 2015).

The biotrophic interaction zone also facilitates the acquisition of nutrients, such as carbon. In most higher plants, sucrose is the primary form of assimilated carbon. The uptake of sucrose and sucrose-derived hexoses by pathogens is facilitated by sugar transporters located in the membrane (Voegele and Mendgen, 2011; Doidy *et al.*, 2012). Pathogens that prefer glucose over sucrose as their main carbon source secrete invertases to cleave sucrose, which has been shown to increase the levels of available hexoses in the biotrophic interaction zone (Doidy *et al.*, 2012; Lemoine *et al.*, 2013). Invertase-caused changes in extracellular glucose concentration can be sensed by the plant, which can consequently induce defense responses (Ehness *et al.*, 1997). *U. maydis* avoids triggering such responses by expressing the sucrose-specific transporter Srt1. Srt1 has a very high substrate affinity, efficiently providing carbon for the fungus (Wahl *et al.*, 2010; Wittek *et al.*, 2017). It is assumed that sucrose rather than hexoses is the preferred carbon source of *U. maydis*. This was deducted from the observation that *srt1* deletion mutants were less virulent than mutants in which the hexose transporter Hxt1 was deleted (Schuler *et al.*, 2015).

Besides *U. maydis*, other hemi- and biotrophs have developed a large variety of different strategies to establish an environment allowing their biotrophic development. Intercellularly growing obligate biotrophs, including powdery mildews, rusts and many oomycetes have evolved highly specialized feeding structures called haustoria. These are branch extensions of hyphae that penetrate a plant cell wall and expand inside that cell. They can be highly complex, like the ones of *Blumeria graminis*, or simpler and more bulbous, such as the those of rust fungi (Yi and Valent, 2013). Haustoria-forming hyphae only invaginate, but do not perforate the host plasma membrane. The hereby formed extrahaustorial membrane (EHM) is continuous with the plant plasma membrane. The EHM is a spezialized membrane and appears to lack several common plant plasma membrane proteins. Instead, the EHM has a unique composition, even possessing its own set of transmembrane proteins (Koh *et al.*, 2005; Micali *et al.*, 2011; Caillaud *et al.*, 2014). The interface between the haustorial cell wall and the EHM is called the extrahaustorial matrix (EHMx). Depending on the pathosystem, it is either continuous

with the host's apoplast or sealed off by a neck-band structure creating an interfacial apoplastic compartment. The EHMx is a gel matrix, enriched with carbohydrates and proteins from both the fungus and the host. It creates an environment for the exchange of molecules and signals between fungus and the host (Yi and Valent, 2013; Oliveira-Garcia and Valent, 2015).

## 1.3 The plant immune system

### 1.3.1 Pattern-triggered immunity

Plants are resistant to the majority of pathogens as they are protected by two preformed physical barriers, the cuticle and the cell wall (Bellincampi *et al.*, 2014). Pathogens that manage to overcome these barriers, face the plant's immune system. Plants do not have an adaptive immune system, but instead rely on each individual cell to autonomously initiate immune responses upon pathogen detection (Jones and Dangl, 2006). The first line of defense reactions is triggered by the recognition of conserved pathogen-specific structures, so-called pathogen- or microbe-associated molecular patterns (PAMPs/ MAMPs) or host-plant-derived damage-associated molecular patterns (DAMPs) (Figure 1.2) (Boller and Felix, 2009). These are recognized through pattern recognition receptors (PRRs) located in the membrane, which subsequently induce PAMP-triggered immunity (PTI). The majority of plant PRRs described to date are receptor-like kinases (RLKs) or receptor-like proteins (RLPs). RLKs have single-pass transmembrane domains and cytoplasmic kinase domains, whereas RLPs lack the kinase domain. PRRs are further characterized by a ligand-binding ectodomain, which classifies them according to the ligand they recognize (Zipfel, 2014; Couto and Zipfel, 2016). Leucine-rich repeat (LRR)-containing PRRs have been extensively studied. They preferentially bind to proteins or peptides, such as the evolutionarily conserved 22-residue peptide of bacterial flagellin (flg22), or the elf18 epitope of the bacterial elongation factor-Tu (EF-Tu) (Gómez-Gómez and Boller, 2000; Zipfel *et al.*, 2006). Other well-known PRRs contain lysine motifs (LysM), which bind carbohydrate-based ligands, such as fungal chitin or bacterial peptidoglycans (Miya *et al.*, 2007; Willmann *et al.*, 2011; Liu *et al.*, 2012; Cao *et al.*, 2014).

Immediately after ligand binding, the PRRs recruit co-receptors to form an active complex, resulting in transphosphorylation of the respective kinase domains. Signaling via this active complex can be mediated directly through receptor-like cytoplasmic kinases (RLCKs), which are specifically recruited to different PRR complexes and provide a link between extracellular ligand perception and downstream signaling (Böhm *et al.*, 2014; Couto and Zipfel, 2016).

The network of signaling pathways is highly complex and results in a series of inter-

twined molecular, cellular and physiological responses. One of the first PTI responses is a rapid calcium influx into the cytosol, which also induces the opening of other membrane transporters. This ultimately leads to an extracellular alkalization and depolarization of the plasma membrane as well as a rapid generation of apoplastic reactive oxygen species (ROS) (Yuan *et al.*, 2017). The activation of plant-membrane-localized NADPH oxidases as well as cell-wall-associated peroxidases mediates the ROS increase, often referred to as ROS burst (Figure 1.2). ROS can have antimicrobial activity and just like $Ca^{2+}$ contribute to further defense signaling and feedback regulations with other small molecules involved in stress signaling, such as nitric oxide and phosphatidic acid (Bigeard *et al.*, 2015; Yu *et al.*, 2017).

Mitogen-activated protein kinase (MAPK) activation is another early and universal PTI response. MAPK cascades are signaling modules that usually consist of three evolutionary conserved kinases, an MAPK, an MAPK kinase (MAPKK), and an MAPK kinase kinase (MAPKKK). These kinases sequentially activate each other by phosphorylation to mediate signaling from receptors to downstream targets (Figure 1.2) (Meng and Zhang, 2013). Another signal transduction pathway is based on the activation of calcium-dependent protein kinases (CDPKs) (Boudsocq and Sheen, 2013). Once activated, these pathways lead to extensive transcriptional reprogramming, which constitutes the main link between the signal transduction and the implementation of induced defenses (Couto and Zipfel, 2016). These include the synthesis of defense hormones and various antimicrobial compounds (Pieterse *et al.*, 2012; Berens *et al.*, 2017). Among these are enzyme inhibitors, toxins and fungal CWDE, such as chitinases and glucanases (Figure 1.2) (Loon *et al.*, 2006; Ahuja *et al.*, 2012; Gupta *et al.*, 2013). Regions exposed to pathogen attacks often form cell wall thickenings, known as papilla. These constitute mechanical and chemical barriers to slow down pathogen invasion (Voigt, 2014; Andersen *et al.*, 2018).

The PTI responses combined with the preformed barriers are usually resilient enough to prevent non-adapted pathogens from colonization. In contrast, adapted pathogens can avoid early defense responses by secreting effector molecules (virulence factors) to suppress PTI and render the plant susceptible to their attack, leading to effector-triggered susceptibility (ETS) (Figure 1.2) (Jones and Dangl, 2006).

### 1.3.2 Effector-triggered immunity

To counteract ETS, plants have evolved a second layer of immunity relying on intracellular resistance proteins (R proteins) that detect the presence of specific effectors, so-called avirulence proteins (Avrs). The subsequently induced defense response is part of the effector-triggered immunity (ETI) (Cui *et al.*, 2015). These receptor proteins usually

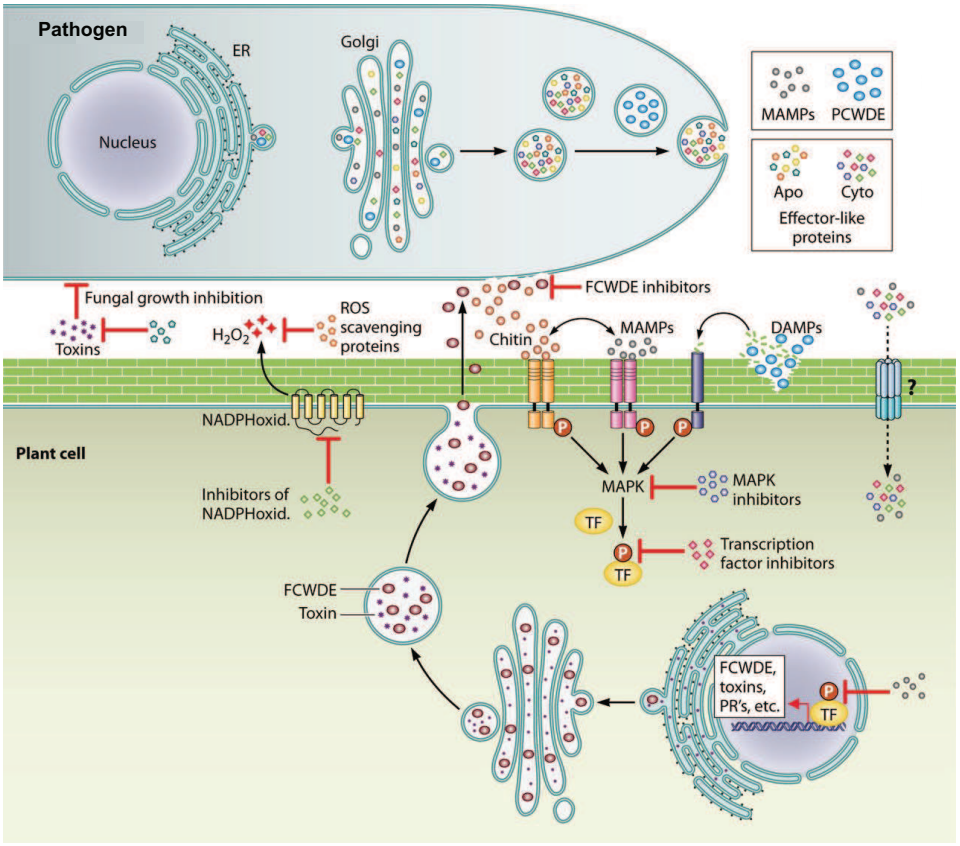


**Figure 1.2: Plant immune responses and sites of action of secreted pathogen effectors.** The model depicts the plant's immune responses upon recognition of microbe-associated molecular patterns (MAMPs), such as the fungal cell wall component chitin, or host-plant-derived damage-associated molecular patterns (DAMPs). DAMPs can be released by plant-cell-wall-degrading enzymes (PCWDE). MAMPs/DAMPs get recognized through membrane-localized receptors, which subsequently induce defense responses through a variety of phosphorylation-mediated signaling pathways (P in red circle). Defense responses include the expression of pathogenesis-related proteins (PRs), toxins, and fungal CWDE (FCWDE). Filamentous pathogens secrete proteins that supress these plant defence responses. These effector-like proteins are usually secreted through the endoplasmic reticulum-golgi pathway. They can remain in the apoplast (Apo) or be further translocated into the cytoplasm (Cyto) by an unknown transporter or mechanism. Figure has been modified from Schmoll *et al.* (2016).

contain a nucleotide-binding domain and leucine-rich repeats (NLR). They can be classified depending on their N-terminal domain (Dodds and Rathjen, 2010; Monteiro and Nishimura, 2018).

Effector recognition may occur through direct binding or indirectly by sensing the activity of an effector interacting with a host component (Cesari, 2018). In addition to reactivating and amplifying PTI-triggered defense responses, ETI often involves a form of localized plant cell death referred to as the hypersensitive response (HR). HR is a very effective method to prevent biotrophic pathogens from spreading (Mur *et al.*, 2008). ETI responses are not only local, but can also induce longer lasting systemic immunity, so-called systemic acquired resistance (SAR). Signals such as the accumulation

of salicylic acid (SA) lead to the systemic expression of *pathogenesis-related* (*PR*) genes and prime uninfected tissues against subsequent pathogen attacks (Fu and Dong, 2013). Pathogens are then forced to develop new effectors or lose the Avrs to circumvent ETI, reinstating ETS. To illustrate this interplay between the plant (PTI/ ETI) and the pathogens (MAMPs/ effectors/ ETS), the zigzag model was postulated by Jones and Dangl (2006). The zigzag model presents the successive steps of this interaction and reflects the evolutionary arms race for new effectors and plant receptors, respectively.

## 1.4 Effectors in plant-pathogenic interactions

### 1.4.1 Effector translocation

Effectors can be grouped based on their target site in the host plant, either remaining in the apoplast (apoplastic effectors) or translocated into the plant cell and function as cytoplasmic effectors. Regardless of the effector type, efficient delivery of effectors to the plant is required for successful infection (Lo Presti *et al.*, 2015). Most fungal and oomycete effectors are secreted through the endoplasmic reticulum-golgi pathway, based on the presence of a secretory signal at the N-terminus of the protein. By means of exocytosis, they are released into the extracellular milieu, which can be the apoplast, the EHMx or the extra-invasive hyphal space depending on the pathogen (Figure 1.2) (Giraldo *et al.*, 2013; Petre and Kamoun, 2014; Viotti, 2016).

Fungal translocated effectors lack conserved amino acid motifs that can be linked to effector uptake and it is unknown whether they use common or divergent routes for translocation (Lo Presti *et al.*, 2016). Interestingly, in the *M. oryzae*-rice pathosystem, a special structure seems to be involved in the translocation of effectors. Cytoplasmic effectors are targeted to an unconventional, golgi-independent, secretory pathway. Afterwards, they accumulate in the biotrophic interfacial complex (BIC) (Khang *et al.*, 2010; Giraldo *et al.*, 2013). Independent of the BIC, apoplastic *M. oryzae* effectors are secreted into the extracellular space between the fungal cell wall and the extra-invasive hyphal membrane (Zhang and Xu, 2014; Shipman *et al.*, 2017).

In oomycetes, many secreted effector proteins share common N-terminal host-targeting motifs associated with effector uptake. RxLR (Arg-x-Leu-Arg) motifs are located about 30 amino acids downstream of the signal peptide and are often followed by a dEEr (Asp-Glu-Glu-Arg) amino acid sequence (Rehmany *et al.*, 2005; Anderson *et al.*, 2015). The RxLR motif of the *Phytopthora infestans* effector Avr3a has been the first one shown to be required for translocation into the host cell (Whisson *et al.*, 2007). However, the proposed translocation mechanism and the specific role of the RxLR motif is still being debated (Wawra *et al.*, 2012; Wawra *et al.*, 2013; Tyler *et al.*, 2013). It was also recently

shown that the RxLR motifs of the AVR3a effector from *P. infestans* is cleaved off before it is secreted from the pathogen (Wawra *et al.*, 2017). Other classes of oomycete effectors are Crinkler proteins with the LxLFLAK motif and the *Albugo laibachii* effectors that share a CHxC signature. Their mechanisms of uptake are currently unknown (Torto *et al.*, 2003; Schornack *et al.*, 2010; Kemen *et al.*, 2011).

### 1.4.2 Molecular functions of fungal effectors

Biotrophic fungi deploy effectors to evade and manipulate the plant's immune system as well as alter the physiology of the host plant (Figure 1.2) (Rodriguez-Moreno *et al.*, 2018). To avoid recognition by the plant and thereby evade PTI, several fungal pathogens secrete effectors to interfere with the different steps of this process. The Avr4 effector of *Cladosporium fulvum* harbors an "invertebrate chitin binding" domain that allows it to bind to chitin in the fungal cell wall, where it blocks the access of host chitinases (Burg *et al.*, 2006; vanEsse *et al.*, 2007). Other effectors, such as the *C. fulvum*-derived Ecp6 or Slp1 from *M. oryzae* bind to chitin fragments after they have already been liberated from the fungal cell wall by plant chitinases. Their chitin-binding affinity is so high that it can outcompete binding to the chitin receptors of the host (Jonge *et al.*, 2010; Mentlak *et al.*, 2012; Sanchez-Vallet *et al.*, 2013).

Effectors are also widely involved in countering all aspects of PAMP-triggered defense responses. The *Verticillium dahliae* effector VdSCP41 targets the plant nucleus and interferes with the DNA-binding activity of the *Arabidopsis thaliana* transcription factors CBP60g and SARD1, thereby abolishing the induction of defense genes (Qin *et al.*, 2018). Furthermore, tomato-papain-like cysteine proteases PIP1 and RCR3 can also be effector targets. They are inhibited in the apoplast by the *C. vulvum* effector AVR2 (Rooney *et al.*, 2005; Van Esse *et al.*, 2008). Effectors do not have to directly target components of the defense apparatus, but can also modulate the plant's physiology for their own benefit. Several effectors interfere with the hormone signaling network that is involved in the regulation of plant growth, development and defense (Shen *et al.*, 2018). SA is important for resistance to biotrophic and hemibiotrophic pathogens and is also required for the induction of SAR (Tanaka *et al.*, 2015). To lower the SA accumulation in the plant cell, *V. dahliae* unconventionally secretes the effector VdIsc1. Vdlsc1 is an isochorismatase that hydrolyzes the host's isochorismate, a precursor of SA, thereby disrupting the SA metabolism (Liu *et al.*, 2014).

### 1.4.3 Effector proteins of *U. maydis*

The *U. maydis* genome is predicted to encode 476 secreted proteins. These include 215 novel effectors that lack any known structural or functional domain. In the *U. maydis* genome, many of these effector genes reside in clusters (Kämper *et al.*, 2006; Schirawski *et al.*, 2010; Lanver *et al.*, 2017; Schuster *et al.*, 2018). The *U. maydis* effectors that contain orthologues in all plant-pathogenic smut fungi are considered to be core effectors, whereas accessory effectors can be found only in a subset of species. A comparative genomic analysis of the secretomes of five plant-pathogenic smut fungi, identified 72 core families of secreted proteins with known domains and 24 families of novel core effectors (Schuster *et al.*, 2018).

Many effectors were shown to contribute to virulence, but so far only the six effectors Rsp3, Pit2, Pep1, Cmu1, Tin2 and See1 are functionally characterized (Kämper *et al.*, 2006; Schirawski *et al.*, 2010; Schilling *et al.*, 2014; Stirnberg and Djamei, 2016; Lanver *et al.*, 2017). The effector Rsp3 binds to the fungal cell wall and protects hyphae from the mannose-binding antifungal proteins AFP1 and AFP2 of maize. By blocking their antifungal activity, Rsp3 contributes to virulence (Ma *et al.*, 2018). The other two apoplastic effectors, Pit2 and Pep1, are involved in the initial establishment of a compatible interaction. Pit2 functions as an inhibitor of a set of apoplastic maize cysteine proteases (Mueller *et al.*, 2013). Pep1 inhibits the activity of the plant peroxidase POX12, a major generator of $H_2O_2$ in the apoplast (Hemetsberger *et al.*, 2012; Hemetsberger *et al.*, 2015). Upon the deletion of *pep1*, mutants arrest after penetration and are subsequently recognized by the plant. This leads to the activation of plant defense responses such as callose formation, accumulation of ROS and local cell death (Doehlemann *et al.*, 2009). The translocated effector Cmu1 interferes with the synthesis of SA (Djamei *et al.*, 2011), whereas another translocated effector, Tin2, targets the plant's secondary metabolism by inducing the production of anthocyanin. An induced anthocyanin production lowers the availability of pre-cursors needed for the lignification of plant cell walls (Tanaka *et al.*, 2014). The third translocated effector, See1, induces the reactivation of plant DNA synthesis during leaf tumor progression (Redkar *et al.*, 2015a; Redkar *et al.*, 2015b).

### 1.4.4 Regulation of effector gene expression

Reacting and responding of the pathogen to the encountered environment is a fine-tuned process. Pathogen sensors can activate signal transduction pathways and downstream transcription factors that regulate genes required for adaptation to the host environment. This goes hand in hand with changes in global gene expression of pathogens, leading to secretion of effectors, enzymes and secondary metabolites, which can then aid the infection process (Does and Rep, 2017).

Effector expression can vary spatially as well as temporally during the infection process. Successive waves of effector gene expression were described in a variety of pathosystems (Toruno *et al.*, 2016; Gervais *et al.*, 2017). These are often associated with a specific period of the infection process. A prominent example is the conversion from a biotrophic to a necrotrophic lifestyle (Kleemann *et al.*, 2012; O'Connell *et al.*, 2012; Jupe *et al.*, 2013). Differential expression throughout the course of infection is also exhibited by biotrophic fungi such as *B. graminis* f. sp. *hordei*, *B. graminis* f. sp. *tritici* and *Puccina striiformis* f. sp. *tritici* (Hacquard *et al.*, 2013; Dobon *et al.*, 2016; Zeng *et al.*, 2017).

For *U. maydis*, an in-depth transcriptional profiling of the plant-associated development (0.5 - 12 days post infection (dpi)), revealed that its effector expression also occurs in waves (Lanver *et al.*, 2018). In the analysis, all *U. maydis* genes were assigned to one of 14 discovered expression modules according to their characteristic expression profile during the course of an infection. The putative secreted effector proteins were present in 12 of the 14 expression modules (Figure 1.3).

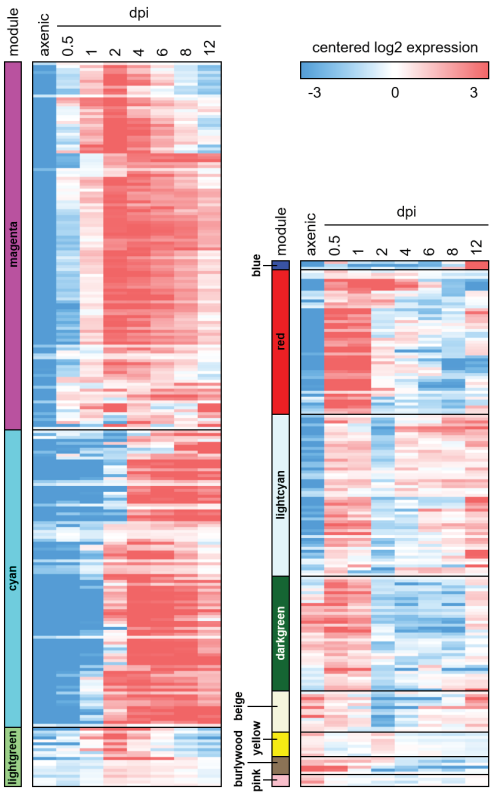


**Figure 1.3: Expression of the *U. maydis* secretome.** A heatmap illustrating co-expression modules of genes encoding putative secreted proteins. Secreted *U. maydis* proteins are assigned to different modules according to their characteristic expression profile across all stages of infection (0.5 to 12 dpi). The different modules are indicated by different colors. Axenic refers to expression in axenic culture. For each module genes were hierarchically clustered, and log2 expression values are shown relative to the mean expression across all stages. Red marks genes that are upregulated and blue that are downregulated. Modified from Lanver *et al.* (2018).

The effectors were enriched in three distinct modules. Effectors in the red module are mainly expressed on the plant surface (0.5 - 1 dpi). Effectors in the magenta module are most strongly induced 0.5 to 2 dpi and their expression is maintained up to 12 dpi. This module is associated with the establishing and maintenance of biotrophy. All of the functionally characterized effectors are part of this module. Effectors in the cyan module are most likely involved with the induction of tumors at 2 - 4 dpi. Effectors that are part of these modules are likely the key determinants for *U. maydis* virulence.

## 1.5 Aim of this study

It is crucial to understand the molecular function and biochemical activity of effectors and thereby elucidate their role in the interplay between *U. maydis* and its host maize. This will not only shed light on the mechanisms of pathogenicity, but also reveal new aspects of plant immunity and defense. Ultimately, this knowledge can be utilized to develop new strategies for plant protection and resistance breeding in agriculture.

The aim of this study was the identification and functional analysis of novel *U. maydis* effectors. It mainly focused on the putative effectors of the magenta module, whose expression is linked to the stage in which biotrophy is established. A systematic deletion approach highlighted the novel effectors *stp2*, *stp3* and *stp4* as very interesting candidates to study plant-pathogen interaction due to their strong phenotype. These were investigated in detail with the regard to their localization and function. Part of this effort was the search for interaction partners, which led to the discovery of an effector complex. This effector complex and its members were subsequently included in the functional characterization.

# 2 Results

## 2.1 Identification of novel effectors

### 2.1.1 Selection and expression of candidates

Initially, a systematic deletion approach was used to identify novel putative effectors and find potential candidates to be functionally characterized. The focus was hereby on novel, single effectors from the magenta module. The expression of the five chosen candidate genes, *UMAG_10030*, *UMAG_10067*, *UMAG_00715*, *UMAG_12197* and *UMAG_05819*, is induced at 12 hours post infection (hpi), the time point of appressoria formation (Figure 2.1). The five genes show a similar expression pattern during the early biotrophic stage. A strong increase of expression can be observed after 24 hpi, and expression peaks at 2 dpi for *UMAG_10030*, *UMAG_00715* and *UMAG_12197* and at 4 dpi for *UMAG_10067* and *UMAG_05819*. At later stages expression declines but is maintained up to 12 dpi (Lanver *et al.*, 2018).

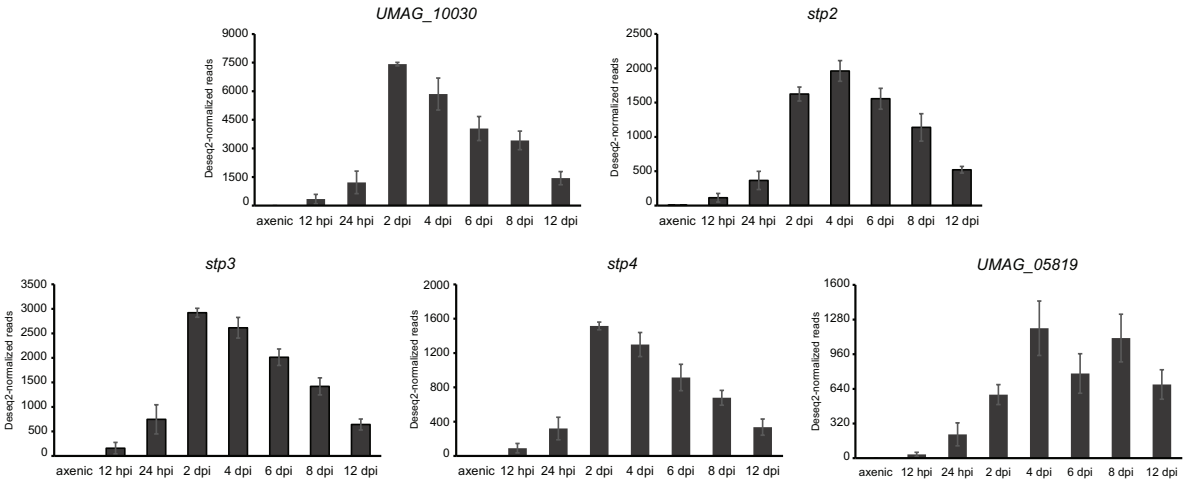


**Figure 2.1: Expression of five candidate genes of the magenta module during biotrophic development.** RNAseq data are from Lanver *et al.* (2018), in which plants were infected with FB1 and FB2 and samples were collected at the indicated time points. Axenic refers to expression in axenic culture. Read counts were normalized using DEseq2. Error bars indicate standard deviation of three biological replicates.

### 2.1.2 Three novel effector proteins are essential for virulence

Deletion mutants of the candidate genes were generated in the solopathogenic haploid strain SG200 by gene replacement using a polymerase chain reaction (PCR)-based approach (Kämper, 2004). To test their virulence, seven-day-old maize plants were infected with the deletion mutants. Infected plants were assessed for disease symptoms at 12 dpi and, depending on their strongest symptoms, assigned to a disease category (Figure 2.2A). The infections were conducted in three biological replicates, with three independently generated deletion strains per deletion mutant. In all cases, the three independently generated deletion strains had comparable phenotypes (not shown). A representative strain is shown in Figure 2.2. In comparison to the wild type SG200, the three deletion mutants SG200ΔUMAG_10067, SG200ΔUMAG_00715 and SG200ΔUMAG_12197 showed neither tumor nor anthocyanin formation. Only light chlorosis and occasional necrotic spots could be observed (Figure 2.2A and B). The mutant phenotype of these strains resembled previously identified *stp1* (*stop after penetration 1*) deletion mutants (Schipper, 2009). The new effector genes were designated *stp2* (*UMAG_10067*), *stp3* (*UMAG_00715*) and *stp4* (*UMAG_12197*). The other two deletion mutants SG200ΔUMAG_10030 and SG200ΔUMAG_05819 showed symptoms comparable to the wild type and were therefore not further investigated in this work (Figure 2.2A and B).

In order to verify that the strong phenotype, caused by deleting the three *stp* genes, is linked to the respective gene, a single copy of this gene under the control of its native promoter was re-integrated into the *ip* (*iron-sulphur protein*) locus of the respective deletion strain. In all three cases the loss of virulence could be fully complemented (Figure 2.2C).

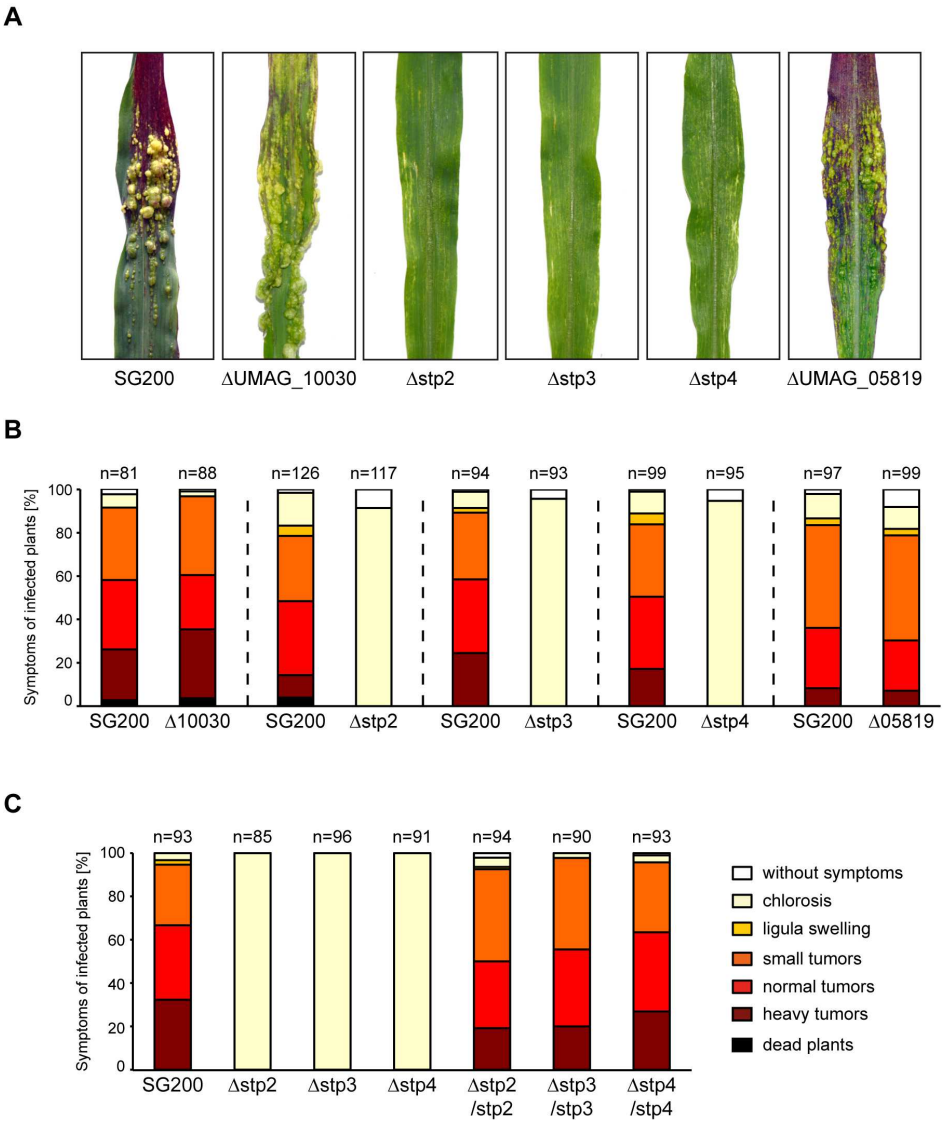


**Figure 2.2: Virulence of candidate gene deletion mutants.** (A) Representative leaves of infections with the wild type SG200 and the five effector deletion mutants at 12 dpi. (B) Plants were infected with indicated strains and assessed for disease symptoms at 12 dpi. Depending on their strongest symptom they were assigned to a disease category. The color code for the symptom categories is given on the bottom right. The infections were conducted in three biological replicates and average values are expressed as percentage of the total number of infected plants (n), shown above each column. (C) Virulence of Δstp2, Δstp3 and Δstp4 complementation strains. Plants were infected with indicated strains and analyzed as described in B.

## 2.2 Phenotypic characterization of the *stp2*, *stp3* and *stp4* deletion mutants

Investigating at which stage the *stp* deletion strains are impaired in establishing a successful biotrophic interaction, early stages of their development were examined in more detail. This included examination of saprophytic growth, stress sensitivity, the formation of filaments and *in planta* growth.

### 2.2.1 Deletion of *stp2*, *stp3* and *stp4* does not affect saprophytic growth

When grown in liquid culture, the three *stp* deletion mutants showed similar growth behaviour as their progenitor strain SG200. Also on potato dextrose media plates colony morphology was indistinguishable from SG200 (not shown). Furthermore, when spotted on potato dextrose (PD)-charcoal plates all three *stp* deletion mutants were able to switch to filament formation (Figure 2.3A). The solopathogenic SG200 is able to form white filaments on charcoal-containing medium due to an active bE/bW complex and autocrine pheromone stimulation (Kämper *et al.*, 2006).

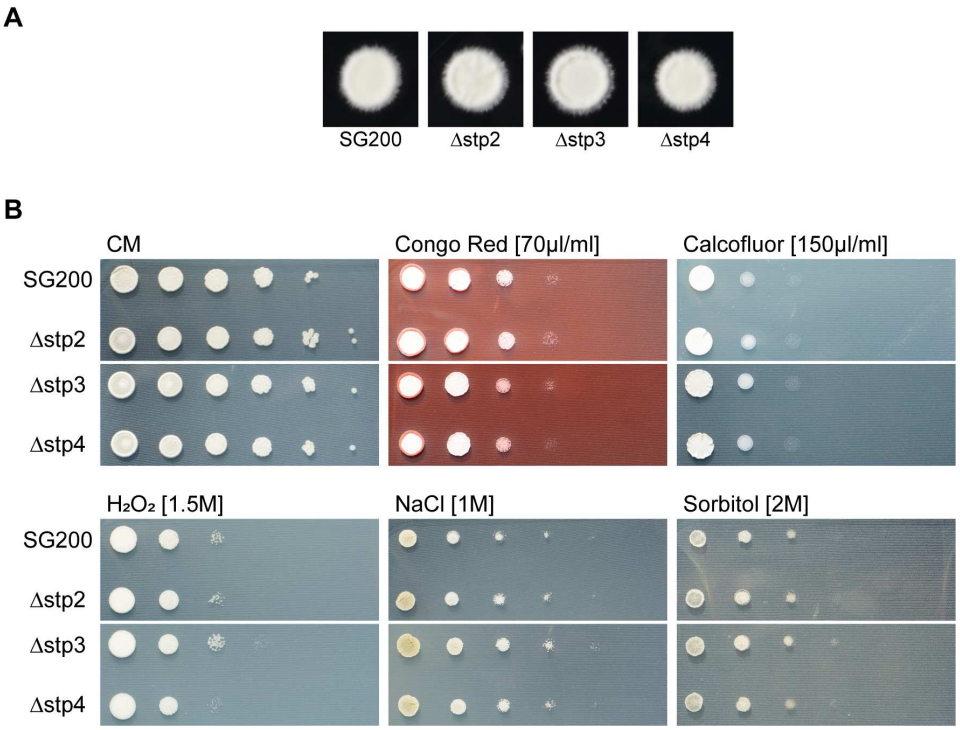


**Figure 2.3: Filamentous growth and stress sensitivity of *stp* deletion strains.** (A) Filamentous growth of the indicated strains on PD-charcoal plates. (B) Serial ten-fold dilutions of the indicated strains were spotted on complete media (CM) and stress plates with indicated supplements. Plates were incubated for 48 h at 28°C.

To test whether the *stp* mutants show an altered sensitivity to stresses that can occur during the colonization process, the mutants were grown on different stress plates. Complete media (CM) plates served as a control. Stress plates were CM plates to which different stress-inducing supplements were added. These supplements induced cell wall stress (congo red and calcofluor white), osmotic stress (sorbitol and sodium chloride) or oxidative stress (hydrogen peroxide). SG200Δstp2, SG200Δstp3 and SG200Δstp4 mutants grown on stress plates were similar in growth and morphology to SG200 (Figure 2.3B).

### 2.2.2 SG200Δstp2, SG200Δstp3 and SG200Δstp4 mutants stop after penetration

After the infection with the deletion mutants, no macroscopic disease symptoms were observed on top of the plant surface (Figure 2.2A). To investigate at which stage the fungal development is impaired, the early stages of the infection were examined microscopically by confocal laser microscopy at 3 dpi. The plant cell wall was stained with propidium iodide and the fungal hyphae were stained with AF488-conjugated WGA (wheat germ agglutinin), a lectin with a high affinity to chitin. In SG200 infected leaves, a strong colonization by fungal hyphae was observed, whereas intracellular hyphae of the *stp* deletion mutants did not spread in the plant tissue. The *stp* deletion strains were able to form appressoria and could penetrate epidermal maize cells, but arrested directly after penetration and failed to colonize mesophyll tissue. For all three deletion mutants, strong autofluorescence was observed around the penetration site, likely due to plant defense responses (Figure 2.4).

As the defect of the deletion mutants manifested itself early after penetration, live cell microscopy was conducted at 1 dpi. In order to observe the deletion mutants in living cells, *stp2*, *stp3* and *stp4* were deleted in the SG200 derivative SG200AN1. This strain carries an appressorial marker gene in which 3×GFP (green fluorescent protein) is fused to a promoter that is strongly expressed during appressoria formation (Mendoza-Mendoza *et al.*, 2009). Already at 1 dpi SG200 was detected in the mesophilic tissue and also started to branch (Figure 2.5A). Confirming previous observations, the *stp* deletion mutants were able to form appressoria and penetrate the plant cell, but stopped very early during infection. In most cases the SG200AN1Δstp2 strain was confined to the epidermal cell layer (Figure 2.5B). SG200AN1Δstp3 and SG200AN1Δstp4 were also largely restricted to the epidermal layer, but in several cases hyphae were detected in the mesophyll. However, the hyphae appeared thin and crippled in comparison to SG200 (Figure 2.5C and D). All three *stp* deletion mutants were unable to form clamp structures, suggesting that mitotic cell division did not occur.

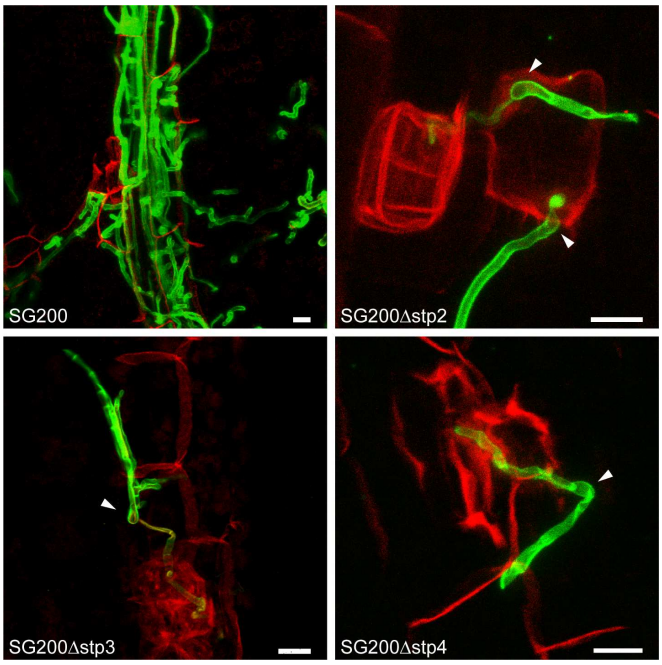


**Figure 2.4: Microscopic analysis of early development of *stp* deletion strains.** Maize seedlings infected with the indicated *U. maydis* strains were observed at 3 dpi by confocal microscopy. Fungal hyphae were stained with WGA-AF488 (green). Plant cell walls were stained with propidium iodide (red). White arrows indicate appressoria. Pictures are maximum projections of confocal z-stacks. The scale bar represents 10 $\mu$m.

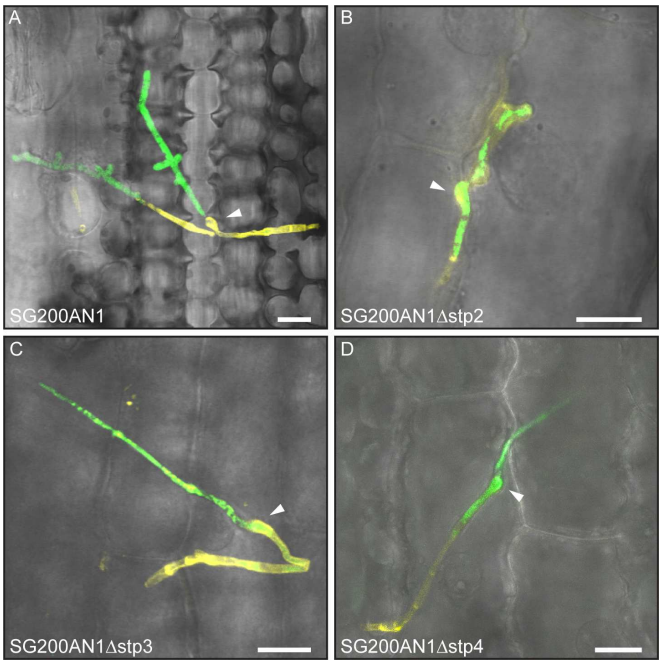


**Figure 2.5: Live cell microscopy of early development of *stp* deletion strains.** Maize seedlings infected with the indicated *U. maydis* strains were observed at 1 dpi by confocal microscopy. Confocal pictures show an overlay of GFP signal (green) UV-laser-induced autofluorescence (yellow) and bright-field projection (grey). Bright-field shows the mesophilic cell layer (A) and epidermal cells (B-D). White arrows indicate appressoria. Pictures are maximum projections of confocal z-stacks. The scale bar represents 10 $\mu$m.

When inducing autofluorescence with an ultraviolet (UV) laser, the calcofluor white stained hyphae (Figure 2.5A and C) and the empty septa of unstained hyphae (Figure 2.5B and D) could be detected on the leave surface. Additionally, the UV laser induced autofluorescence in the deletion mutants, in particular around the intracellular hyphal tip area. In several cases it appeared as if the hyphae was encased by it. For *stp3*, *stp4* deletion mutants and the wild type autofluorescence was not observed.

## 2.3 Comparison of effectors essential for biotrophy

Deletion mutants lacking *stp2*, *stp3* and *stp4* effectors showed similar virulence phenotypes to those observed for mutants of the previously described effectors *stp1* (Schipper, 2009) and *pep1* (Doehlemann *et al.*, 2009; Hemetsberger *et al.*, 2012; Hemetsberger *et al.*, 2015). Effectors *stp1* and *pep1* also reside in the magenta module, indicating that all five essential effectors are co-expressed (Supplementary Figure S1). Consequently, Stp1 and Pep1 were included in subsequent studies for comparison. Even though their virulence phenotype is comparable, the genomic sequences of the effectors are not similar. The differ with regard to size, chromosome location or cysteine content (Table 2.1). While *stp1*, *stp3* and *pep1* lack introns, *stp2* and *stp4* have one predicted intron each. All five essential effectors exist as single genes and only *stp1* is part of a cluster (Kämper *et al.*, 2006). All five are predicted to be secreted and all five lack known sequence motifs associated with enzymatic functions (Table 2.1).

**Table 2.1:** Table showing the length in amino acids, the length of the predicted signal peptide, the predicted molecular weight after secretion, the chromosome location and the number and position of cysteines for each of the essential effectors.

| Protein name | Length (aa) | Length of signal peptide (aa) | Location | Cysteine residues | Predicted molecular weight after secretion (kDa) |
|---|---|---|---|---|---|
| Stp1 | 515 | 28 | Chromosome 5 | 2 (C 125, 460) | 47.62 |
| Stp2 | 218 | 25 | Chromosome 5 | 2 (C 61, 104) | 20.66 |
| Stp3 | 327 | 24 | Chromosome 1 | 14 (C 55, 56, 71, 93, 112, 127, 199, 200, 215, 229, 264, 279, 298, 313) | 32.76 |
| Stp4 | 129 | 23 | Chromosome 7 | 8 (C 32, 38, 56, 67, 82, 95, 97, 104) | 11.45 |
| Pep1 | 178 | 26 | Chromosome 3 | 4 (C 59, 75, 94, 112) | 15.75 |

None of the five essential effectors has a paralog in the *U. maydis* genome. However, orthologs were detected in sequenced plant parasitic smut fungi indicating that the genes belong to the core effectors (Rabe *et al.*, 2016; Schuster *et al.*, 2018). Amino acid sequence identity, alignment and pairwise comparison of the essential effectors with orthologs from the other smuts is shown in Table 2.2 and Supplementary Figure S2.

**Table 2.2:** Table showing the percent identity of amino acid sequences of the essential effectors with the sequences of the orthologs from related smut species.

| *Ustilago maydis* | Stp1 | | Stp2 | | Stp3 | | Stp4 | | Pep1 | |
|---|---|---|---|---|---|---|---|---|---|---|
| | Gene ID | Identity (%) | Gene ID | Identity (%) | Gene ID | Identity (%) | Gene ID | Identity (%) | Gene ID | Identity (%) |
| *Sporisorium reilianum* f. sp. *zeae* | sr_10918.2 | 51.75 | sr_10759 | 59.40 | sr_12002 | 69.46 | sr_13927 | 62.60 | sr_12947 | 65.38 |
| *S. reilianum* f. sp. *sorghi* | srs_10918 | 37.64 | srs_10759 | 60.18 | srs_12002 | 69.46 | srs_13927 | 62.60 | srs_12947 | 65.93 |
| *Sporisorium scitamineum* | SPSC_05474 | 47.19 | SPSC_06156 | 64.09 | SPSC_01978 | 68.26 | SPSC_06609 | 64.66 | SPSC_03260 | 61.54 |
| *Ustilago bromivora* | UBRO_12209 | 45.39 | UBRO_03606 | 53.10 | UBRO_01096 | 67.38 | UBRO_04531 | 60.15 | UBRO_02965 | 60.44 |
| *Ustilago hordei* | UHOR_12209 | 40.00 | UHOR_03606 | 53.10 | UHOR_01096 | 62.73 | UHOR_04531 | 60.15 | UHOR_02965 | 60.44 |
| *Melanopsichium pennsylvanicum* | MEPE_00854 | 44.76 | MEPE_04171 | 49.79 | MEPE_02823 | 60.61 | MEPE_02537 | 43.75 | MEPE_01593 | 52.49 |

## 2.4 Characterization of plant responses after infection with essential effector mutants

In order to characterize plant defense responses, maize tissue infected with *stp1*, *stp2*, *stp3*, *stp4* and *pep1* deletion mutants was examined by confocal laser microscopy at 24 to 48 hpi. Different stains were used to visualize certain plant defense reactions. Additionally, an RNA sequencing (RNAseq) dataset was generated from infected tissue at 24 hpi, allowing a more detailed comparison of defense responses triggered by the *stp* and *pep1* deletion mutants.

### 2.4.1 *stp2* and *pep1* deletion mutants induce strong callose deposition after penetration

An early plant reaction towards pathogen infection is the formation of papillae that provide a physical barrier against the invading pathogen. To show whether any of the essential effector mutants induces this type of defense, callose, a component of this cell wall apposition, was stained with aniline blue. For SG200AM1Δstp1 (Schipper, 2009), SG200AN1Δstp3 and SG200AN1Δstp4, callose staining was highly localized at penetration sites and there was no or only very little signal located at the intracellularly growing hyphae. This was very similar to what was observed for the wild type SG200AN1 (Figure 2.6). In contrast, SG200AN1Δstp2 as well as SG200Δpep1RFP (Doehlemann *et al.*, 2009) showed a strong callose-derived signal encasing the entire intracellularly growing hyphae from the penetration site (Figure 2.6). For SG200AN1Δstp2 and SG200Δpep1RFP, the formation of papillae could also be observed in the bright-field channel (Figure 2.6).

### 2.4.2 *stp* deletion mutants induce plant cell death after penetration

Plants that were infected with *stp* deletion mutants, developed necrotic patches (Figure 2.1A). These patches could be an indication for cell death, a plant reaction which is usually very efficiently suppressed by biotrophic plant pathogens. To establish whether

cell death occurs as a reaction to the colonization by the *stp* deletion strains, infected plant material was stained with FM4-64, a stain visualizing the plant membrane. Calcofluor white staining was used to visualize fungal hyphae when the AN1-marker associated GFP signal was no longer detectable. In cells infected with SG200AN1, intracellular hyphae were encased completely by an intact plant plasma membrane (Figure 2.7). Plant cells that were penetrated by the *stp* and *pep* deletion mutants often showed a disintegrated plant plasma membrane and formation of intracellular vesicles (Figure 2.7). These are typical signs of programmed cell death (PCD) (Teh and Hofius, 2014). PCD could be seen already at 20 hpi and was even more prominent at 48 hpi. These results indicate that all deletion mutants induce plant cell death.

### 2.4.3 RNAseq reveals a high degree of similarity in defense responses induced by *stp* mutants

To be able to compare the plant defense responses triggered by the *stp* deletion mutants, a transcriptome analysis was conducted using RNAseq. For these samples, maize seedlings were infected with SG200Δstp1, SG200Δstp2, SG200Δstp3, SG200Δstp4, SG200Δpep1, SG200 as well as water (mock). Samples were collected at 24 hpi, the time point around which the deletion mutants arrest. This was done in three biological replicates. A principal component analysis (PCA) confirmed that there were only minor variations between the biological replicates for each sample (Figure 2.8A). Furthermore, the distribution of the samples within the PCA showed that mock- and SG200-infected samples were different from each other and the samples infected with the deletion mutants. However, the PCA found that the deletion mutants of *stp1*, *stp2*, *stp3*, *stp4* and *pep1* were very similar as they clustered together.

Differentially expressed plant genes induced by the deletion mutants in comparison to SG200 were identified (Figure 2.8B). The comparison resulted in 221 (Δstp1), 204 (Δstp2), 401 (Δstp3), 241 (Δstp4) and 326 (Δpep1) significantly upregulated maize genes (expression doubled at an adjusted significance level of $p < 0.01$) and 127 (Δstp1), 156 (Δstp2), 431 (Δstp3), 166 (Δstp4) and 308 (Δpep1) significantly downregulated maize genes (expression halved at an adjusted significance level of $p < 0.01$) (Figure 2.8B). Focusing on the significantly upregulated genes, 122 were represented in all five deletion mutant samples and 207 genes were present in at two, three or four of the deletion mutant samples. The number of genes specifically expressed in each sample was the highest for Δstp3 (97) followed by Δpep1 (52), Δstp1 (12), Δstp4 (11) and Δstp2 (10).

Gene ontology (GO) term-enrichment analysis was performed with the agriGOv2.0 software (Tian *et al.*, 2017) to determine whether the differentially expressed genes,

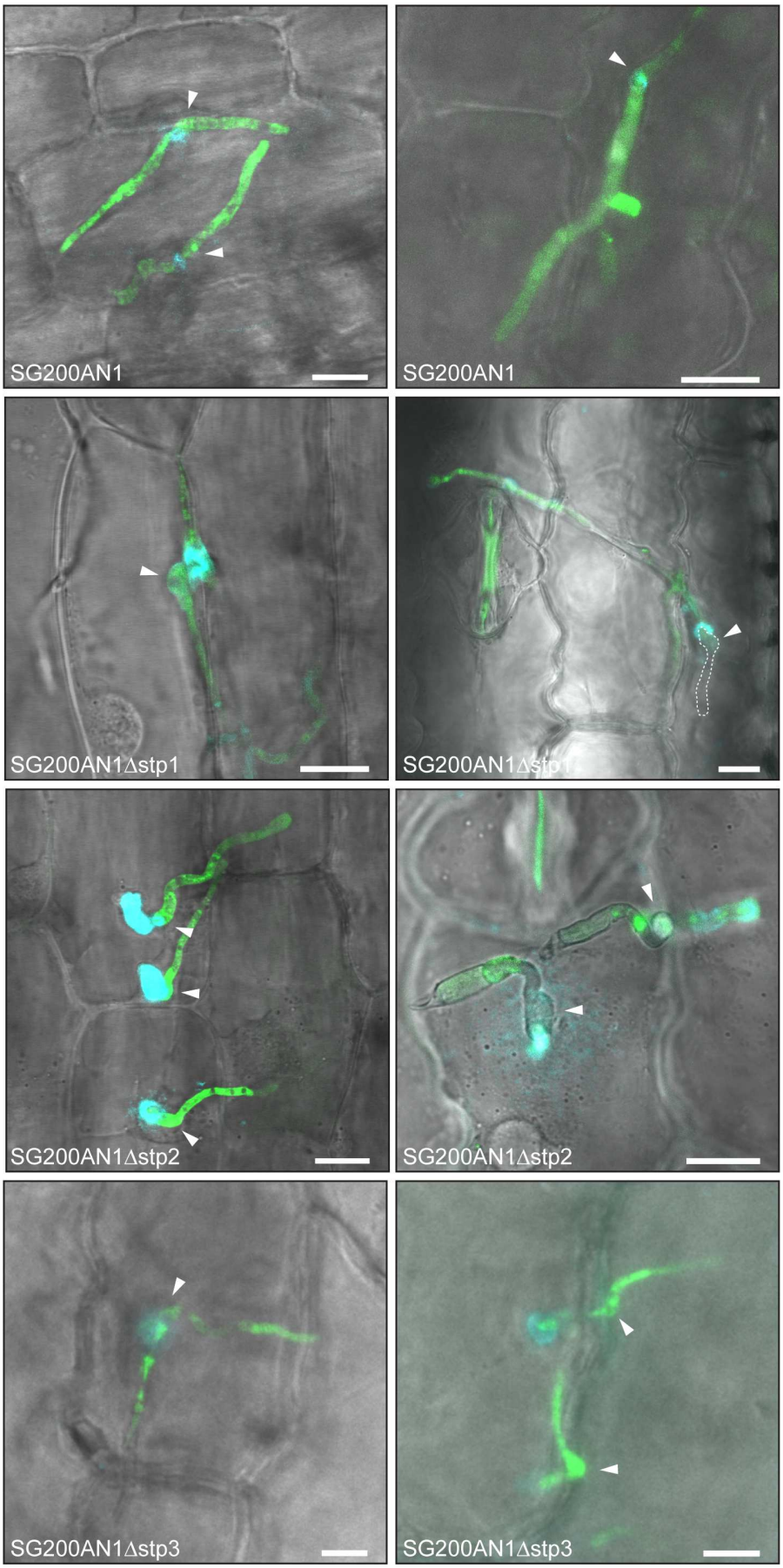
SG200AN1
SG200AN1
SG200AN1Δstp1
SG200AN1Δstp1
SG200AN1Δstp2
SG200AN1Δstp2
SG200AN1Δstp3
SG200AN1Δstp3

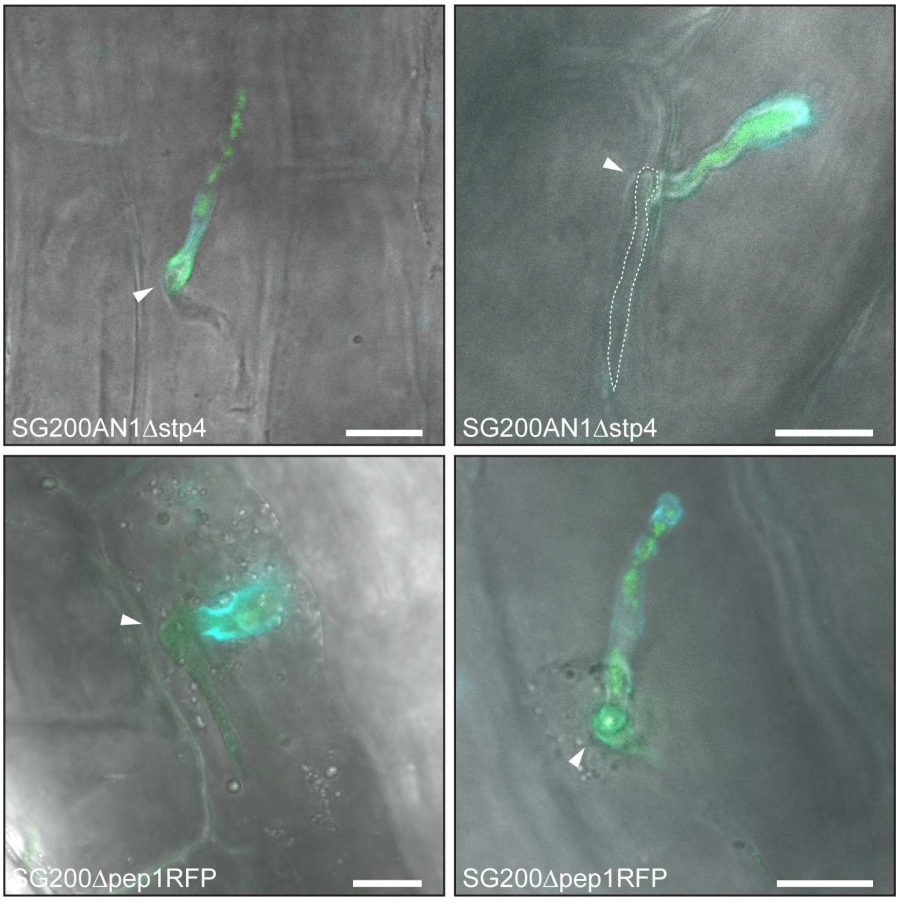


**Figure 2.6: Detection of callose deposition after infection with *stp* and *pep1* deletion strains.** Maize seedlings infected with the indicated *U. maydis* strains were observed at 1 dpi by confocal microscopy. Confocal pictures are showing an overlay of GFP signal (green), aniline blue stained callose depositions (cyan) and bright-field projection (grey). Callose is formed primarily below penetration sites in SG200AN1, SG200AN1Δstp1, SG200AN1Δstp3 and SG200AN1Δstp4 or encases the entire intracellularly growing hyphae in SG200AN1Δstp2 and SG200Δpep1RFP. Dotted lines mark hyphae and appressoria on the plant surface. White arrows indicate appressoria. Pictures are maximum projections of confocal z-stacks. The scale bar represents 10 $\mu$m.

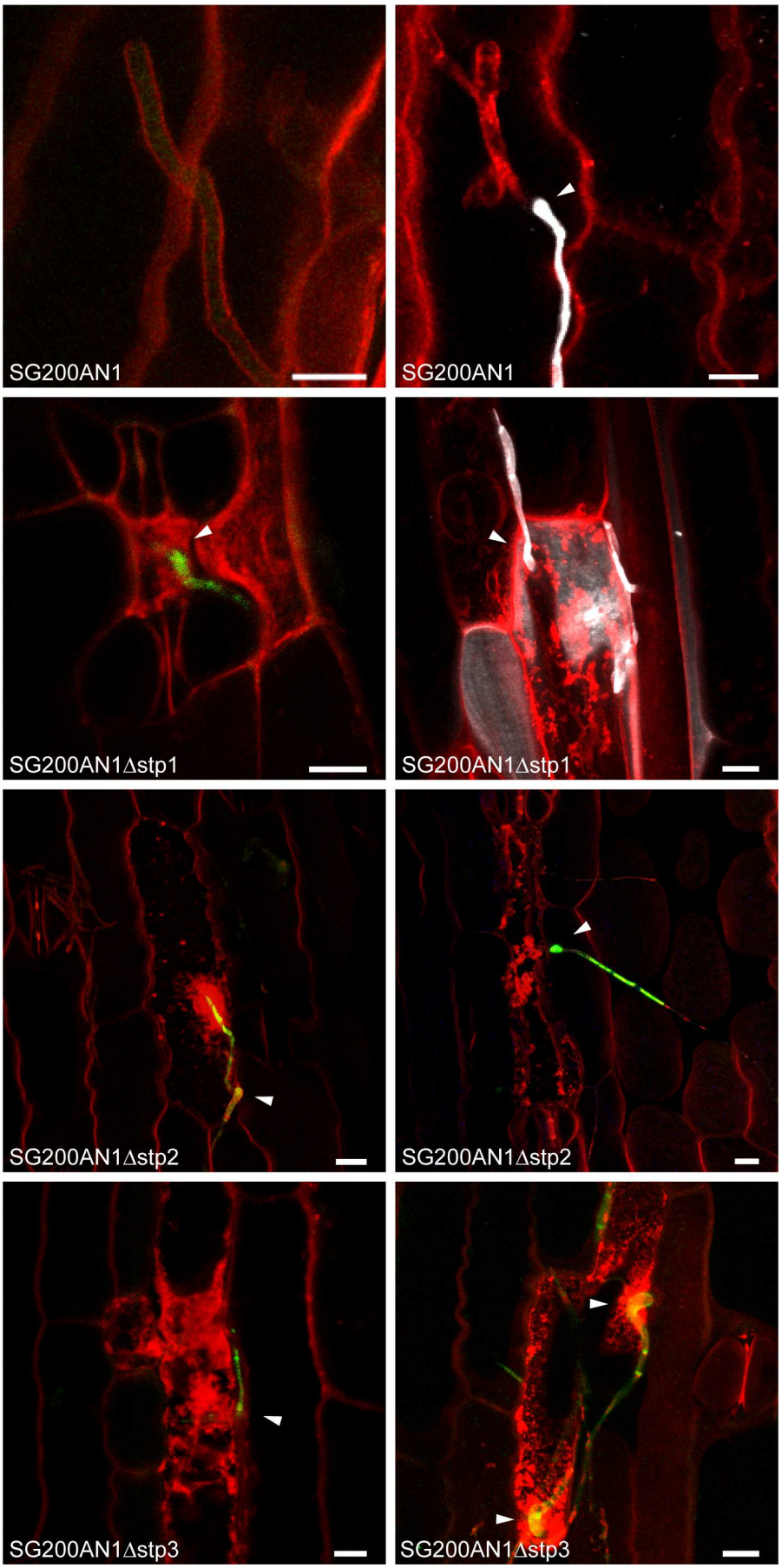
SG200AN1
SG200AN1
SG200AN1Δstp1
SG200AN1Δstp1
SG200AN1Δstp2
SG200AN1Δstp2
SG200AN1Δstp3
SG200AN1Δstp3

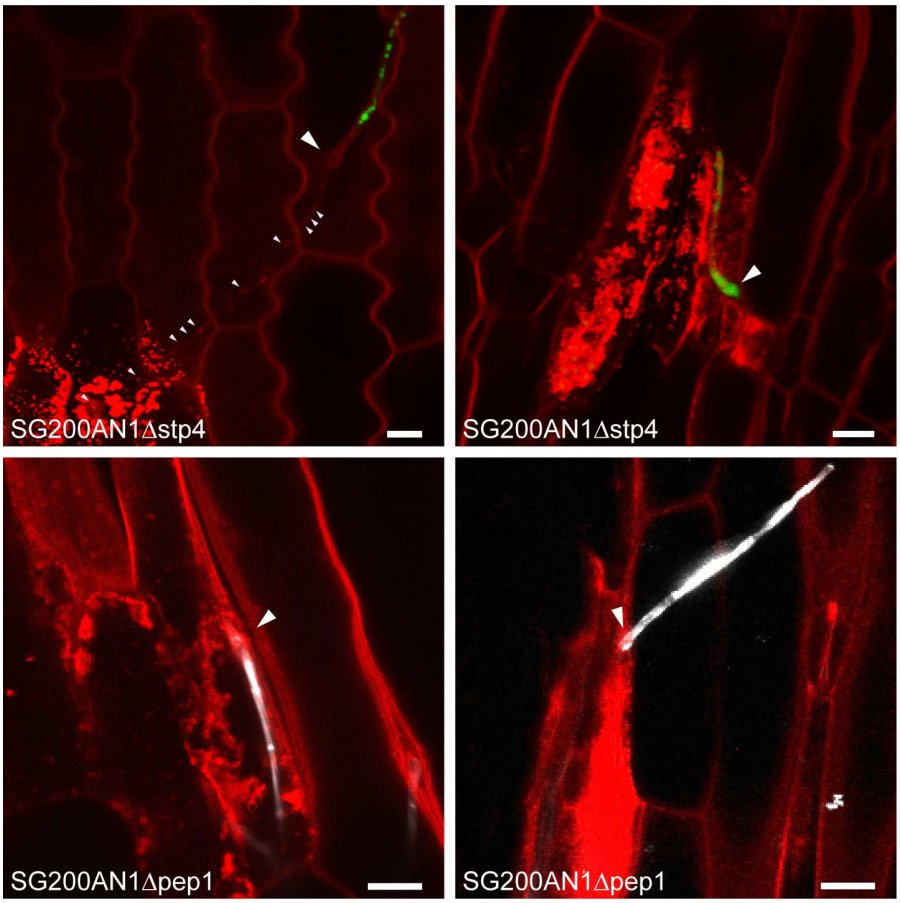


**Figure 2.7: Detection of plant cell death after the infection with *stp* and *pep1* deletion strains.** Maize seedlings infected with the indicated *U. maydis* strains were observed over a time period of 20 hpi to 48 hpi by confocal microscopy. Confocal pictures are showing an overlay of GFP signal (green) and FM4-64 stained plant plasma membrane (red). Older fungal hyphae on leaf surface are stained with calcofluor white (white). White arrows indicate appressoria. Small, light purple arrows point at intracellularly growing hyphae. Pictures are maximum projections of confocal z-stacks. The scale bar represents 10 $\mu$m.

upregulated in all five deletion mutant samples, had any functional role in defense. The genes upregulated with all deletion strains, were mostly assossiated with the GO terms "transcription factor activity", "binding" and "kinase activity". Other upregulated genes could be linked to plant defense responses such as serine/threonine kinases (Cross *et al.*, 2000), WRKY transcription factors (Pandey and Somssich, 2009) or the putative disease resistance protein RGA3, a member of the disease resistance NB-LRR family (Sekhwal *et al.*, 2015).

Even though in these preliminary results no specific defense pathway for the individual *stp* deletion mutant was identified, the RNAseq dataset illustrates the differential gene expression between the compatible and incompatible interactions. The large overlap between the five deletion mutants could indicate a similar function.

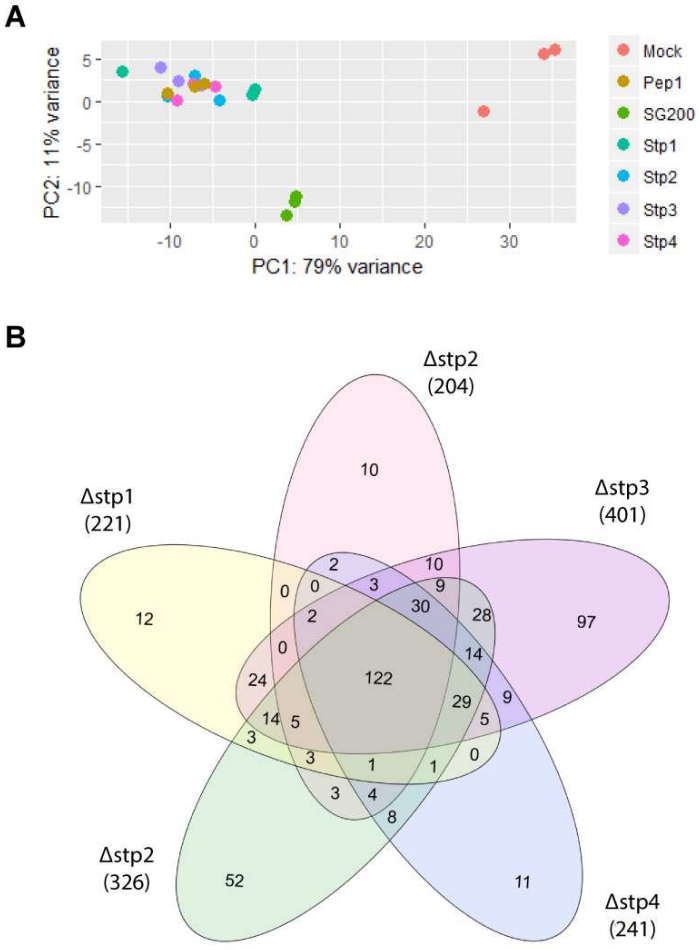


**Figure 2.8: Differentially expressed genes after maize infection with *stp* and *pep1* deletion mutants and SG200.** (A) PCA of RNAseq data. Each circle represents one biological sample, infected with strain SG200, SG200Δstp1 , SG200Δstp2, SG200Δstp3, SG200Δstp4, SG200Δpep1. Mock infected leaves treated with water served as control. (B) The Venn diagram displays the overlap of the significantly upregulated maize genes after infection with the *stp* and *pep1* mutant strains compared with SG200.

## 2.5 Secretion and localization of Stp effector proteins

Spatially locating the areas in which effectors take effect, helps to understand the effector's role in virulence. Based on the presence of a signal peptide, all five essential effectors are predicted to be secreted through the classical ER-Golgi route. Using the bioinformatic tool ApoplastP, which predicts the location of effectors, all five essential effectors were predicted to be apoplastic (Sperschneider *et al.*, 2018). To verify these predictions, microscopic and biochemical methods were implemented.

### 2.5.1 Stp effector proteins can be epitope-tagged and immunoprecipitated

Epitope tags represent a common way of detecting and visualizing proteins without having to generate protein-specific antibodies. Strains were generated in which the *stp* deletion mutants were complemented with C-terminal, HA-tagged versions of the respective gene, expressed under its native promoter and introduced in single or multiple copies. Stp1-HA- and Pep1-HA-expressing strains were generated similarly. To verify that the tags do not interfere with effector function, plant infection assays were conducted with strains harboring single or multiple copies of the tagged effector genes (Figure 2.9A). All strains fully complemented, except for the Pep1-HA-expressing strain carrying multiple integrations, which showed slightly reduced virulence (Figure 2.9A). To test expression and stability of the essential effectors during infection, effector proteins were immunoprecipitated from total lysates of infected plant tissue. Plants were infected with strains containing single copies of the tagged genes and harvested at 3 dpi. 3 dpi is a time point at which all the essential effectors are highly expressed (Figure 2.1 and Supplementary Figure S1). The strain SG200Pcmu1-Spcmu1-mCherryHA was included as a positive control (Djamei *et al.*, 2011). The subsequent western blot analysis revealed that all five fusion proteins are expressed. Stp2-HA, Stp4-HA and Pep1-HA showed a signal of the predicted size, whereas the molecular weights of Stp1-HA and Stp3-HA were 10 kDa higher than predicted (Figure 2.9B).

Schipper (2009) showed that Stp1 becomes posttranslationally modified and deglycosylating Stp1 reduced its size by about 10 kDA. To investigate whether Stp3 is also glycosylated, the precipitate from the Immunoprecipitation (IP) was treated with a protein deglycosylation mix and subsequently analyzed via western blot. Stp1, used as a positive control, did shift indeed. After the treatment the molecular weight of Stp3-HA decreased, but not to the extent that it matched the predicted size (Figure 2.9C). This could indicate that Stp3-HA has either abnormal behavior in SDS gels or carries other post-translational modifications.

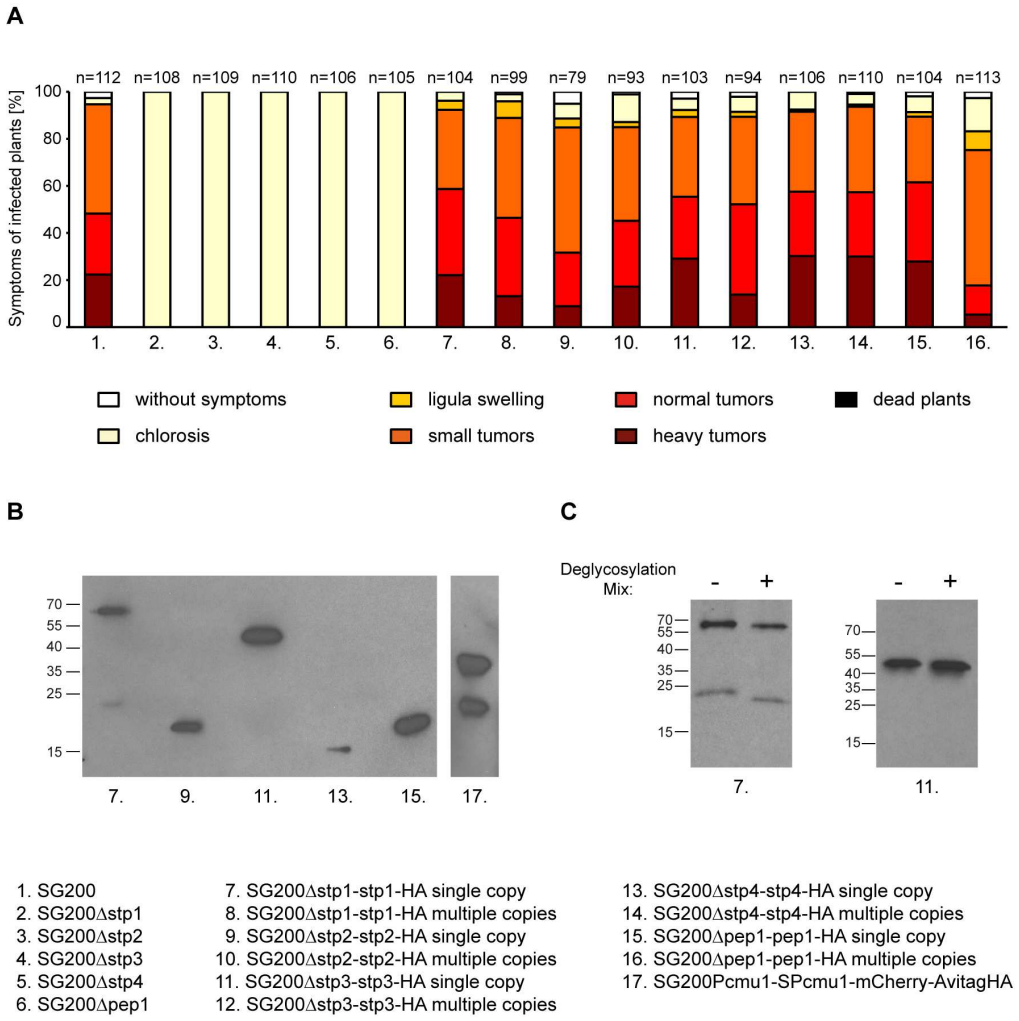


**Figure 2.9: Biological activity of HA fusion strains of essential effectors and integrity in infected tissue.** (A) Plants were infected with the strains listed under 1-16. Plants were assessed for disease symptoms at 12 dpi and depending on their strongest symptom assigned to a disease category. The color code for the symptom categories is given underneath the graph. The infections were conducted in three biological replicates and average values are expressed as percentage of the total number of infected plants (n), shown above each column. (B) Immunoprecipitation of HA-tagged essential effectors. The respective fusion proteins were immunoprecipitated from soluble protein extracts from maize tissue infected with indicated *U. maydis* strains listed under 1-17 and analyzed via an anti-HA western blot. Plant material was harvested at 3 dpi. Numbers on the left indicate the size in kDa. (C) Deglycosylation of Stp1-HA and Stp3-HA. The respective fusion proteins were immunoprecipitated from soluble protein extracts from maize tissue infected with the respective *U. maydis* strain and subsequently treated with either the deglycoslylation mix (+) or mock (-) and analyzed via an anti-HA western blot. Numbers on the left indicate sizes in kDa.

### 2.5.2 Stp effector proteins can be secreted

To experimentally prove the secretion of the Stp effectors, they were C-terminally HA-tagged and fused to a constitutive promoter and integrated into the *ip* locus of the AB33 strain. The strain AB33 can be induced to filament by shifting the cells from ammonium-containing medium to nitrate-containing medium (Brachmann *et al.*, 2001). After shifting the cells for six hours, supernatant was collected and proteins were TCA-precipitated and subjected to western blot analysis in parallel with an analysis of the cell pellet. The full-length version of Stp2, Stp3 and Stp4 could be detected in supernatants as well as in the pellet fractions (Figure 2.10). In both, the molecular weight of Stp4 was higher than predicted and several high molecular weight forms were detected. No signal was observed for control strain AB33. Furthermore, the presence of tubulin was used as a cytoplasmic marker to exclude the possibility that the detected signals were due to cell lysis. Western blot analysis of the proteins revealed that tubulin could only be detected in the cell pellet and was absent from the supernatant of the samples. Since secretion was previously shown for constitutive expressed Stp1-HA and Pep1-HA (Doehlemann *et al.*, 2009; Schipper, 2009), it can be concluded that the five essential effectors can be secreted and carry a functional secretion signal.

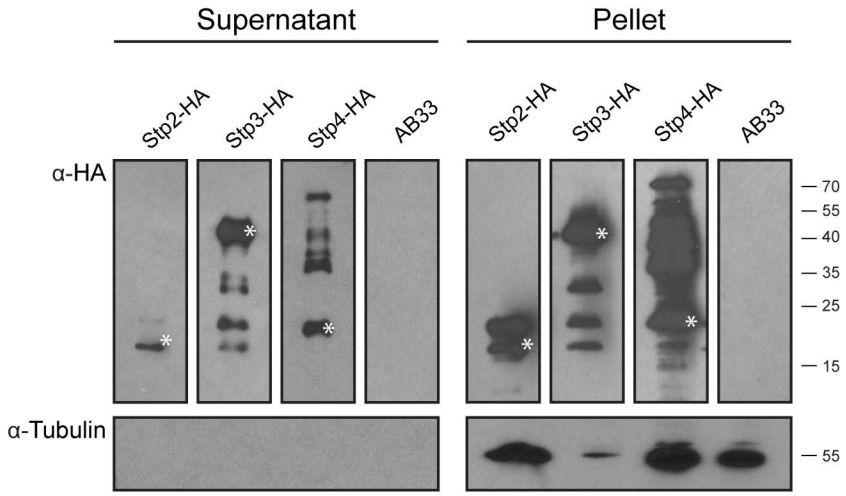


**Figure 2.10: Secretion of Stp2, Stp3 and Stp4.** Western blot analysis of the secreted effectors in the supernatant as well as in the pellet of the AB33-derived strains in which Stp2-HA, Stp3-HA and Stp4-HA are expressed from a constitutive promoter using anti-HA antibodies. Detection of tubulin via an anti-tubulin antibody served as a lysis control. Effector proteins of the expected size are marked. No signal was observed for control strain AB33. Proteins of the expected size are marked with an asterisk. Numbers on the right indicate sizes in kDa.

### 2.5.3 Stp effector proteins are secreted during biotrophic development

In order to visualize the essential effectors *in planta*, the effectors were C-terminally fused to mCherry-HA under the control of their respective native promoters into the *ip* locus of the respective deletion strain. The functionality of these alleles was confirmed by plant infections. In all cases, disease symptoms similar to SG200 were observed (Supplementary Figure S3A). Additionally, the integrity of the fusion proteins was tested by western blot analysis, using total cell lysates from plant material harvested at 3 dpi. This revealed proteins with the expected sizes for the full-length fusion proteins. In addition, two smaller fragments were detected, which were most likely cleaved mCherry and a smaller, C-terminal degradation product (Supplementary Figure S3B).

The apoplastic effector Pit2 served as the secretion control (Mueller *et al.*, 2013). The localization of the fusion proteins was observed at 2 dpi using confocal microscopy. Intracellularly growing hyphae of all strains were surrounded by the mCherry fluorescence signal, which in particular accumulated at the hyphal tips in which secretion occurs (Figure 2.11). A strong signal could also be detected at cell-cell passages, where it could be seen diffusing into the apoplast away from the fungal hyphae (Figure 2.11J). Pit2-mCherry showed a rather uniform distribution around the biotrophic hyphae (Figure 2.11M and N) whereas Stp1-, Stp3-, Stp4- and Pep-mCherry all showed a spotted pattern (Figure 2.11A, B, F, G, H, I, K, L). The cross section of the Stp1-mCherry hyphae in Figure 2.11B indicates that speckles appear to reside on the surface of the hyphae. Stp2-mCherry distribution appeared intermediate, also depicting these speckled structures. However, a smoother distribution was found in other parts (Figure 2.11D and E). It is currently unclear, whether this reflects a different distribution or is caused by the high amount of potentially free mCherry, which is cleaved off this fusion protein (Supplementary Figure S3B). These observations indicate that essential effector fusion proteins are secreted from biotrophic hyphae.

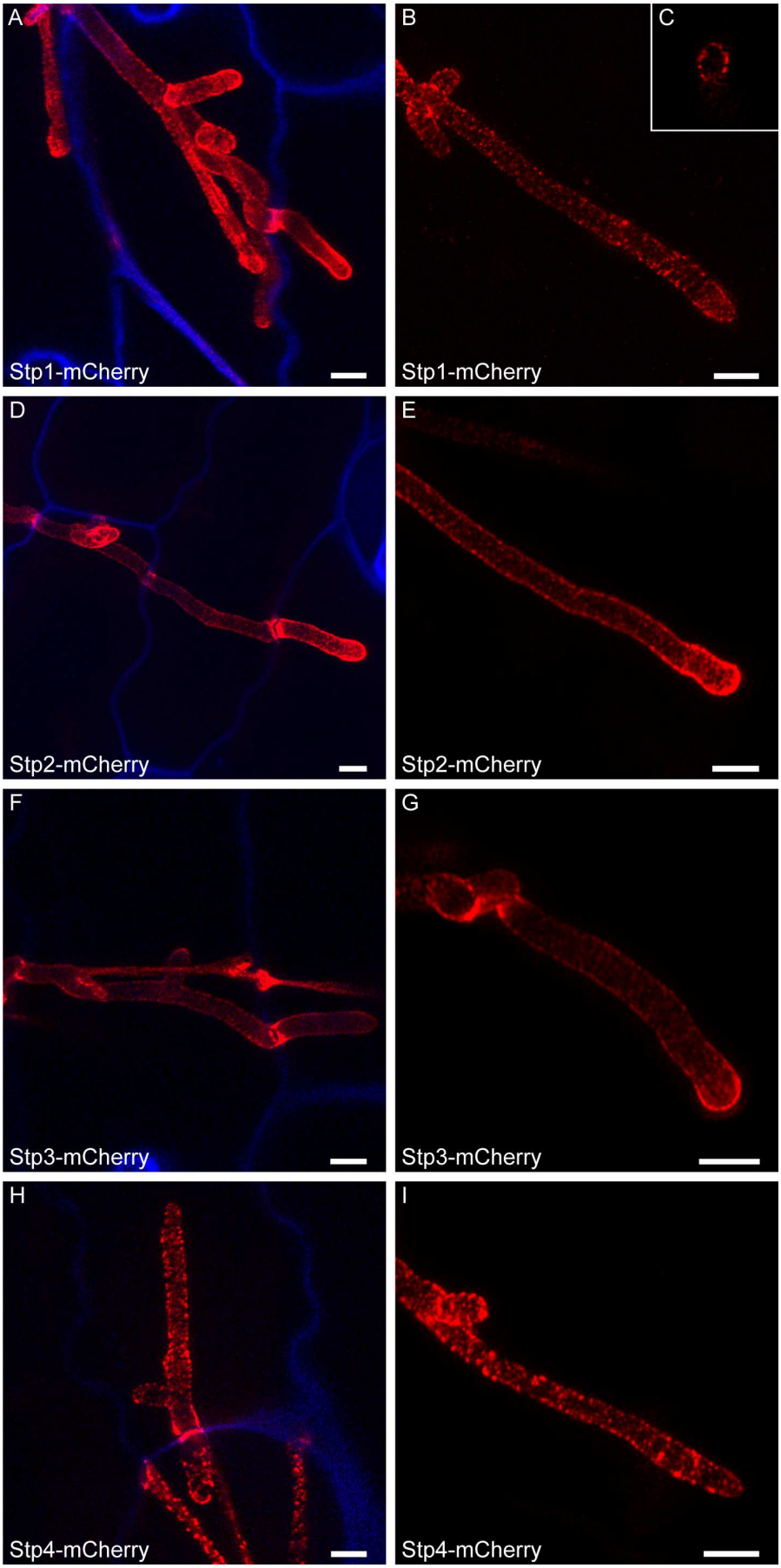
A
Stp1-mCherry
B
C
Stp1-mCherry
D
Stp2-mCherry
E
Stp2-mCherry
F
Stp3-mCherry
G
Stp3-mCherry
H
Stp4-mCherry
I
Stp4-mCherry

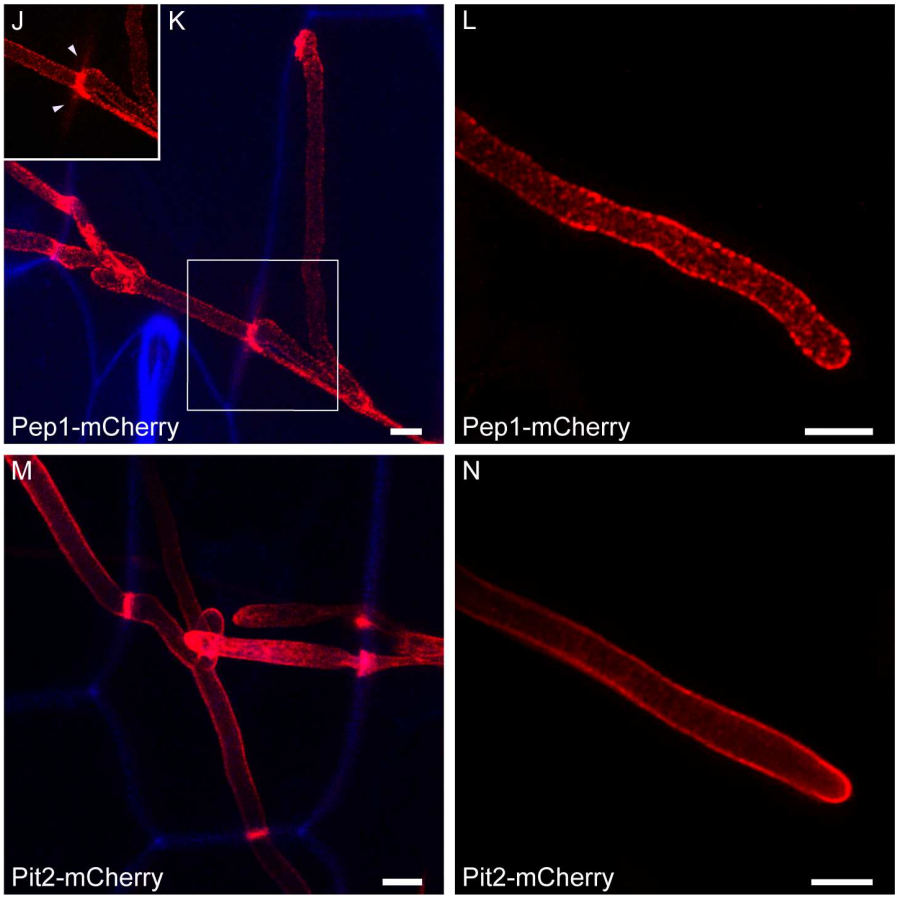


**Figure 2.11: Localization of essential effector-mCherry fusion proteins during biotrophic development.** Maize seedlings infected with the indicated *U. maydis* strains were observed at 2 dpi by confocal microscopy. Confocal pictures show an overlay of mCherry signal (red) and UV-laser-induced cell wall autofluorescence (blue). (J) Cell-cell passage without UV-laser-induced cell wall autofluorescence. White arrows point at mCherry signal spreading from the fungal hyphae. The scale bar represents 5 $\mu$m.

### 2.5.4 Stp effector proteins diffuse freely in the apoplast

To test whether the essential effectors localize at the plant plasma membrane, the fungal cell wall or the apoplastic space, the apoplast was enlarged by inducing plasmolysis. As it was previously demonstrated for Stp1-mCherry and Pep1-mCherry (Doehlemann *et al.*, 2009; Schipper, 2009), the mCherry fusion proteins showed an even distribution in the enlarged apoplastic space (Figure 2.12).

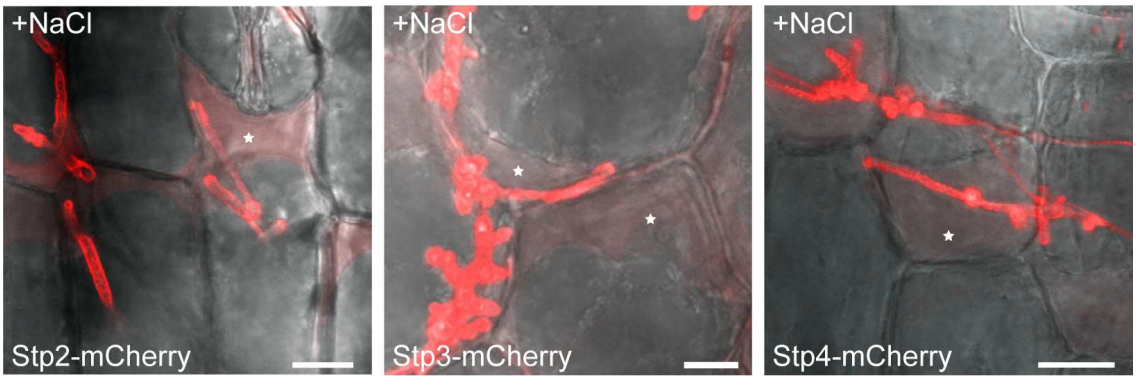


**Figure 2.12: Secretion of mCherry fusion proteins into the maize apoplast.** Maize seedlings infected with the indicated *U. maydis* strains were observed at 4 dpi by confocal microscopy. Confocal pictures show an overlay of mCherry signal (red) and bright-field projection (grey). Plasmolysis was induced by 1 M NaCl and the resulting enlarged apoplastic spaces are indicated by white stars. Pictures are maximum projections of confocal z-stacks. The scale bar represents 10 $\mu$m.

These observations indicate that Stp2, Stp3 and Stp4 were secreted by the fungus and diffuse freely in the apoplast. However, there was still a significant amount of signal surrounding the hyphae, making it unclear whether the effectors were still attached to the hyphae or whether the plant plasma membrane just did not detach properly.

To investigate this, the maize line ZmPIN1a-YFP was used, which expresses a YFP-tagged version of the PIN1a protein that locates to the plant plasma membrane (Gallavotti *et al.*, 2008). When these plants were infected with the strains expressing the Pit2-mCherry and Stp3-mCherry fusion strains, a tight encasement of the fungal hyphae by the plant plasma membrane could be observed (Figure 2.13A). As could be observed for a penetrating Stp3-mCherry hyphae, the YFP (yellow fluorescent protein) signal from the plasma membrane began right underneath the appressorium, simultaneously with Stp3-mCherry secretion (Figure 2.13B).

After inducing plasmolysis in ZmPIN1a-YFP plants infected with SG200Pit2-mCherry, a mCherry signal could be observed in the enlarged apoplastic space. The apoplast could be clearly identified due to the network-like structure and fine strands in the periplasmic space. These so-called Hechtian strands link the protoplast to the inner side of the cell wall of plasmolyzed cells (Giraldo and Valent, 2013). Even though plasmolysis is induced and the plant plasma membrane is detached from the cell wall, it still remains, at least

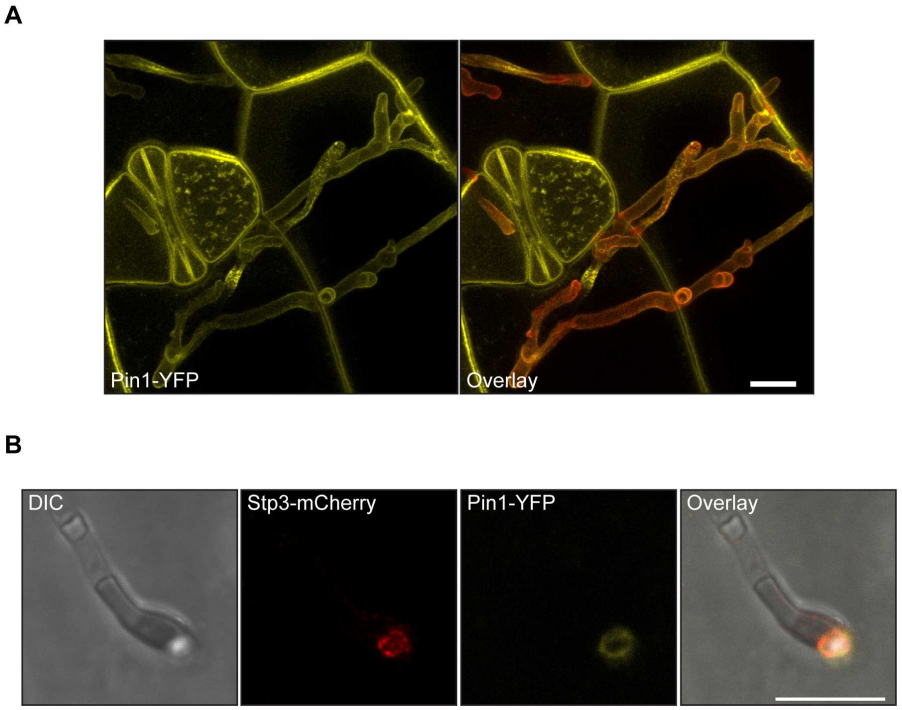


**Figure 2.13: Microscopy of intracellularly growing *U. maydis* hyphae.** (A) ZmPIN1a-YFP seedlings infected with SG200Pit2-mCherry were observed at 2 dpi by confocal microscopy. Confocal pictures show Pin1a-YFP signal (yellow) on the left or an overlay of mCherry (red) and Pin1a-YFP signals on the right. Pictures were kindly provided by S. Reißmann. (B) ZmPIN1a-YFP seedlings infected with SG200 Stp3-mCherry were observed at 1 dpi by confocal microscopy. Confocal pictures show DIC bright-field (grey), Stp3-mCherry (red), PIN1a-YFP (yellow) and an overlay of those channels. Pictures are maximum projections of confocal z-stacks. The scale bar represents 10 $\mu$m.

partially, attached to the fungus (Figure 2.14). This observation indicates that there is a very tight attachment between the plant plasma membrane and the fungus.

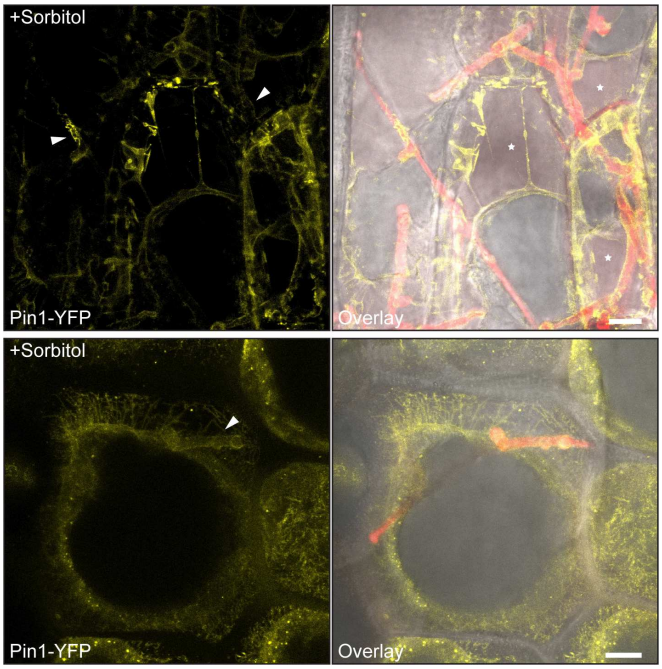


**Figure 2.14: Microscopy of intracellularly growing *U. maydis* hyphae in ZmPIN1a-YFP plants after plasmolysis.** ZmPIN1a-YFP seedlings infected with SG200Pit2-mCherry were observed at 2 dpi by confocal microscopy. Confocal pictures show Pin1a-YFP signal (yellow) on the left or an overlay of mCherry (red) and Pin1a-YFP signals on the right. Plasmolysis was induced by 1 M Sorbitol and the resulting enlarged apoplastic spaces are indicated by white stars. White arrows indicate plant plasma membrane attachment sites. Pictures are maximum projections of confocal z-stacks. The scale bar represents 10 $\mu$m. Pictures were kindly provided by S. Reißmann.

### 2.5.5 Stp effector proteins are not translocated into the plant cell

Due to the limitations of microscopy-based approaches, a biochemical assay was conducted to investigate the translocation of secreted effectors Stp2, Stp3 and Stp4. The assay utilizes transgenic maize lines that express the bacterial biotin ligase BirA in their cytoplasm. BirA has the ability to biotinylate any protein that has a short peptide termed the Avitag. Effectors tagged with an Avitag are biotinylated in case of translocation into the cytoplasm and can then be immunoprecipitated from infected leaves of the BirA plants using streptavidin beads (Lo Presti *et al.*, 2016). In addition to the Avi-HA-tagged Stp2, Stp3 and Stp4, the generated strains expressed the Avi-HA-tagged cell wall-bound invertase Suc2. Suc2 serves as an internal negative control for biotinylation that might occur during cell lysis. Virulence, which is indicative of the fusion proteins, was confirmed through infection assays (Supplementary Figure S4). Infected leaves were harvested at 3 dpi and proteins from the lysate were immunoprecipitated with HA-coated magnetic beads in order to ensure protein expression during infection and with streptavidin (Strp)-coated magnetic beads to detect the potentially biotinylated proteins. Samples were subsequently analyzed via western blot analysis. When BirA plants were infected with

strains expressing either Stp2-AvitagHA, Stp3-AvitagHA or Stp4-AvitagHA, protein expression could be detected but biotinylation was not observed (Figure 2.15A).

To rule out the possibility that Stp2-AvitagHA, Stp3-AvitagHA and Stp4-AvitagHA were not biotinylated due to the inaccessibility of their Avitag, the assay was repeated promoting biotinylation of proteins during the cell lysis. In the subsequently developed western blots, biotinylation of Suc2-AvitagHA as well as Stp2-AvitagHA, Stp3-AvitagHA and Stp4-AvitagHA could be observed, indicating that all of them can be biotinylated (Figure 2.15B). This experiment provided strong evidence that Stp2, Stp3 and Stp4 are not translocated into the plant cell, but rather act outside the plant cell. This is in agreement with what was observed for Stp1-AvitagHA and Pep1-AvitagHA (Lo Presti *et al.*, 2016).

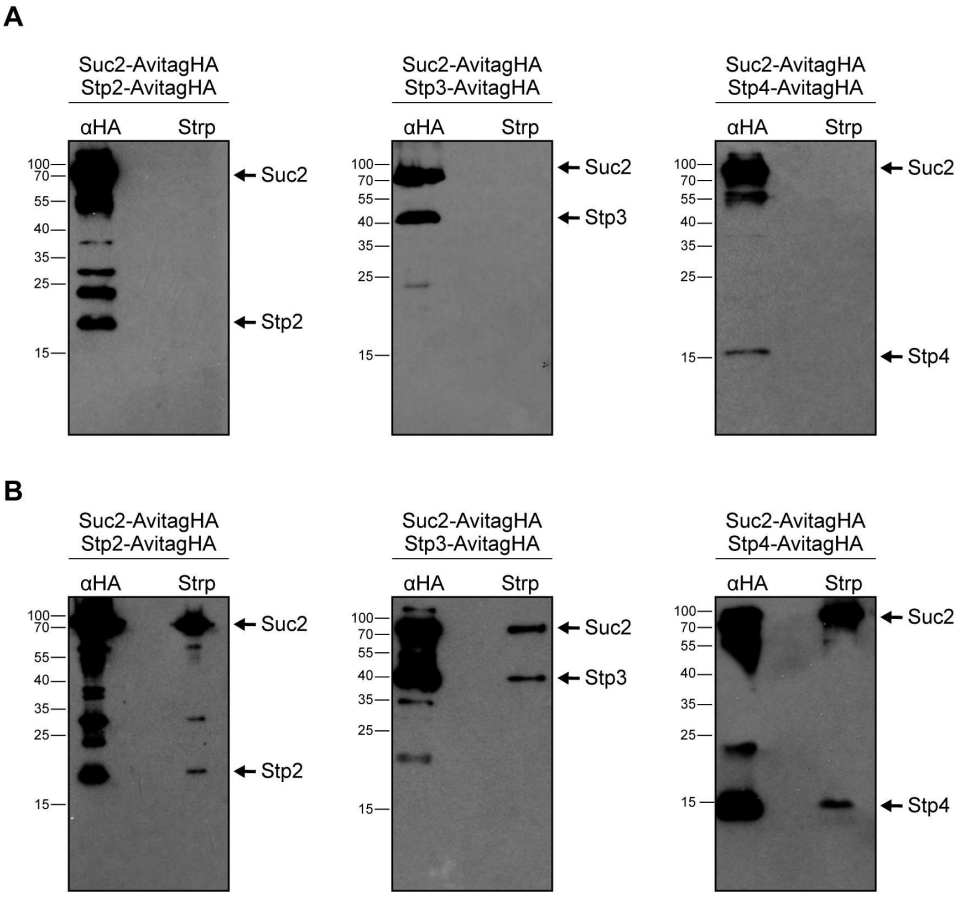


**Figure 2.15: BirA-based translocation assay for Stp2, Stp3 and Stp4.** (A) Seven-day-old BirA maize seedlings were infected with the indicated strains. At 3 dpi, plant lysates were either immunoprecipitated with HA-coated magnetic beads or with streptavidin-coated magnetic beads and analyzed via anti-HA western blot. (B) The assay was repeated as described in A while promoting biotinylation of proteins during cell lysis. Numbers on the left indicate sizes in kDa.

### 2.5.6 Localization of Stp3-HA reveals an association with membranous structures

To obtain an independent assessment for the localization of Stp3, an immuno-transmission electron microscopy (Immuno-TEM) approach was implemented in cooperation with K. Snetselaar (Saint Joseph's University, PA, USA). It was only possible to label Stp3-HA on fungal filaments residing in plant cells that were cut open during the sample preparation. This observation indicates that the cytoplasm including the plant plasma membrane leaked out making the epitope accessible. However, these preliminary results imply that Stp3-HA localizes in membranous protrusions, which appear to originate from the fungal hyphae and extend into the plant tissue (Figure 2.16A). At this point it is unclear whether Stp3-HA localizes exclusively at the tip of these protrusions or if its further spread is limited.

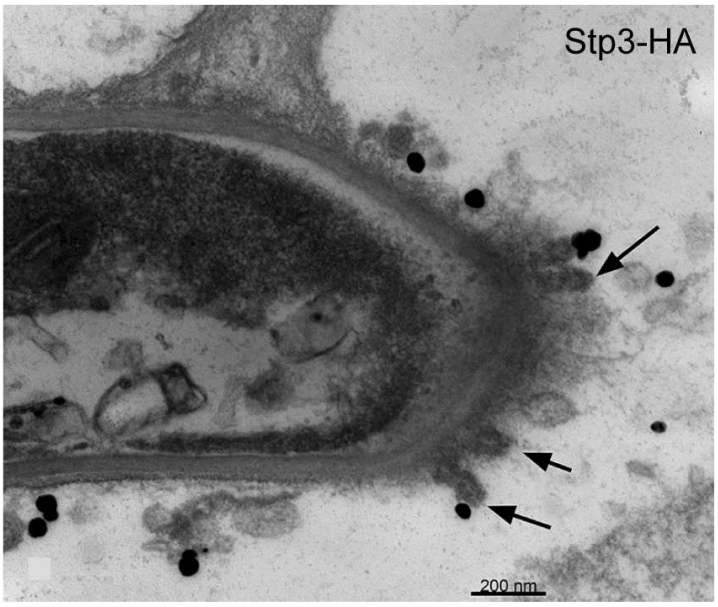


**Figure 2.16: Immuno-transmission electron microscopy of maize tissue infected with strains expressing Stp3-HA.** Arrows indicate membranous protrusions. Scale bar as indicated. These preliminary results were generated and were kindly provided by K. Snetselaar (Saint Joseph's University, PA, USA).

## 2.6 Identification of interaction partners for Stp effector proteins

To obtain clues about the processes affected by pathogen effectors, it is common practice to identify interacting plant protein. To find plant interactors of Stp2, Stp3 and Stp4, a mass spectrometry-based proteomics approach was conducted using all essential effectors as bait proteins.

### 2.6.1 Stp1, Stp3, Stp4 and Pep1 form a complex

To generate material for the immunoprecipitation, plants were infected with SG200Δstp1-stp1-HA, SG200Δstp2-stp2-HA, SG200Δstp3-stp3-HA, SG200Δstp4-stp4-HA and SG200 Δpep1-pep1-HA expressing a single HA-tagged copy. SG200Pcmu1-Spcmu1-mCherry-HA infected plants served as negative control. Plant material was harvested at 3 dpi. Samples were analyzed by liquid chromatography tandem mass spectrometry (LC-MS/MS) in collaboration with T. Glatter (Max Planck Institute for Terrestrial Microbiology). Instead of finding interacting plant proteins as expected, Stp1, Stp3, Stp4 and Pep1 were found to interact (Table 2.3). The interaction between these four effectors was observed by individually using each of them as bait protein. Interestingly, Stp2 did not interact with any of the four other effectors, irrespective of whether Stp1-HA, Stp3-HA, Stp4-HA or Pep1-HA were used as bait and Stp2-HA failed to co-precipitate any of the four other effectors. These findings of an effector complex consisting of Stp1, Stp3, Stp4 and Pep1, were confirmed in three biological replicates. Secreted mCherry-HA showed no interaction with any of the essential effectors. The interaction between the four effector proteins was initially shown for a strain with multiple integrations of Stp1-HA (L. Liang, personal communication).

Repeating the experiment including SG200Δstp2-stp2-HA and SG200Δstp3-stp3-HA strains with multiple copies of Stp2-HA and Stp3-HA, showed that overexpressing one member did not influence complex formation (Supplementary Table S6). This surprising result again indicates that a plant target for these essential effector proteins most likely does not exist. These experiments also failed to detect POX12 peroxidase, the published apoplastic target for Pep1 (Hemetsberger *et al.*, 2012).

**Table 2.3:** Total spectrum counts of unique peptides for respective proteins are shown for three biological replicates (I, II, III). Secreted mCherry-HA served as negative control. Proteins with confirmed interactions are indicated by colored background.

| Protein / Peptides | Stp1-HA | | | Stp2-HA | | | Stp3-HA | | | Stp4-HA | | | Pep1-HA | | | mCherry-HA | | |
|---|---|---|---|---|---|---|---|---|---|---|---|---|---|---|---|---|---|---|
| | I | II | III | I | II | III | I | II | III | I | II | III | I | II | III | I | II | III |
| Stp1 | 18 | 77 | 65 | 0 | 0 | 0 | 6 | 41 | 13 | 11 | 28 | 21 | 5 | 27 | 17 | 0 | 0 | 0 |
| Stp2 | 0 | 4 | 0 | 2 | 13 | 0 | 0 | 1 | 0 | 0 | 6 | 0 | 0 | 2 | 0 | 0 | 0 | 0 |
| Stp3 | 0 | 40 | 27 | 0 | 0 | 0 | 1 | 20 | 9 | 2 | 25 | 13 | 3 | 22 | 11 | 0 | 0 | 0 |
| Stp4 | 0 | 18 | 6 | 0 | 0 | 0 | 3 | 6 | 1 | 5 | 19 | 7 | 3 | 10 | 4 | 0 | 0 | 0 |
| Pep1 | 1 | 37 | 21 | 0 | 0 | 0 | 5 | 24 | 6 | 4 | 19 | 10 | 3 | 19 | 12 | 0 | 0 | 0 |
| mCherry | 0 | 0 | 0 | 0 | 0 | 0 | 0 | 0 | 0 | 0 | 1 | 0 | 0 | 0 | 0 | 57 | 105 | 132 |

### 2.6.2 Stp2 interacts with two other essential *U. maydis* effectors

In addition to not being part of the Stp1, Stp3, Stp4 and Pep1 effector complex, Stp2 also did not consistently interact with a specific plant protein. However, recent CO-IP/MS experiments using extracts from SG200Δstp2-stp2-HA revealed that Stp2 seems to be interacting with three other *U. maydis* proteins (Table 2.4). Mutants of the putative effectors *UMAG_01695 (pst1)* and *UMAG_04342 (stp5)* have the same apathogenic phenotype as the other five essential effectors (Vranes, 2006) (P. Happel, personal communication). The deletion of the third interactor *UMAG_06315*, a secreted protein with two predicted transmembrane domains, did not have an influence on virulence (J. Kämper, personal communication). Due to their related expression pattern and phenotype, it is very likely that Stp2, Pst1 and the novel effector Stp5 form another effector complex (Supplementary Figure S5).

**Table 2.4:** Total spectrum counts of unique peptides for respective proteins are shown for three biological replicates (I, II, III). mCherry-HA was used as negative control.

| Protein / Peptides | Stp2-HA | | | mCherry-HA | | |
|---|---|---|---|---|---|---|
| | I | II | III | I | II | III |
| Stp2 | 2 | 13 | 2 | 0 | 0 | 0 |
| Pst1 | 16 | 69 | 14 | 0 | 0 | 0 |
| Stp5 | 7 | 20 | 2 | 0 | 0 | 0 |
| UMAG_06315 | 2 | 49 | 6 | 0 | 4 | 1 |
| mCherry | 0 | 0 | 0 | 57 | 105 | 52 |

## 2.7 Visualization of the effector complex

To visualize the complex, validate the interaction of its members and see where the effectors co-localize, bimolecular fluorescence complementation (BiFC) was attempted by tagging the effectors with half- as well all the full-length versions of fluorescent proteins.

### 2.7.1 The formation of the effector complex is critical for the pathogenic development of *U. maydis*

BiFC is based on the reconstitution of two non-fluorescent fragments of a fluorescent protein *in vivo*. Upon interaction, these will form a fluorescent complex whose signal can be visualized by confocal microscopy. For this purpose, Stp1 was tagged C-terminally with the N-terminal part of YFP, whereas Stp3 was tagged C-terminally with the C-terminal part of YFP. Tagging was done at the endogenous loci of both genes in the same strain. Control strains were generated in which only one of the effectors was tagged with either full-length YFP or the C-or-N-terminal half of YFP. The control strains SG200stp1-YFP, SG200stp3-YFP and SG200pep1-YFPC induced virulence symptoms similar to SG200, whereas SG200stp1-YFPN and SG200stp3-YFPC showed reduced virulence (Figure 2.17). However, the strain SG200stp1-YFPC stp3-YFPN was unable to cause disease and arrested right after penetration, comparable to the *stp* deletion strains. No YFP signal could be observed by fluorescent microscopy (Supplementary Figure S6). Strains in which the tags were switched to SG200stp1-YFPN stp3-YFPC were also unable to cause disease (Figure 2.17). In the strain SG200stp4-YFPN pep1-YFPC, which co-expressed the other two complex members, all virulence was abolished (Figure 2.17). It is either simultaneous modification of two complex members with large tags or the association of the split YFP parts that interferes with pathogenic development.

In the next step, strains expressing Stp1-YFPC and Stp3-YFPN in the SG200 background were created. In these strains, all four complex members were present and the two tagged genes were additionally incorporated into the *ip* locus. Stp1-YFPC and Stp3-YFPN were inserted in single, double and multiple copies. While the strains with single and double copies showed slightly reduced virulence symptoms in comparison to SG200, the strains with multiple and especially the one with a very high number of additional copies was severely attenuated in virulence (Figure 2.18A). Even though the latter strain still showed the formation of tumors, these were so small that they could be rather felt by touch than seen by eye (Figure 2.18B). This dominant negative phenotype is strong evidence that not only the presence of complex members is important, but that the formation of the complex is critical for pathogenic development of *U. maydis*.

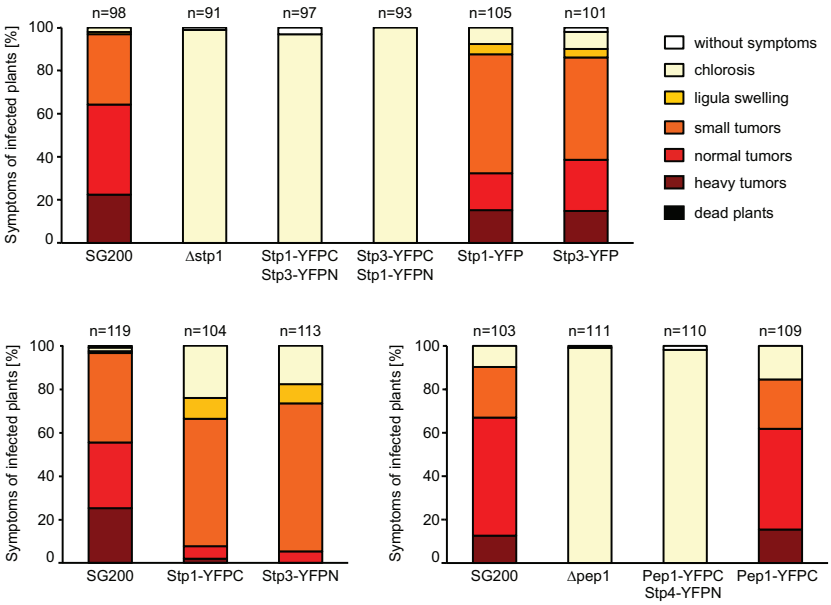


**Figure 2.17: Virulence of strains expressing effector complex members with large tags.** Plants were infected with the indicated *U. maydis* strains and assessed for disease symptoms at 12 dpi. Depending on their strongest symptom they were assigned to a disease category. The color code for the symptom categories is given on the top right. The infections were conducted in three biological replicates and average values are expressed as percentage of the total number of infected plants (n), shown above each column. Infection with SG200stp4-YFPN pep1-YFPC was done by D. Aßmann.

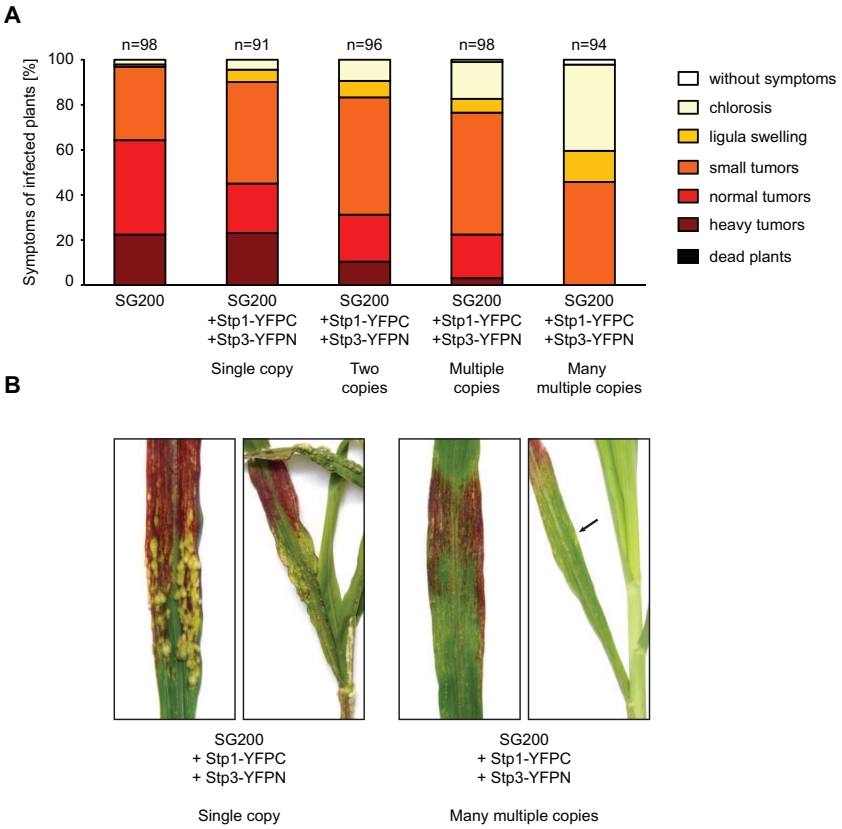


**Figure 2.18: Virulence of SG200 with additional Stp1-YFPC and Stp3-YFPN copies.** (A) Plants were infected with the wild type SG200 and SG200stp1-YFPC stp3-YFPN strains carrying single, double, multiple and many multiple integrations of Stp1-YFPC and Stp3-YFPN. Plants were assessed for disease symptoms at 12 dpi. Depending on their strongest symptom they were assigned to a disease category. The color code for the symptom categories is given on the right. The infections were conducted in three biological replicates and average values are expressed as percentage of the total number of infected plants (n), shown above each column. (B) Representative leaves of infections with SG200stp1-YFPC stp3-YFPN with single and many multiple integrations of Stp1-YFPC and Stp3-YFPN at 12 dpi. Arrow indicates small tumor.

## 2.7.2 Stp1 and Stp3 co-localize

To test whether simultaneously tagging two complex members with large tags interferes with the complex formation or whether it is the ability of the YFPN and YFPC tags to associate, a strain was generated, in which Stp1 was tagged with full-length YFP and Stp3 was tagged with full-length mCherry in locus. Compared to SG200, the strain SG200stp1-YFP stp3-mCherry showed reduced disease symptoms, but did not show the deletion phenotype (Figure 2.19A). When visualized by fluorescent microscopy, both Stp1YFP and Stp3mCherry showed the speckled structures around the hyphae (Figure 2.19B). Combining the two fluorescent channels revealed that the signals co-localize in these structures.

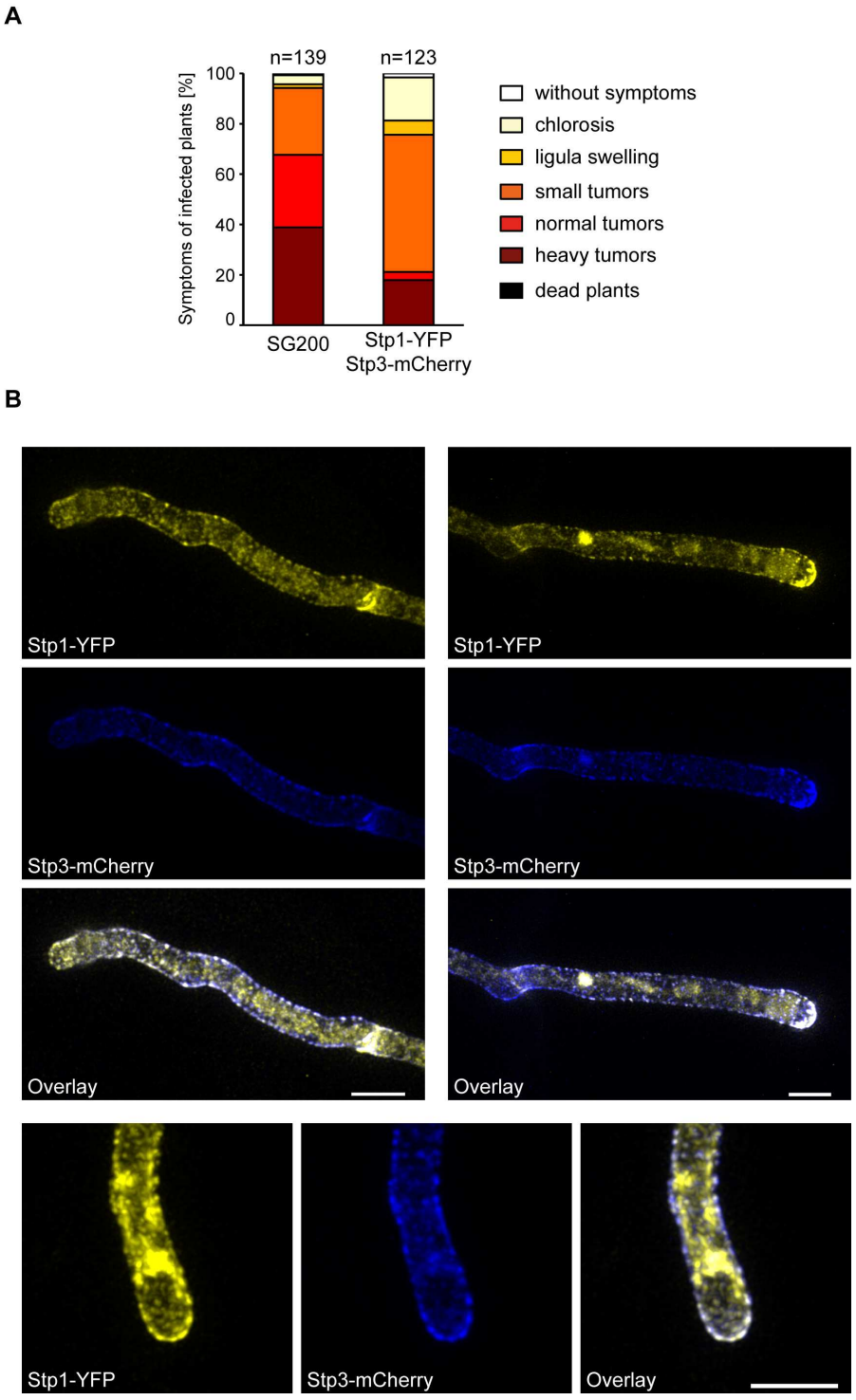


**Figure 2.19: Co-localization of Stp1-YFP and Stp3-mCherry during biotrophic development.** (A) Plants were infected with the wild type SG200 and SG200stp1-YFP stp3-mCherry and assessed for disease symptoms at 12 dpi. Depending on their strongest symptom they were assigned to a disease category. The color code for the symptom categories is given on the right. The infections were conducted in three biological replicates and average values are expressed as percentage of the total number of infected plants (n), shown above each column. (B) Maize seedlings infected with SG200stp1-YFP stp3-mCherry were observed at 3 dpi by confocal microscopy. Confocal pictures are showing the fluorescent signals of Stp1-YFP (yellow) and Stp3-mCherry (blue). An overlay of the two fluorescent channels is indicated in each subfigure. At locations where Stp1-YFP and Stp3-mCherry overlap the fluorescent signal appears white. Pictures are maximum projections of confocal z-stacks. The scale bar represents 10 $\mu$m.

## 2.8 Interaction studies of effector complex members in *Saccharomyces cerevisiae*

To investigate whether individual complex members interact directly or indirectly, a yeast two-hybrid (Y2H) system was used, where effector complex members were tested for binary, ternary and quaternary interaction.

### 2.8.1 Pairwise interaction between complex members

The *stp1*, *stp3*, *stp4* and *pep1* genes were cloned into both the bait vector pGBKT7 and the prey vector pGADT7, generating in-frame fusions with the gene encoding the yeast GAL4 binding (BD) and activation domain (AD), respectively. After co-tranformation, reporter gene transcription is activated if the two fusion proteins interact in the yeast nucleus. The *S. cerevisiae* strain AH109 harbors the reporter genes *ADE2* and *HIS3*, which encode for two enzymes that are crucial for adenine and histidine biosynthesis and thereby enable nutritional selection as a read-out for the interaction between proteins (James *et al.*, 1996).

In the following experiments, growth on high-stringency medium (SD -Leu -Trp -Ade -His) was used to study the interaction between the complex members. Additionally, strains were also grown on low-stringency medium (SD -Leu -Trp) to confirm their viability. Expression of the fusion proteins was confirmed by analyzing total cell extracts via western blot using anti-HA (AD fusion proteins) and anti-myc (BD fusion proteins) antibodies. All experiments were done with three independent transformants to exclude false positives due to spontaneous mutations. When tested for autoactivation, BD-Stp4 showed an activation of the reporter genes and was therefore used exclusively when fused to the AD. Neither BD-Stp1, BD-Stp3 nor BD-Pep1 showed autoactivation (not shown). Testing strains containing all possible combinations of the four complex members revealed that all strains could grow on low-stringency plates. The yeast strains expressing AD-Stp3/BD-Stp1 and AD-Pep1/BD-Stp1 were able to grow on high-stringency plates, proving that there is direct interaction between the respective protein pairs. For AD-Stp4/BD-Stp1 expressing strains, growth could be observed on high-stringency plates, but appeared much weaker, suggesting a weaker, more transient interaction between Stp4 and Stp1. Combinations of AD-Stp3/BD-Pep1, AD-Stp4/BD-Stp3 and AD-Stp4/BD-Pep1 failed to provide for growth on high-stringency plates, indicating that there is no direct interaction between the respective protein pairs (Figure 2.20B). Except for Stp4, which was excluded because of autoactivation, the effector pairs showed the same results when AD and BD fused proteins were switched (not shown). All bait and prey proteins were expressed in the respective yeast strains (Figure 2.20A).

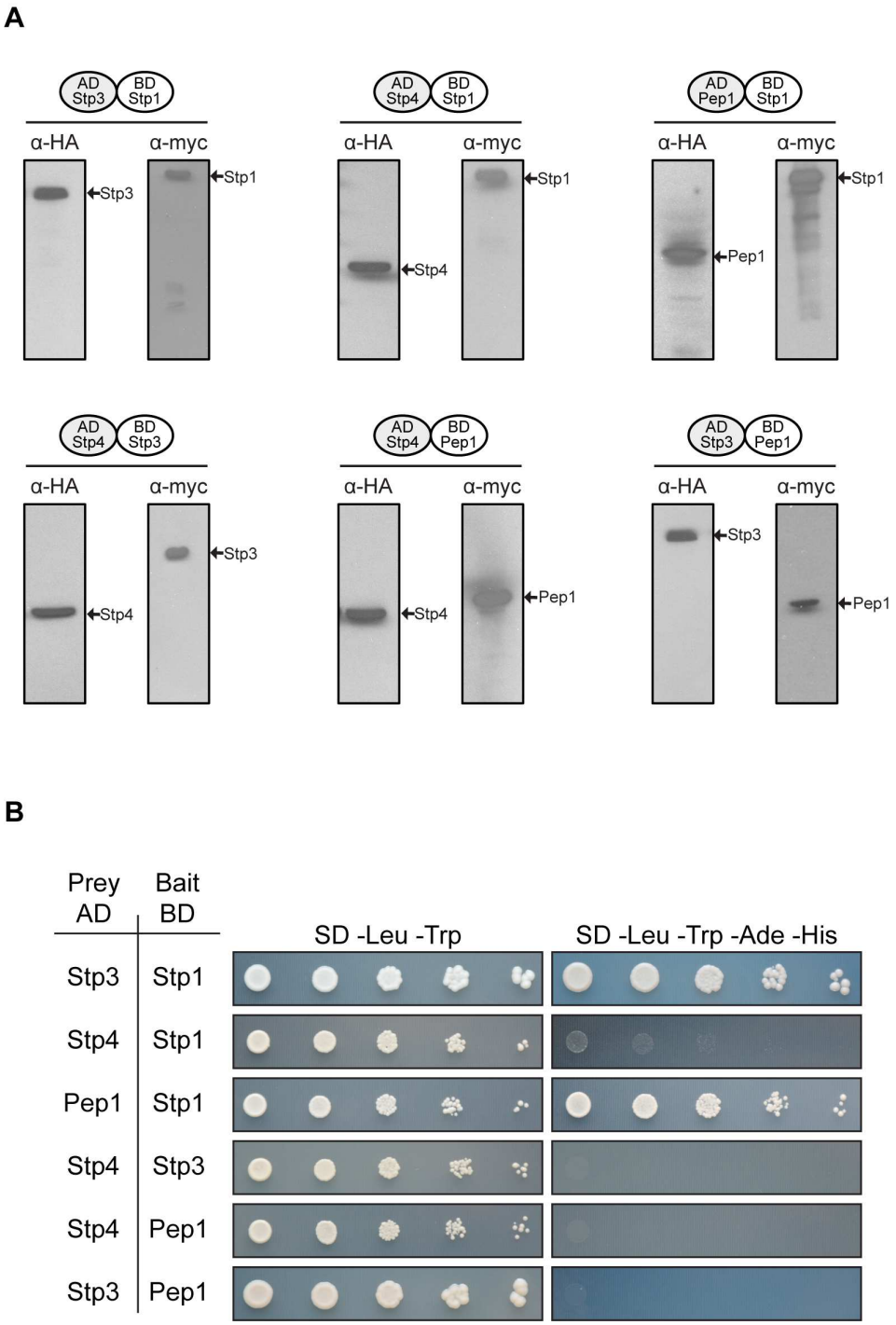


**Figure 2.20: Yeast Two-Hybrid analysis of pairwise interactions of effector complex members.** Potential interactions of the four effector proteins were tested in indicated pairwise combinations consisting of a bait plasmid (AD fused to the indicated complex member) and a prey plasmid (BD fused to the indicated complex member). (A) Total cell extracts were analyzed by immunoblotting using anti-HA antibodies for the AD fusion proteins and anti-myc antibodies for the BD fusion proteins. (B) Ten-fold dilutions series of AH109 yeast cells containing plasmids expressing the indicated proteins were spotted onto low-stringency medium (SD -Leu -Trp) and onto high-stringency medium (SD -Leu -Trp -Ade -His). Plates were incubated for 3 days at 28°C.

### 2.8.2 Stp1, Stp3, Stp4 and Pep1 form discrete ternary complexes

It has been shown that by introducing a third protein into the Y2H system, transcriptional activation can be promoted or induced if this protein provides a bridge between two proteins that did not interact or interact weakly (Sandrock *et al.*, 2001). Therefore, it was tested whether an additional complex member could increase interaction between the weakly interacting AD-Stp4/BD-Stp1 and the non-interacting effectors Stp3, Stp4 and Pep1.

To this end, both myc-Pep1 and myc-Stp3 were cloned into the vector pYEA and co-transformed with AD-Stp4/BD-Stp1. pYEA contains an *ADE2* nutritional marker allowing the selection on medium lacking adenine (Sandrock and Egly, 2001). The yeast strains expressing AD-Stp4/BD-Stp1/myc-Stp3 and AD-Stp4/BD-Stp1/myc-Pep1 showed full growth on both low (SD -Leu -Trp -Ade) and high (SD -Ade -His -Leu -Trp)-stringency plates (Figure 2.21). This demonstrates that the weak interaction between Stp1 and Stp4 is stabilized or strengthened when either Stp3 or Pep1 are present. In the pairwise Y2H analysis, the effectors Stp3, Stp4 and Pep1 have already been shown to directly interact with Stp1. To test whether Stp1 is essential for interaction between complex members, Stp3, Stp4 and Pep1 were co-transformed as AD-Pep1/BD-Stp3/myc-Stp4. All three proteins were expressed (Figure 2.21A) and growth could be observed on low and high-stringency plates (Figure 2.21B).

### 2.8.3 The reconstitution of the quaternary complex in yeast

To test whether yeast is suitable for the formation of the entire effector complex, a strain expressing all four complex members was generated. To allow a subsequent screen for a small molecule which inhibits complex formation, Wong *et al.* (2017) used a strain, in which nine ABC transporter-related genes are deleted, making it highly permeable. To prove that ABC9Δ behaves like its progenitor strain AH109 with regard to expressing the complex members, several representative Y2H interaction assays for complex members were conducted. In all cases, the results were the same as previously observed in the AH109 background (Supplementary Figure S7). Therefore, ABC9Δ expressing AD-Stp4/BD-Stp1/myc-Pep1 was used and myc-Stp3 was additionally expressed from the PYEA plasmid. The strain AD-Stp4/BD-Stp1/myc-Pep1/myc-Stp3 was able to grow on both high- and low-stringency plates (Figure 2.22A and B). Its formation was verified by a Co-IP/MS experiment in which the total lysate was incubated with HA-coated magnetic beads to immunoprecipitate the HA-tagged AD-Stp4. The strain AD-empty/BD-Stp1/myc-Pep1/myc-Stp3 was included as a control. Samples were analyzed by LC-MS/MS. The results showed an interaction between the four effector proteins. (Figure 2.22C).

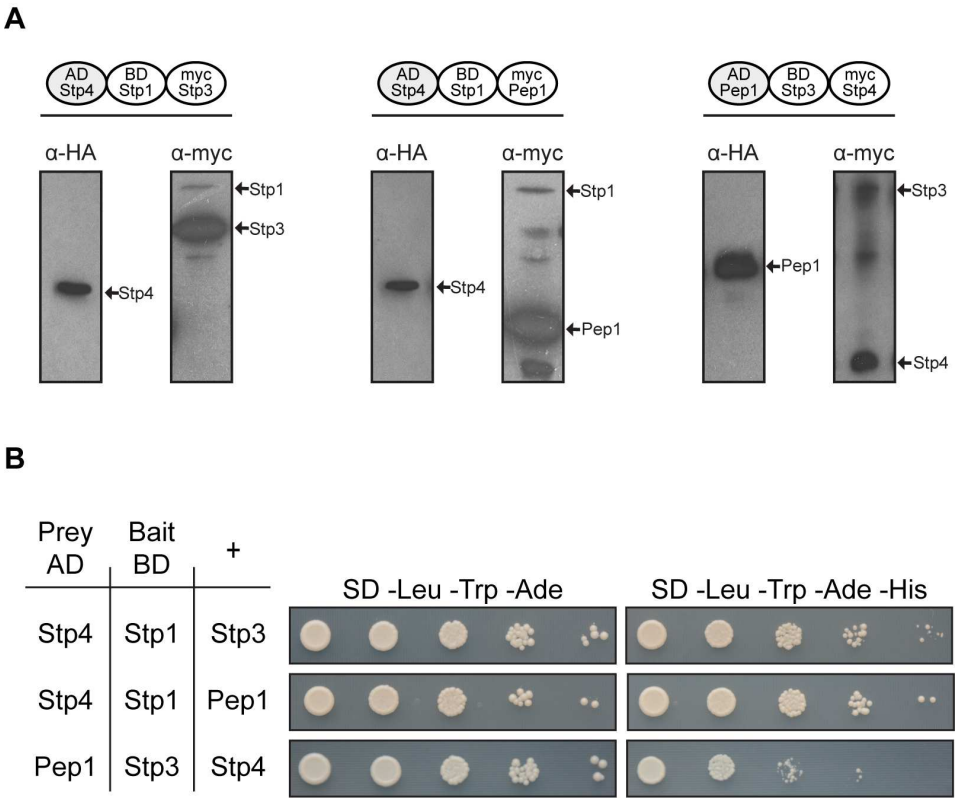


**Figure 2.21: Ternary complex formation by effectors revealed by yeast three-hybrid analysis.** Potential interactions of the four proteins were tested in indicated combinations. These consisted of a bait plasmid (AD fused to indicated complex member), a prey plasmid (BD fused to indicated complex member) and an additional plasmid carrying the gene sequence of the indicated complex member (+). (A) Total cell extracts were analyzed by immunoblotting using anti-HA antibodies for the AD fusion proteins and anti-myc antibodies for the BD fusion proteins and the additional myc-tagged protein (+). (B) Ten-fold dilutions of AH109 yeast cells containing the plasmids were spotted onto low-stringency medium (SD -Leu -Trp -Ade) and onto high-stringency medium (SD -Leu -Trp -Ade -His). Plates were incubated for 3 days at 28°C.

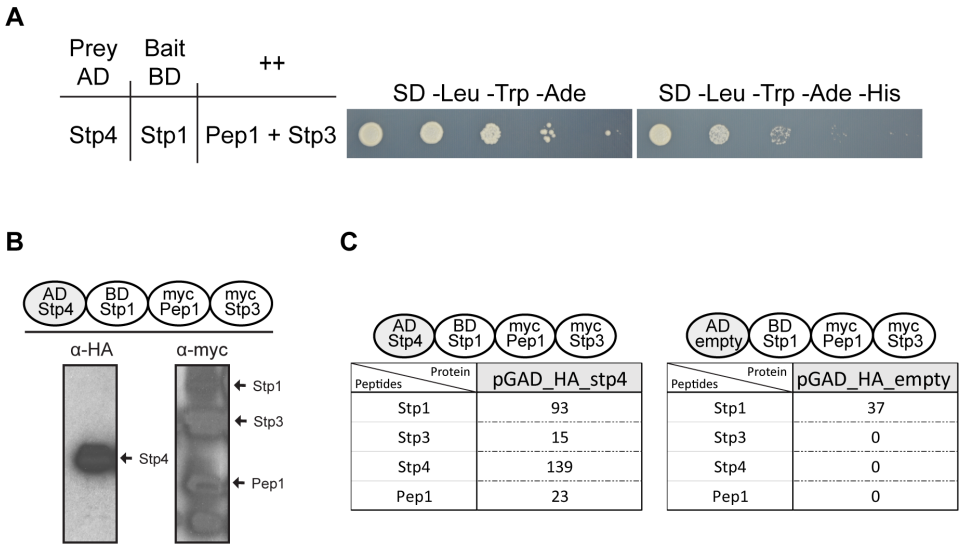


**Figure 2.22: Quaternary complex formation by effectors.** The interaction of all four complex members was tested with the strain ABC9Δ AD-Stp4/BD-Stp1/myc-Pep1/myc-Stp3. (A) Ten-fold dilutions of ABC9Δ yeast cells containing plasmids expressing the indicated proteins were spotted onto low-stringency medium (SD -Leu -Trp -Ade) and onto high-stringency medium (SD -Leu -Trp -Ade -His). Plates were incubated for 3 days at 28°C. (B) Total cell extracts were analyzed by immunoblotting using anti-HA antibodies for the AD fusion proteins and anti-myc antibodies for the BD fusion proteins and the additional myc-tagged proteins (++). (C) Co-immunoprecipitation reveals quaternary complex formation. Total cell lysates of strain ABC9Δ AD-Stp4/BD-Stp1/myc-Pep1/myc-Stp3 and the control strain AH109 AD-empty/BD-Stp1/myc-Pep1/myc-Stp3 were incubated with HA-coated magnetic beads to immuno-precipitate the HA-tagged protein at the activation domain. Samples were analyzed by LC-MS/MS by T. Glatter. Tables shows the total spectrum counts of unique peptides for the respective proteins. The experiment was done in one biological replicate.

# 3 Discussion

In this study, I identified three effectors whose deletion mutants were no longer able to cause disease. Deletion mutants of these three effectors, named *stp2*, *stp3* and *stp4* (stop after penetration) were still able to form appressoria and penetrate the plant, but arrested in the epidermal cell layer. The arrest was accompanied by plant defense responses, including a disruption of the plant plasma membrane surrounding the fungal hyphae. A similar phenotype was observed for the previously described effectors *stp1* and *pep1*. Co-IP/MS experiments using each of these essential effectors revealed that Stp1, Stp3, Stp4 and Pep1 form an effector complex. The four complex members did not interact with Stp2 or plant proteins. Recent experiments suggest that Stp2 interacts with at least two other *U. maydis* effectors, which have a virulence phenotype comparable to *stp2* deletion strains. Finally, I provided evidence that the formation of the complex itself and not just the presence of the individual complex members is necessary for a successful colonization.

## 3.1 The *stp* effector genes are essential for virulence

The three *stp* deletion mutants, *stp2*, *stp3* and *stp4*, did not exhibit any growth defects during their saprophytic phase and were unchanged in their ability to respond to osmotic, cell wall and oxidative stress. Furthermore, their ability to form filaments on charcoal-containing media was not impaired. Using live cell microscopy, the formation of appressoria and the penetration into the plant cell could be observed for all deletion mutants. With respect to appressorium formation and penetration, they behaved very similar to the *stp1* deletion strain, which has been shown to not have an appressorium formation or penetration defect (Schipper, 2009). The *stp* deletion strains arrested in growth in the epidermal cell layer. In rare cases, mutants were able to reach the mesophyll layer, but never exhibited any branching or clamp formation like SG200. Absence of a phenotype in axenic culture and the importance of the *stps* during the early biotrophic interaction phase matches with their expression pattern. The genes are not expressed in axenic culture and are induced upon plant contact. Previous studies have shown that the *stp* genes are among those, which are surface-cue-induced (Lanver *et al.*, 2014). Their highest expression coincides with onsetting biotrophic interaction.

Expression only after contact with the plant is a common feature of fungal effectors (Lo Presti *et al.*, 2016). Most functionally characterized fungal effectors manipulate the plant immune system (Selin *et al.*, 2016). One of the first plant defense responses upon sensing an intruder is the formation of cell wall appositions, so-called papillae. Papillae contain callose and often accumulate ROS (Voigt, 2014). A thin patch of callose was detected underneath the penetrating appressoria of SG200 and the *stp1*, *stp3* and *stp4* deletion strains. Invading hyphae of these strains were not inhibited growing through these patches, suggesting that they did not impose a barrier (Hemetsberger *et al.*, 2012). For the *pep1* deletion strain, a strong callose deposition was observed, which started around the penetration site and encased the entire intracellularly growing hyphae. Hyphal tips were not detected below these callose plugs, suggesting that callose was blocking hyphal growth. Such a phenotype was also observed after infection with *stp2* deletion mutants. Hemetsberger *et al.* (2012) have shown that formation of these papillae was also associated with a strong $H_2O_2$ accumulation. When silencing the peroxidase POX12, an apoplast interactor of Pep1, the plant defense reaction was much weaker. POX12 was initially identified in Doehlemann *et al.* (2009) as a gene that is significantly upregulated after infection with the *pep1* deletion strain in comparison to infections with SG200. This could be confirmed in this study, as the POX12-encoding gene was one of the genes that were upregulated after infection with the *pep1* deletion strain, but not after infection with the *stp1*, *stp2*, *stp3* and *stp4* deletion strains. Interestingly, among the ten genes that are uniquely upregulated in *stp2* mutants is another plant peroxidase, which is suspected to be involved in cell wall fortification (Kolattukudy *et al.*, 1992; Chen *et al.*, 2016). It will be interesting to find out, if this peroxidase is inhibited by Stp2. As Stp2 and Pep1 have a similar defense phenotype, it is conceivable that Stp2 has a similar function as Pep1 in terms of inhibiting early defense responses.

Staining infected plant cells with FM4-64 was used to visualize plant cell death, which could be observed after infection with *stp1*, *stp2*, *stp3*, *stp4* and *pep1* deletion mutants. This supports the macroscopic observations concerning the necrotic spots, which were visible on the leaves of plants infected with mutants lacking essential effectors. A similar plant reaction was also observed for the *pit1* and *pit2* deletion strains, but it occurred later (Doehlemann *et al.*, 2011). Plant cell death can be induced when unspecific defense is triggered by the perception of a PAMP and is subsequently not suppressed by the pathogen (Thomma *et al.*, 2011). This indicates that mutants lacking the essential effectors fail to suppress PTI responses. Alternatively, one could consider that cell death is just a secondary effect to an impaired biotrophic interaction and not the actual reason for the growth arrest. In this scenario, other secreted effectors might be missing or unable to fulfill their function. This could also explain why the deletion mutants of the essential effectors cause a similar plant cell death reaction.

The similarities in plant responses to essential effector deletion mutants could also be observed in the RNAseq dataset generated at 24 hpi, the time point when *U. maydis* has just penetrated the plant tissue. When focusing on significantly upregulated genes, there was a large overlap between all five deletion strains and additional genes that were upregulated in at least two of the deletion strains. Such a high overlap likely reflects that all essential effectors might function together. The *stp2* deletion strain shared the majority of its significantly upregulated genes with mutants lacking *stp1*, *stp3*, *stp4* and *pep1*. GO terms associated with the genes upregulated after infection with all five effector deletion strains were mainly associated with cell regulation and cell signaling. Considering the early time point of sample collection, the respective genes could be part of the signaling network facilitating pathogen recognition. Currently, the transcriptome data indicate that *stp1*, *stp2*, *stp3*, *stp4* and *pep1* deletion mutants cause a strong defense reaction in comparison to the wild type. Future analysis may exhaustively explore the generated dataset and additionally focus on deletion-strain-specific upregulated genes.

## 3.2 Effectors essential for virulence form a complex

A common approach to understand the function of effector candidates, is the identification of plant protein interaction partners. Protein-protein interaction assays are able to find effector targets (Varden *et al.*, 2017). CO-IP/MS has been recently applied in the *U. maydis* - *Z. mays* pathosystem. This technique was used to identify the antifungal proteins AFP1 and AFP2 as interaction partners of the effector Rsp3 (Ma *et al.*, 2018). Using this methodology, the effector complex consisting of Stp1, Stp3, Stp4 and Pep1 was discovered. Surprisingly, there was no reliable identification of plant interaction partners. The experiments also failed to detect the POX12 peroxidase, which is the published apoplastic target of Pep1. In Hemetsberger *et al.* (2012), the interaction between Pep1 and POX12 was shown by Y2H. A CO-IP approach has the advantage that proteins are present in their native form and are expressed in their natural physiological environment (Rao *et al.*, 2014). Therefore, a reason for not detecting POX12 could be the time point at which the plant samples were collected. POX12 shows strong upregulation at 12 hpi and at 12 dpi, and is only very weakly expressed in between (Lanver *et al.*, 2018). CO-IP at other time points than 3 dpi, the value used in this study, might have detected potential plant interaction partners for the other effectors. I have tried CO-IP with plant samples that were collected at 24 hpi with all the previously used strains. However, the CO-IP/MS experiments using this plant material failed to even detect the bait protein (not shown), which is most likely due to the presence of under 0.5% of fungal material at this stage (Lanver *et al.*, 2018). The conditions at earlier time

points should be optimized in future experiments. The results presented in Table 2.3 and Table 2.4 were generated using a protocol which was optimized during the course of this study and could consistently identify the quadruple effector complex. In an attempt to identify potential plant interaction partners, different buffer compositions and incubation conditions were tried as well as first attempts to cross-link proteins in the cell lysate before proceeding with the Co-IP experiments (not shown). In most of these conditions, the effector complex could be detected (not shown). This was also the case when strains carrying multiple integrations of the gene encoding the bait protein were used. The finding that such strains were indistinguishable in virulence from strains carrying the complex-encoding genes in single copy suggests that complex formation is unlikely to be affected.

Interestingly, the initial Co-IP/MS experiments failed to identify interaction partners for Stp2. This changed in more recent trials, which makes it likely that Stp2 is part of a second effector complex, whose individual members are also essential for virulence. A potential reason could be improved lysis conditions. While the early samples, in which the Stp1, Stp3, Stp4 and Pep1 complex was identified, were grinded by hand, newer samples were prepared with a grinding machine. It will be interesting to see whether the second complex can be confirmed using Stp5 and Pst1 as bait. Due to the highly similar phenotype of mutants of all essential effector deletion mutants and the fact that all seven essential effectors reside in the magenta module, the question arises whether there are two separate effector complexes or whether these two complexes are connected. The subcomplexes might only very transiently interact, which could be hard to detect without cross-linking. However, in one trial of CO-IP/MS with an especially good lysis and a high number of detected peptides, Stp2, Pst1 and Stp5 were fished by Stp1, Stp3, Stp4 and Pep1 (Table 2.3).

The finding that secreted effectors of plant pathogens interact with each other and that this interaction is necessary for their function, is novel for eukaryotic pathogens. In *Legionella pneumophila*, the causative agent of Legionnaires' disease, the effectors interact directly and indirectly with each other after being secreted into the host cell. In comparison to other bacteria, such as *Salmonella enterica* and *Escherichia coli*, *L. pneumophila* possesses a large number of secreted effector proteins (Ensminger, 2016). Among these are effectors that act in antagonistic or synergistic fashion and target the same pathways as well as effectors that physically interact within the host cell. These were termed metaeffectors or effectors of effectors (Urbanus *et al.*, 2016). The authors speculate that *L. pneumophila* uses a subset of its effectors to regulate others after release into the host cell. An example is the metaeffector LegL1, which directly inactivates the RavJ effector by inhibiting its catalytic activity (Urbanus *et al.*, 2016; Huett, 2017).

## 3.3 Pep1, an effector with a dual function?

Pep1 is one of the few effectors whose function has been at least partially elucidated. Hemetsberger *et al.* (2012) have shown that Pep1 functions as an inhibitor of plant peroxidases, including the maize peroxidase POX12. It was demonstrated that the *pep1* deletion mutant defect could be partially restored by virus-induced gene silencing of POX12. However, the described partial complementation after silencing of POX12 was just referred to the ability of the deletion mutant to pass more than one cell layer. This could be due to the absence of the callose plug. Virulence symptoms like anthocyanin and tumor formation were never observed. Furthermore, in POX12-silenced plants the longer hyphae of the *pep1* deletion mutant failed to branch and were unable to develop clamp connections (Hemetsberger *et al.*, 2012). This extended growth phenotype very much resembles the development of *stp1*, *stp3* and *stp4* deletion mutants after infection. Therefore, it is conceivable that Pep1 has two functions. Initially, Pep1 might inhibit POX12 at a very early time point, and its second and essential function could be forming the effector complex. This hypothesis is supported by the finding that POX12 is highly expressed at 12 hpi and 12 dpi, while the expression of *pep1* peaks at 3 dpi (Lanver *et al.*, 2018). Additionally, Doehlemann *et al.* (2009) observed a strain expressing *pep1* under the *otef* promoter. The promoter exhibits strong expression during the early biotrophic phase of *U. maydis*, but is shut down during the late biotrophic phase. The used strains exhibited a strong reduction in virulence compared to the wild type strain expressing *pep1* under its native promoter. This indicates that Pep1 remains essential during the entire biotrophic phase, which is inconsistent with its sole role as inhibitor of POX12.

## 3.4 The effector complex functions outside the plant cytosol

The essential effectors were predicted to be secreted. This was verified for Stp2, Stp3 and Stp4 after the respective genes were fused to a constitutive promotor and the proteins were detected in the supernatants. Stp2 und Stp3 were detected as full-length proteins, but the culture also showed degradation products, whereas the molecular weight of Stp4 was higher than predicted and several very high molecular weight forms were detected. Since Stp4 is very cysteine-rich, the high molecular weight forms could result from inter-molecular disulphide bridges that might form faster than the correct intra-molecular ones. However, after immunoprecipitating from the total plant lysates, Stp2, Stp3 and Stp4 were all detectable as single bands in the predicted sizes.

Utilizing the biochemical BirA translocation assay, it could be shown that Stp2-

AvitagHA, Stp3-AvitagHA and Stp4-AvitagHA are not translocated into the apoplast. This is in agreement with what was previously observed for Stp1-AvitagHA and Pep1-AvitagHA (Lo Presti *et al.*, 2016). However, the assay cannot distinguish between soluble apoplastic effectors and those bound to the fungal cell wall or plant plasma membrane. During the intracellular growth, the plant plasma membrane encloses the fungus very tightly, which makes the secreted mCherry fusion proteins seem to surround the fungal hyphae. This experiment was already conducted with several apoplastic and translocated *U. maydis* effectors, such as Pit2, Tin2 and Cmu1 (Doehlemann *et al.*, 2011; Djamei *et al.*, 2011; Tanaka *et al.*, 2014). In all cases, the detected mCherry signal showed a smooth, even distribution around the fungus. In contrast, the mCherry signal from Stp1, Stp2, Stp3, Stp4 and Pep1 fusion proteins accumulated in speckles surrounding the hyphae. The same formation of speckles was also reported after *in situ* immunolocalization of Pep1 and Stp1, proving that the speckles are not just artefacts from the fluorescent tags (Doehlemann *et al.*, 2009; Schipper, 2009). As such speckles were detected for the essential effectors, it is very likely that they stem from the complex formed by these effectors. This was further strengthened by showing co-localization of Stp1-YFP and Stp3-mCherry in the speckles. As a next step it would be interesting to co-localize the other complex members as well as members of the Stp2 complex. In case the observed speckles actually originate from the complex, this would indicate that there is a very high number of constantly formed complexes, which also seem to remain in place while the fungus continues to grow.

Since the plant plasma membrane is tightly attached to the hyphae, it cannot be distinguished whether the fusion proteins are attached to the fungus, the plant plasma membrane or soluble in the apoplast. Plasmolysis experiments were conducted to detach the plant plasma membrane from the fungus and enlarge the apoplast. Plasmolysis experiments were done already for several *U. maydis* effectors to prove their secretion into the apoplast (Mueller *et al.*, 2013; Tanaka *et al.*, 2014; Stirnberg and Djamei, 2016; Seitner *et al.*, 2018). Similar to those studies, the mCherry signal of the Stp1, Stp2, Stp3, Stp4 and Pep1 fusion proteins could be detected in the apoplast (Doehlemann *et al.*, 2009; Schipper, 2009). In all cases, there was still a high amount of mCherry signal surrounding the hyphae. To investigate whether the effectors remain attached to the hyphae or whether the plant plasma membrane just does not detach properly, PIN1a-YFP plants were used to visualize the plant plasma membrane. When inducing plasmolysis in PIN1a-YFP plants infected with SG200pit2-mCherry, it could be observed that the plant plasma membrane did not fully detach from fungal hyphae. Whether the plant plasma membrane attaches at specific sites and whether these attachment sites co-localize with the speckles could unfortunately not be resolved. Attempts to remove the plant plasma membrane from the intracellularly growing hyphae included applying

a mixture of plant mazerating enzymes. After the tissue was loosened-up, intracellular growing hyphae were enriched by binding to WGA-coupled magnetic beads. Preliminary results suggest that hyphae continue to show mCherry signal in speckles (not shown). In future, PIN1a-YFP plants will have to be used in such experiments to ensure full removal of the plant plasma membrane. Further indications that the complex could be actually associated with or even connected to the fungus are preliminary immuno-TEM pictures. These images, generated in collaboration with K. Snetselaar (Saint Joseph's University, PA, USA), show that Stp3-HA localizes at membranous protrusions, which appear attached to the fungal hyphae, and extend into the host. It remains to be shown, whether these structures are part of the fungus or just residual plant plasma membrane that stays attached to the fungus.

Distinct structures containing secreted effector proteins were also observed in the biotrophic interaction between the crucifer anthracnose fungus *C. higginsianum* and *A. thaliana*. In this system, confocal microscopy identified RFP-tagged effectors in multiple fluorescent foci, called interfacial bodies that localized between the biotrophic hyphae of *C. higginsianum* and the plant plasma membrane (Kleemann *et al.*, 2012). Immuno-TEM analysis confirmed the formation of interfacial bodies as well as the accumulation of the tagged effector within. Studies on *C. orbiculare* and its host cucumber also revealed the accumulation of fluorescently tagged effectors in multiple dotted structures located around the biotrophic hyphal surface. In this system, the effectors also located at a ring-like structure around the neck region of primary invasive hyphae (Irieda *et al.*, 2014; Irieda *et al.*, 2016).

In the *M. oryzae* - rice pathosystem another type of structure is formed during its biotrophic development. The biotrophic interfacial complex (BIC) is a plant-derived membrane-rich structure external to the hyphae (Giraldo *et al.*, 2013; Khang *et al.*, 2010). It develops at the tip of the primary biotrophic hyphae and as the hyphae develops and the tip swells, the BIC is positioned on the side. In contrast to the many speckles that cover the intracellular hyphae of *U. maydis*, the BIC constitutes a large and solitary structure. It is speculated that the BIC is involved in the translocation of effectors as it was demonstrated that cytoplasmic effectors accumulate in the BIC before translocating into the plant cells. However, its exact role remains unclear (Giraldo *et al.*, 2013; Khang *et al.*, 2010).

## 3.5 The formation of the complex is essential for *U. maydis* virulence

Initially, BiFC was planned to visualize the effector complex and verify its localization in speckles. However, tagging two complex members in their endogenous locus with the halves of YFP lead to a complete loss of virulence. When examined by confocal microscopy, it was evident that the tagged strains showed a phenotype similar to the *stp* deletion mutants. Introducing additional copies of Stp1-YFPC and Stp3-YFPN into a wild type background lead to a reduction in virulence, which correlated with the number of additional copies introduced. This dominant negative effect indicates that the formation of the complex is essential for virulence of *U. maydis*. It is likely that the two halves of the YFP interfere with the complex formation because they assemble and it is conceivable that this pushes the complex apart. It was also speculated that the two large tags interfere with complex formation. However, this possibility was excluded, after fusing full-length YFP and full-length mCherry to Stp1 and Stp3 in the same strain. This strain was fully virulent and even allowed to co-localize the effectors in speckles.

## 3.6 Stp1, Stp3, Stp4 and Pep1 interact also in *S. cerevisiae*

Interaction studies using CO-IP/MS provided very consistent results about Stp1, Stp3, Stp4 and Pep1 forming a complex. Utilizing a Y2H system, pairwise interactions were tested to investigate whether there is a specific order in which these four proteins assemble or whether each complex member contacts each of the others in the complex. After testing all effector combinations, it appeared as if Stp1 is a central component, interacting with all the other effectors whereas the others did not interact among themselves. Initially, there was only a weak interaction between Stp1 and Stp4, which could be strengthened by adding either Stp3 or Pep1. In this case, Stp3 and Pep1 might fulfill a bridging function or full interaction between Stp4 and Stp1 might require a combination of interacting surfaces from Stp4 and Stp3 or Pep1 (Xing *et al.*, 2016). The possibility that only the presence of two proteins could open up the interaction site for the third partner to bind and connect to them could also be a possible explanation for the successful interaction in the strain AD-Pep1/BD-Stp3/myc-Stp4, in which none of the three effectors interacted when tested in pairs (Maruta *et al.*, 2016). Furthermore, this finding indicated that the presence of Stp1 is not mandatory for a formation of a subcomplex, but without it Stp3, Stp4 and Pep1 need to be present to form a stable complex. The gained knowledge about the composition of subcomplexes which can form, is expected to be instrumental

for future structural studies.

Since a strain harboring only three out of the four complex members could already grow on high-stringency plates, nutritional selection could not be used as a readout for the interaction between Stp1, Stp3, Stp4 and Pep1. Therefore, a CO-IP using the total cell lysate of the yeast strain expressing all four complex members was conducted. The subsequent mass spectrometry revealed that Stp4, as a bait, fished all the other complex members as interactors. The strain expressing all four complex members should not only serve to verify complex formation, but can also be used in an experiment to further prove its biological relevance. Planned is a screening approach for a small molecular compound, which inhibits complex formation. Yeast has proven to be a good model for conducting high-throughput screens of small-molecule libraries (Stefanini *et al.*, 2013; Zimmermann *et al.*, 2018). Wong *et al.* (2017) describe a Y2H assay, which they used in a high-throughput manner to screen for small-molecule protein-protein interaction inhibitors. They used a strain, in which nine ABC transporter-related genes were deleted to make it highly permeable to small molecules. We are currently testing this strain for optimal growth conditions in a high-throughput setup (Jung *et al.*, 2015). Subsequently the small molecule screen will be conducted in collaboration with the compound management and screening center (comas) at Max Planck Institute of Molecular Physiology in Dortmund. If a small compound that destroys the complex can be identified, it is expected to inhibit biotrophic development of *U. maydis*. It could also enable the development of a new antifungal drug against smut fungi.

## 3.7 Essential effector proteins are core effectors

There are currently 53 core effectors based on a comparative genomics analysis of the secretomes of eleven strains belonging to ten species of plant pathogenic smut fungi (M. Schuster, personal communication). The deletion of core effectors from the magenta module was part of a shared effort to delete all core effectors of *U. maydis*. After deleting all core effectors, it became evident that *U. maydis* possesses seven essential core effectors. These are the previously identified Stp1 and Pep1 as well as the in the course of this work identified Stp2, Stp3 and Stp4. The other two essential effectors, which became apparent as putative interactors of Stp2, were not part of the original set of core effectors. Stp5 and Pst1 were initially excluded as they did not fit the chosen selection criteria. Stp5 was excluded since it did not contain a predicted signal peptide based on the chosen SignalP threshold, whereas Pst1 harbors a predicted transmembrane domain (M. Schuster, personal communication). During the course of this study, a paper about Stp4 and its phenotype was published. In the publication, Stp4 was termed Cce1

(Cysteine-rich core effector 1) (Seitner *et al.*, 2018). Even though its name includes the term core, the authors claim that *cce1* does not have a homolog in *M. pennsylvanicum*. However, having a better sequenced version of the *M. pennsylvanicum*, our group was able to identify this homolog proving that *stp4* truly is a core effector (M. Schuster and G. Schweizer, personal communication). For consistency reasons, the effector remained to be called *stp4* in this work. The fact that the essential effectors are well conserved indicates a crucial function in all smut fungi. This is further strengthened by the fact that *stp1*, *stp4* and *pep1* deletion mutants could be fully complemented with the respective homologs from various smut fungi (Liang, 2012; Hemetsberger *et al.*, 2015; Seitner *et al.*, 2018). Moreover, for the *U. hordei pep1* deletion strain, it was shown that it also arrests in the first cell layer of its host plant barley, demonstrating the importance of *pep1* outside the maize system (Hemetsberger *et al.*, 2015). The essential effectors were also present in anamorphic yeasts from the same family, but seem to be restricted to the Ustilaginaceae (Schuster *et al.*, 2018).

## 3.8 Potential functions of the effector complex

I propose that the major function of the four effectors Stp1, Stp3, Stp4 and Pep1 is carried out in the effector complex. The function of the complex affects the development of *U. maydis* early, with the initiation of and during biotrophic development. The function of the complex must be such that each component is important enough to completely arrest the fungal growth. Additionally, it is necessary for the complex to form properly. Therefore, I propose that the complex members form an essential structure. Here, I discuss the potential function of this structure in three different models (Figure 3.1). In all three cases, the elicited plant defense responses are a secondary effect based on the malfunction of the effector complex. The discussed models cover a function in translocation of other effectors, in nutrient acquisition or in the establishment of a biotrophic interaction zone. An open question for all models is whether there are two effector complexes or a single large one and whether there might even be more components not found so far. In this context, it should be considered that Pst1 is predicted to have a transmembrane domain and that there are additional putative transmembrane proteins whose expression is co-regulated with the effectors in the complex (C. Pellegrin, personal communication). With planned interaction studies relying on cross-linking as well as a collaboration concerning the structural analysis, an answer to these questions could be found in the future.

The first model is based on the idea that the essential effectors could form a structure that functions in delivering effector proteins into the host cell (Figure 3.1B). An example

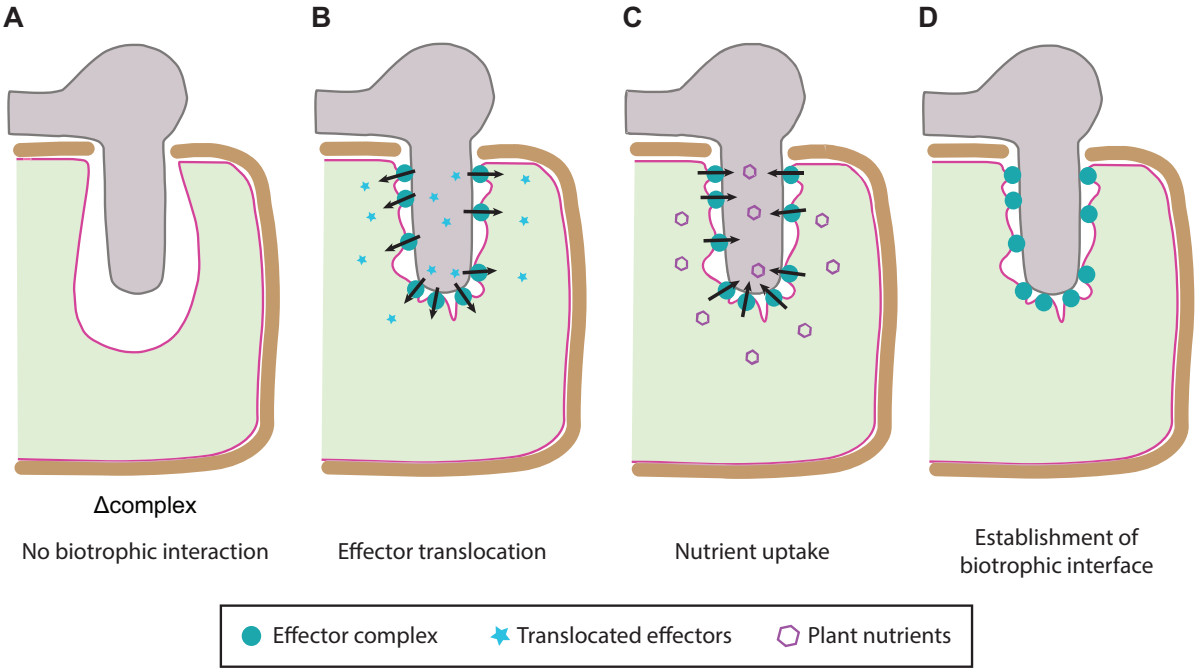


**Figure 3.1: Models for the function of the effector complex.** (A) In the absence of the complex the biotrophic interaction cannot be established. The fungus arrest early in its development. (B) The complex (turquoise circle) creates a structure to aid the translocation of other effectors (blue stars). (C) The effector complex creates a structure to support nutrient uptake (purple hexagon). (D) The effector complex attaches to the plant plasma membrane and establishes a biotrophic interface. Arrows indicate the direction of movement. The pink line represents the plant plasma membrane. Picture modified from S. Reißmann.

for such a machinery is the type III secretion system (T3SS) of gram-negative bacteria that is used to deliver their effectors directly into host cells. The T3SS is a membrane-embedded nanomachine, whose central component is a needle complex. Resembling a molecular syringe, the T3SS forms a channel that crosses the bacterial envelope and the host cell membrane, enabling bacteria to inject numerous effector proteins into the cytoplasm of host cells (Galan *et al.*, 2014). Nematodes also deliver their effectors by piercing the cell wall with a needle-like stylet and injecting them directly into the host cell (Goverse and Smant, 2014). Unlike the nematodes, whose stylet is also a feeding structure firmly attached to their heads, the bacterial needle structure is building its final components upon host contact. Building blocks include the components of the needle filament as well as the translocator proteins, which make up a channel, the so-called translocon, in the host cell membrane. Through this channel other effectors enter the host cell (Wagner *et al.*, 2018). Since *U. maydis* complex members are also only expressed upon plant contact, the proposed machinery may be analogous to that of T3SS.

In the preliminary Immuno-TEM experiments, Stp3 is associated with emerging protrusions. The protrusions might function as a channel structure arising from the fungus. Such a channel would require presorting apoplastic and translocated effectors

with the translocated effectors being unconventionally secreted and transferred via the effector complex. Separate secretion pathways for apoplastic and translocated effectors have been described in bacterial systems and for *M. oryzae* (Zhang and Xu, 2014).

However, known translocated *U. maydis* effectors, such as Tin2 or Cmu1, can also be found in the apoplast when fused to mCherry. They are smoothly and evenly distributed and not associated with the speckles presumably containing the complex. Therefore, another possibility could be a translocon structure that is disconnected from the fungus and transfers effectors from the apoplast to the host cell. An example for such a disconnected effector translocon is the PTEX (Plasmodium translocon of exported proteins) complex in malaria parasites. The PTEX consists of five proteins, but multiple molecules of the three proteins HSP101, PTEX150 and EXP2, form the essential core part of PTEX. EXP2 forms the vacuolar-membrane-spanning part of the channel, whereas HSP101 unfolds proteins destined for export. PTEX150 is thought to play a structural role, connecting the two (Elsworth *et al.*, 2014; Ho *et al.*, 2018).

Fungi also build structures, thought to be associated with the transport of effectors. These structures, such as the BIC of *M. oryzae* or the ring structure and interfacial bodies of *C. higginsianum* and *C. orbiculare* are species-specific and do not resemble needle structures or tunnels, indicating that a universal mechanism to transport effectors to the host does not exist. The effector complex described in this work could form a novel translocation structure specific for smut fungi. Experiments utilizing translocated effectors are currently being conducted in order to prove or disprove that the complex in *U. maydis* is involved in effector translocation.

Instead of facilitating effector delivery to the host, the complex could serve to extract molecules from it (Figure 3.1C). These molecules may be nutrients required to sustain fungal growth in the host environment. The importance of nutrients for virulence was shown in *U. maydis* mutants lacking the saccharose transporter Srt1 (Wahl *et al.*, 2010). The hyphae of essential effector deletion mutants appeared thin and crippled which could reflect that they are starved. Many fungal nutrient transporters are part of the magenta module (Lanver *et al.*, 2018). In this case, the complex would provide a connection between the fungus and the plant cytosol, allowing nutrient influx towards the fungus.

Such a structure does not need to resemble previously described nutrient channels, as was shown for the RhopH complex in *P. falciparum*. The complex consists of at least three proteins that are secreted almost immediately upon invasion. It is speculated that after secretion and assembly the complex shuttles to the membrane of red blood cells, where it helps to increase cell permeability by forming a channel that allows transfer of a wide array of solutes (Counihan *et al.*, 2017; Ito *et al.*, 2017; Sherling *et al.*, 2017). Similar to the speckles of the *U. maydis* complex, multiple channels are distributed along the membrane (Lisk and Desai, 2005). A knockdown of the individual proteins

disrupted the entire complex. Additionally, inhibition of the channel activity resulted in developmental arrest (Pillai *et al.*, 2012).

Rather than proposing a direct function of the complex in effector delivery or nutrient acquisition, the complex structure could also be involved in establishing and maintaining the biotrophic interaction zone (Figure 3.1D). We have shown that the plant plasma membrane is extremely tightly attached to the fungus. This tight attachment might be necessary to facilitate efficient exchange of molecules via extracellular vesicles.

While the exact function of the effector complex remains to be elucidated in future and ongoing studies the *U. maydis* - *Z. mays* system is likely to be the most tractable system to allow this to happen. Due to the crucial importance of the complex for virulence and its conservation in smut fungi, it could also serve as a potential drug target.

# 4 Material and methods

## 4.1 Material and source of supplies

### 4.1.1 Chemicals

Chemicals used in this study were predominantly obtained from Becton Dickinson (Heidelberg, Germany), GE Healthcare (Munich, Germany), Invitrogen (Karlsruhe, Germany), Merck (Darmstadt, Germany), Roche Diagnostics (Mannheim, Germany), Roth (Karlsruhe, Germany) and Sigma-Aldrich (Munich, Germany).

### 4.1.2 Buffers and solutions

Standard buffers and solutions were prepared according to Ausubel (2002). If required, media and buffer were autoclaved for 5 minutes at 121°C. Heat-sensitive solutions were filter-sterilized (Pore size 0.22 $\mu$m; Merck).

### 4.1.3 Enzymes and antibodies

All restriction enzymes were obtained from New England Biolabs (NEB) (Frankfurt, Germany). Phusion DNA polymerase was obtained from Thermo Fisher Scientific (Waltham, MA, USA). Enzymatic digestion of cell walls was accomplished using Novozym 234 (Interspex Products, Foster City, CA, USA). Antibodies were obtained from Sigma-Aldrich and Cell Signaling Technology (Leiden, Netherlands). A table of all antibodies can be found in Table 4.3.

### 4.1.4 Commercial kits

For purification of PCR products and DNA fragments from agarose gels, the Wizard SV Gel and PCR Clean-Up System from Promega (Mannheim, Germany) was used. The isolation and purification of plasmid DNA from bacterial cultures was carried out with QIAprep Mini Plasmid Kit from Qiagen. For the assembly of multiple DNA fragments the Gibson Assembly Cloning Kit (NEB) was used. For digoxigenin labeling of PCR products, the DIG High Prime kit (Roche) was used. The ECL Plus Western blot

detection reagent (GE Healthcare) was used for chemiluminescence detection. More specific kits are listed in the respective method sections.

## 4.2 Cell cultivation and media

### 4.2.1 Cultivation of *E. coli*

*E. coli* bacteria were cultivated in dYT liquid medium or on YT solid medium (Ausubel *et al.*, 1987; Sambrook *et al.*, 1989). Antibiotics were added as selection markers as needed (ampicillin, 100 $\mu$g/ml, kanamycin 40 $\mu$g/ml). Liquid cultures were incubated at 37°C and 200 rpm. Solid media were incubated under aerobic condition at 37°C.

| Solution | Composition | Notes |
|---|---|---|
| dYT liquid medium | 1.6% (w/v) Tryptone<br>1.0% (w/v) Yeast-extract<br>0.5% (w/v) NaCl | Dissolve in $H_2O_{bid}$ and autoclave |
| YT solid medium | 1.6% (w/v) Tryptone<br>0.8% (w/v) Tryptone<br>0.5% (w/v) Yeast-extract<br>0.5% (w/v) NaCl<br>1.3% (w/v) Bactoagar | Dissolve in $H_2O_{bid}$ and autoclave |
| dYT glycerol medium | 1.6% (w/v) Tryptone<br>1.0% (w/v) Yeast-extract<br>0.5% (w/v) NaCl<br>80.0% (v/v) 87% Glycerol (f.c. 69.6%) | Dissolve in $H_2O_{bid}$ and autoclave |

### 4.2.2 Cultivation of *U. maydis*

*U. maydis* was grown on PD solid medium and in $YEPS_{Light}$ liquid medium at 28°C. Selection markers were added when needed.

| Selection marker | Final concentration |
|---|---|
| Hygromycin B (H) | 200 $\mu$g/ml |
| Geneticin (G) | 400 $\mu$g/ml |
| Nourseothricin (clonNAT) (N) | 75 $\mu$g/ml |
| Carboxin (C) | 2 $\mu$g/ml |

Liquid cultures were incubated at 28°C and 200 rpm. Solid media were incubated under aerobic condition at 28°C. Glycerol stocks for long-term storage at -80°C were created by mixing a dense liquid culture with NSY-glycerol at a 1:1 ratio.

| Medium | Composition | Notes |
|---|---|---|
| $YEPS_{Light}$ liquid medium | 1.0% (w/v) Yeast-extract<br>0.4% (w/v) Peptone<br>0.4% (w/v) Sucrose | Dissolve in $H_2O_{bid}$ and autoclave |
| PD solid medium | 2.4% (w/v) Potato dextrose broth<br>2.0% (w/v) Bactoagar | Dissolve in $H_2O_{bid}$ and autoclave |
| PD charcoal solid medium | 2.4% (w/v) Potato dextrose broth<br>1.0% (w/v) Charcoal<br>2.0% (w/v) Bactoagar | Dissolve in $H_2O_{bid}$ and autoclave |
| NSY glycerol medium | 0.8% (w/v) Nutrient broth<br>0.1% (w/v) Yeast-extract<br>0.5% (w/v) Sucrose<br>69.6% (v/v) Glycerol | Dissolve in $H_2O_{bid}$ and autoclave |

For stress assays, CM plates were used as a base. Sorbitol (2 M) and NaCL (1 M) were added prior to autoclaving. Congo red (70 $\mu$g/ml), calcofluor white (150 $\mu$g/ml) and $H_2O_2$ (1.5 M) were supplemented after autoclaving. In order to test the sensitivity of strains to the stressors, *U. maydis* strains were grown overnight at 28°C and 200 rpm in $YEPS_{Light}$. The cells were diluted in fresh $YEPS_{Light}$ and grown until reaching an $OD_{600}$ of 0.8 and then set to OD of 1 in $H_2O_{bid}$. Serial ten-fold dilutions of the cell suspensions (8$\mu$l) were spotted on the respective plates. The plates were incubated for 48 hours at 28°C. To test filamentous growth, the cell suspensions were spotted on PD-charcoal plates.

| Medium | Composition | Notes |
|---|---|---|
| CM<br>(Holliday, 1974) | 0.4% (w/v) Casaminoacids<br>0.2% (w/v) Yeast-extract<br>2.0% (v/v) Vitamin solution<br>25.0% (v/v) Salt solution<br>0.1% (w/v) DNA from herring sperm degr.<br>0.6% (w/v) NH4NO3<br>1.0% (v/v) 1 M Tris/HCl pH 8.0 (f.c. 10 mM)<br>2.0% (w/v) Bactoagar (for solid medium)<br>4.0% (v/v) 50% glucose solution (f.c. 2%) | Dissolve in $H_2O_{bid}$,<br>adjust pH to 7.0 with 5 M NaOH<br>and autoclave |
| Vitamin solution<br>(Holliday, 1974) | 0.1‰ (w/v) Thiamine hydrochloride<br>0.05‰ (w/v) Riboflavin<br>0.05‰ (w/v) Pyridoxine hydrochloride<br>0.2‰ (w/v) D-Pantothenic acid hemicalcium salt<br>0.05‰ (w/v) 4-Aminobenzoic acid<br>0.2‰ (w/v) Nicotinic acid<br>0.2‰ (w/v) Choline chloride<br>1.0‰ (w/v) myo-Inositol | Dissolve in $H_2O_{bid}$,<br>prepare 40 ml aliquots in 50 ml tubes<br>and freeze at -20°C |
| Salt solution<br>(Holliday, 1974) | 16.0‰ (w/v) $KH_2PO_4$<br>4.0‰ (w/v) $Na_2SO_4$<br>8.0‰ (w/v) KCl<br>2.0‰ (w/v) $MgSO_4 \times 7\ H_2O$<br>1.32‰ (w/v) $CaCl_2 \times 2\ H_2O$<br>8.0‰ (v/v) Trace elements | Dissolve in $H_2O_{bid}$<br>and sterile filtrate |
| Trace elements<br>(Holliday, 1974) | 0.06‰ (w/v) $H_3BO_3$<br>0.14‰ (w/v) $MnCl \times 4\ H_2O$<br>0.4‰ (w/v) $ZnCl_2$<br>0.4‰ (w/v) $Na_2MoO_4 \times 2\ H_2O$<br>0.1‰ (w/v) $FeCl_3 \times 6\ H_2O$ | |
| 50% Glucose solution | 55.0% (w/v) Glucose $\times\ H_2O$ | Dissolve in $H_2O_{bid}$<br>and sterile filtrate |
| PD solid medium | 2.4% (w/v) Potato dextrose broth<br>2.0% (w/v) Bactoagar | Dissolve in $H_2O_{bid}$<br>and autoclave |
| PD charcoal solid<br>medium | 2.4% (w/v) Potato dextrose broth<br>1.0% (w/v) Charcoal<br>2.0% (w/v) Bactoagar | Dissolve in $H_2O_{bid}$<br>and autoclave |

The *U. maydis* strain AB33 and its derivatives were cultured in ammonium minimal medium (AM-MM) or nitrate minimal medium (NM-MM) to repress or induce the nitrate-inducible promoter $P_{nar}$.

| Medium | Composition | Notes |
|---|---|---|
| AM-MM (Holliday, 1974) | 0.30% (w/v) $(NH_4)_2SO_4$<br>6.25% (v/v) Salt solution<br>2.00% (w/v) Glucose (after autoclavation) | Dissolve in $H_2O_{bid}$,<br>adjust pH to 7.0 with 5 M NaOH<br>and autoclave |
| NM-MM (Holliday, 1974) | 0.30% (w/v) $KNO_3$<br>6.25% (v/v) Salt solution<br>2.00% (w/v) Glucose (after autoclavation) | Dissolve in $H_2O_{bid}$,<br>adjust pH to 7.0 with 5 M NaOH<br>and autoclave |

### 4.2.3 Cultivation of *S. cerevisiae*

*S. cerevisiae* was grown at 28°C and 200 rpm. YEPD served as full medium. For the auxotrophic strains, SD (Selection Dropout) medium supplemented with the respective amino acids was used. The final concentrations of the amino acid supplements were adenine (0.02 g/l), histidine (0.02 g/l), leucine (0.1 g/l) and tryptophane (0.02 g/l). Glycerol stocks for long-term storage at -80°C were created by mixing a dense liquid culture with NSY-Glycerin at a 1:1 ratio.

For the Y2H interaction studies, the transformants were grown overnight at 28°C and 200 rpm in the according selection medium. The cells were diluted in fresh selection medium and grown until reaching an $OD_{600}$ of 1. Cells were resuspended in $H_2O_{bid}$ and serial ten-fold dilutions of the cell suspensions (8 $\mu$l) were spotted on the respective SD medium. The plates were incubated at 28°C for 3-4 days.

| | | |
|---|---|---|
| YEPD medium | 2.00% (w/v) Pepton<br>1.00% (w/v) Yeast extract<br>2.00% (w/v) Bactoagar (for solid medium) | Dissolve in $H_2O_{bid}$<br>and autoclave |
| SD medium | 0.67% (w/v) Yeast nitrogen base w/o amino acids<br>0.16% (w/v) DO supplements w/o adenine, histidine, leucine and tryptophan<br>2.00% Glucose (after autoclaving)<br>2.00% (w/v) Bactoagar (for solid medium) | Dissolve in $H_2O_{bid}$<br>and autoclave |

### 4.2.4 Determination of cell density

The cell density of liquid cultures was determined using a photometer (Ultrospec 3000 pro UV/Visible spectrophotometer, Biochrom, Cambridge, United Kingdom) at a wave length of 600 nm ($OD_{600}$). To determine the optical density, cell cultures were diluted

1:10 in $H_2O_{bid}$. The $OD_{600}$ of $H_2O_{bid}$ was used as a reference value. For *U. maydis* and *S. cerevisiae* cell cultures at $OD_{600}$ of 1 equals approximately 1-5$\times 10^7$ cells/ml.

## 4.3 Strains, oligonucleotides and plasmids

### 4.3.1 *E. coli* strains

The *E. coli* strains DH5$\alpha$ and TOP10 were used for the cloning and amplification of plasmids:

- DH5$\alpha$ (Thermo Fisher Scientific): (*F-endA1 glnV44 thi-1 recA1 relA1 gyrA96 deoRnupG purB20* $\Phi$*80dlacZ*$\Delta$*M15* $\Delta$*(lacZYA-argF)U169, hsdR17(rK-mK+),* $\lambda$-)
- TOP10 (Invitrogen): (*F-mcrA*$\Delta$*(mrr-hsdRMS-mcrBC)* $\Phi$*80lacZ*$\Delta$*M15* $\Delta$*lacX74 recA1 araD139* $\Delta$*(araleu) 7697 galUgalKrpsL (StrR) endA1 nupG*)

### 4.3.2 *U. maydis* strains

Deletion mutants genes were generated by gene replacement using a PCR-based approach (Kämper, 2004). For the integration of genes into the *ip*-Locus (*sdh2*), plasmids containing a carboxin resistant *ip*-allele ($ip^R$) were used (Broomfield and Hargreaves, 1992). These plasmids were linearized with the restriction enzymes SspI or AgeI and subsequently inserted via homologous recombination with the endogenous, carboxin-sensitive *ip*-allele ($ip^S$) into the genome of *U. maydis*. If not indicated otherwise, the transformed strains carry a single insertion in the *ip*-locus. Resulting strains were verified by Southern blot analysis. Strains can contain phleomycin (P), hygromycin (H), carboxin (C), nourseothricin (N) resistance. All strains are listed in Table 4.1.

**Table 4.1:** *U. maydis* strains used in this study.

| Name | Serial number | Genotype | Resistance | Reference |
|---|---|---|---|---|
| SG200 | NL41 | *a1: mfa2 bW2 bE1* | P | Kämper *et al.* (2006) |
| SG200ΔUMAG_10030 | NL1 | *a1: mfa2 bW2 bE1 ΔUMAG_10030* | P, H | This study, pNL1 |
| SG200Δstp2 | NL5 | *a1: mfa2 bW2 bE1 Δstp2* | P, H | This study, pNL3 |
| SG200Δstp3 | NL7 | *a1: mfa2 bW2 bE1 Δstp3* | P, H | This study, pNL2 |
| SG200Δstp4 | NL113 | *a1: mfa2 bW2 bE1 Δstp4* | P, H | This study, pSW16 |
| SG200ΔUMAG_05819 | NL42 | *a1: mfa2 bW2 bE1 ΔUMAG_05819* | P, H | This study, pNL4 |
| SG200Δstp2-stp2 | NL18 | *a1: mfa2 bW2 bE1 Δstp2, ip$^R$[Pstp2:stp2]ip$^S$* | P, H, C | This study, pNL7 |
| SG200Δstp3-stp3 | NL29 | *a1: mfa2 bW2 bE1 Δstp3, ip$^R$[Pstp3:stp3]ip$^S$* | P, H, C | This study, pNL8 |
| SG200Δstp4-stp4 | NL110 | *a1: mfa2 bW2 bE1 Δstp4, ip$^R$[Pstp4-stp4]ip$^S$* | P, H, C | This study, pSW20 |
| SG200AN1 | NL24 | *a1: mfa2 bW2 bE1 PUMAG_01779:3xegfp:NatR* | P, N | Lanver *et al.* (2014) |
| SG200AN1Δstp2 | NL25 | *a1: mfa2 bW2 bE1 PUMAG_01779:3xegfp:NatR Δstp2* | P, H, N | This study, pNL3 |
| SG200AN1Δstp3 | NL40 | *a1: mfa2 bW2 bE1 PUMAG_01779:3xegfp:NatR Δstp3* | P, H, N | This study, pNL2 |
| SG200AN1Δstp4 | NL97 | *a1: mfa2 bW2 bE1 PUMAG_01779:3xegfp:NatR Δstp4* | P, H, N | This study, pSW16 |
| SG200AM1Δstp1 | NL38 | *a1: mfa2 bW2 bE1 Δstp1 ip$^R$ [PUMAG_01779:gfp] ip$^S$* | P, H, C | Schipper (2009) |
| SG200Δpep1Potef-2RFP | NL63 | *a1: mfa2 bW2 bE1 Δpep1, ip$^R$[Potef-RFP]ip$^S$* | P, H, C | Doehlemann *et al.* (2009) |
| SG200Δpep1 | NL114 | *a1: mfa2 bW2 bE1 Δpep1* | P, H | Doehlemann *et al.* (2009) |
| SG200Δstp1 | NL112 | *a1: mfa2 bW2 bE1 Δstp1* | P, H | Schipper (2009) |
| SG200Δstp1-stp1-HA | NL118 | *a1: mfa2 bW2 bE1 Δstp1, ip$^R$[Pstp1:stp1-HA]ip$^S$* | P, H, C | K. Münch (KM508) |
| SG200Δstp1-stp1-HA (multiple) | NL119 | *a1: mfa2 bW2 bE1 Δstp1, ip$^R$[Pstp1:stp1-HA]ip$^S$* | P, H, C | K. Münch (KM509) |
| SG200Δstp2-stp2-HA | NL52 | *a1: mfa2 bW2 bE1 Δstp2, ip$^R$[Pstp2-stp2-HA]ip$^S$* | P, H, C | This study, pNL12 |
| SG200Δstp2-stp2-HA (multiple) | NL53 | *a1: mfa2 bW2 bE1 Δstp2, ip$^R$[Pstp2-stp2-HA]ip$^S$* | P, H, C | This study, pNL12 |
| SG200Δstp3-stp3-HA (multiple) | NL56 | *a1: mfa2 bW2 bE1 Δstp3, ip$^R$[Pstp3-stp3-HA]ip$^S$* | P, H, C | This study, pNL14 |
| SG200Δstp3-stp3-HA | NL58 | *a1: mfa2 bW2 bE1 Δstp3, ip$^R$[Pstp3-stp3-HA]ip$^S$* | P, H, C | This study, pNL14 |
| SG200Δstp4-stp4-HA | NL120 | *a1: mfa2 bW2 bE1 Δstp4, ip$^R$[Pstp4:stp4-HA]ip$^S$* | P, H, C | K. Münch (KM508) |
| SG200Δstp4-stp4-HA (multiple) | NL121 | *a1: mfa2 bW2 bE1 Δstp4, ip$^R$[Pstp4:stp4-HA]ip$^S$* | P, H, C | K. Münch (KM520) |
| SG200Δpep1-pep1-HA | NL122 | *a1: mfa2 bW2 bE1 Δpep1, ip$^R$[Ppep1:pep1-HA]ip$^S$* | P, H, C | K. Münch (KM503) |
| SG200Δpep1-pep1-HA (multiple) | NL123 | *a1: mfa2 bW2 bE1 Δpep1, ip$^R$[Ppep1:pep1-HA]ip$^S$* | P, H, C | K. Münch (KM502) |

| Name | Serial number | Genotype | Resistance | Reference |
|---|---|---|---|---|
| AB33 | NL128 | *a2: Pnar: bW2 bE1* | P | Brachmann *et al.* (2001) |
| AB33Potef-stp2-HA (double) | NL166 | *a2: Pnar: bW2 bE1* $ip^R$*[Potef:stp2:HA]*$ip^S$ | P, C | This study, pNL27 |
| AB33Potef-stp3-HA (double) | NL169 | *a2: Pnar: bW2 bE1* $ip^R$*[Potef:stp3:HA]*$ip^S$ | P, C | This study, pNL28 |
| AB33Potef-stp4-HA (double) | NL171 | *a2: Pnar: bW2 bE1* $ip^R$*[Potef:stp4:HA]*$ip^S$ | P, C | This study, pNL29 |
| SG200Pcmu1-cmu1SP-mCherry-HA | NL61 | *a1: mfa2 bW2 bE* $ip^R$*[Pcmu1-cmu1SP-cherry-biotagHA]*$ip^S$ | P, C | L. LoPresti (LL106) |
| SG200Δstp1-stp1-mCherry | NL70 | *a1: mfa2 bW2 bE1* Δ*stp1,* $ip^R$ *[Pstp1:stp1:mcherryHA]*$ip^S$ | P, H, C | Schipper (2009) |
| SG200 Δstp2-stp2-mCherry | NL49 | *a1: mfa2 bW2 bE1* Δ*stp2,* $ip^R$*[Pstp2-stp2-cherry-HA]*$ip^S$ | P, H, C | This study, pNL13 |
| SG200 Δstp3-stp3-mCherrry | NL74 | *a1: mfa2 bW2 bE1* Δ*stp3,* $ip^R$*[Pstp3-stp3-cherry-HA]*$ip^S$ | P, H, C | This study, pNL15 |
| SG200Δstp4-stp4-mCherry | NL101 | *a1: mfa2 bW2 bE1* Δ*stp4,* $ip^R$*[Pstp4-stp4-cherry-HA]*$ip^S$ | P, H, C | This study, pSW24 |
| SG200Δpep1-pep1-mCherry | NL87 | *a1: mfa2 bW2 bE1* Δ*pep1,* $ip^R$*[Ppep1:pep1:HA]*$ip^S$ | P, H, C | D. Aßmann (DA46) |
| SG200Δpit2-pit2-mCherry | NL127 | *a1: mfa2 bW2 bE1* Δ*pit2,* $ip^R$*[Ppit2:pit2:mcherry]*$ip^S$ | P, H, C | Doehlemann *et al.* (2011) |
| SG200stp2-AvitagHA | NL33 | *a1: mfa2 bW2 bE1 suc2::suc2-avitag3HA stp2::stp2-avitag-HA* | P, H, N | This study, pNL9 |
| SG200stp3-AvitagHA | NL35 | *a1: mfa2 bW2 bE1 suc2::suc2-avitag3HA stp3::stp3-avitag-HA* | P, H, N | This study, pNL10 |
| SG200stp4-AvitagHA | NL109 | *a1: mfa2 bW2 bE1 suc2::suc2-avitag3HA stp4::stp4-avitag-HA* | P, H, N | This study, pSW25 |
| SG200stp1-YFPC stp3-YFPN | NL88 | *a1: mfa2 bW2 bE1 stp1:HA:HA:YFPC(AS156-239) stp3:V5:HA:YFPN(AS1-155)* | P | D. Aßmann (DA99) |
| SG200stp3-YFPC stp1-YFPN | NL89 | *a1: mfa2 bW2 bE1 stp3:V5:HA:YFPC(AS156-239) stp1:HA:HA:YFPN(AS1-155)* | P | D. Aßmann (DA107) |
| SG200stp1-HA-YFP | NL90 | *a1: mfa2 bW2 bE1 stp1:HA-YFP* | P | K. Münch (KM465) |
| SG200stp3-YFP | NL92 | *a1: mfa2 bW2 bE1 stp3:HA-YFP* | P | K. Münch (KM476) |
| SG200stp1-YFPN | NL158 | *a1: mfa2 bW2 bE1 stp1:HA:HA:YFPN (AS1-155)* | P | D. Aßmann (DA184) |
| SG200stp3-YFPN | NL159 | *a1: mfa2 bW2 bE1 stp3:V5:HA:YFPN (AS1-155)* | P | D. Aßmann (DA186) |
| SG200stp4-YFPN pep1-YFPC | NL179 | *a1: mfa2 bW2 bE1 stp4:myc:HA:YFPN(AS1-155) pep1:strep:HA:YFPC(AS156-239)* | P | D. Aßmann (DA130) |
| SG200pep1-YFPC | NL180 | *a1: mfa2 bW2 bE1 pep1:strep:HA:YFPC(AS156-239)* | P | D. Aßmann (DA131) |
| SG200stp1-YFPN stp3-mCherry (many multiple) | NL126 | *a1: mfa2 bW2 bE1* $ip^R$*[Pstp1-stp1-HA-HA-YFPN-Tnos Pstp3-stp3-V5-HA-YFPC-Tnos]*$ip^S$ | P, C | D. Aßmann (DA136) |
| SG200stp1-YFPN stp3-mCherry (multiple) | NL129 | *a1: mfa2 bW2 bE1* $ip^R$*[Pstp1-stp1-HA-HA-YFPN-Tnos Pstp3-stp3-V5-HA-YFPC-Tnos]*$ip^S$ | P, C | D. Aßmann (DA132) |
| SG200stp1-YFPN stp3-mCherry (double) | NL130 | *a1: mfa2 bW2 bE1* $ip^R$*[Pstp1-stp1-HA-HA-YFPN-Tnos Pstp3-stp3-V5-HA-YFPC-Tnos]*$ip^S$ | P, C | D. Aßmann (DA135) |
| SG200stp1-YFPN stp3-mCherry | NL131 | *a1: mfa2 bW2 bE1* $ip^R$*[Pstp1-stp1-HA-HA-YFPN-Tnos Pstp3-stp3-V5-HA-YFPC-Tnos]*$ip^S$ | P, C | D. Aßmann (DA138) |
| SG200stp1-YFP stp3-mCherry | NL177 | *a1: mfa2 bW2 bE1 stp1:HA-YFP; stp3:mCherry-HA* | P | D. Aßmann (DA205) |

### 4.3.3 *S. cerevisiae* strains

For the Y2H interaction studies in *S. cerevisiae*, the strain AH109 (Clontech, Saint-Germain-en-Laye, France) was used (James *et al.*, 1996). The AH109 strain is auxotrophic for tryptophan, leucine, adenine and histidine. Additionally, an AH109 derivate strain ABC9Δ was used. ABC9Δ and was kindly provided by P. Arumugar (Biomedical Science Institute, Singapore). In this strain, ABC transporter-related genes were deleted by standard methods using PCR product-mediated homologous recombination (Wong *et al.*, 2017).

### 4.3.4 Oligonucleotides

Oligonucleotides used in this study are listed in Table 4.2. They were ordered from Eurofins Genomics (Ebersberg, Germany) and used for plasmid construction and sequencing.

**Table 4.2:** Oligonucleotides used in this study.

| Name | Sequence | Application |
|---|---|---|
| NL2 | CTCGAGTTTTTCAGCAAGATAATATTGCGGACGCACAAGAATAC | Amplification of the *UMAG_10030* left border |
| NL3 | AGAATAGGAACTTCTGGCCATCTAGGCCCTTGAACAGATGTCAGGC | Amplification of the *UMAG_10030* left border |
| NL4 | AGTATAGGAACTTCTGGCCTGAGTGGCCTTGTCATGCGGACATACC | Amplification of the *UMAG_10030* right border |
| NL5 | AGGAGATCTTCTAGAAAGATAATATTGAGGAGCTTGGAGAACTG | Amplification of the *UMAG_10030* right border |
| NL10 | CTCGAGTTTTTCAGCAAGATAATATTGATCAGGTACGCGACAAG | Amplification of the *stp3* left border |
| NL11 | AGAATAGGAACTTCTGGCCATCTAGGCCGTGTGGCGATCGTACGTC | Amplification of the *stp3* left border |
| NL12 | AGTATAGGAACTTCTGGCCTGAGTGGCCGGCGCAAAAAAGCCTTGG | Amplification of the *stp3* right border |
| NL13 | AGGAGATCTTCTAGAAAGATAATATTTCACCGCGGAAGATTCAC | Amplification of the *stp3* right border |
| NL18 | CTCGAGTTTTTCAGCAAGATAATATTTTCAAACGCGGCTAACTC | Amplification of the *stp2* left border |
| NL19 | AGAATAGGAACTTCTGGCCATCTAGGCCTGCAGCAGTGAGAAAGAC | Amplification of the *stp2* left border |
| NL20 | AGTATAGGAACTTCTGGCCTGAGTGGCCACTTGATCTCCTGGCTTC | Amplification of the *stp2* right border |
| NL21 | AGGAGATCTTCTAGAAAGATAATATTCTCTCGTGTCTGTTACTG | Amplification of the *stp2* right border |
| SW37 | CTCGAGTTTTTCAGCAAGATAATATTTGATCCACATCAGCAGTC | Amplification of the *stp4* left border |
| SW38 | TAGAGAATAGGAACTTCTGGCCATCTAGGCCACACCGCTTGAACAAGTG | Amplification of the *stp4* left border |
| SW39 | GAAAGTATAGGAACTTCTGGCCTGAGTGGCCCCAGCCTTCTTGGCATTC | Amplification of the *stp4* right border |
| SW40 | AGGAGATCTTCTAGAAAGATAATATTACAGTGCAGACGACTTTG | Amplification of the *stp4* right border |
| NL26 | CTCGAGTTTTTCAGCAAGATAATATTTGAAGTTGACCCACTCTG | Amplification of the *UMAG_05819* left border |
| NL27 | AGAATAGGAACTTCTGGCCATCTAGGCCTGTGCTGCTTCTTTCTGG | Amplification of the *UMAG_05819* left border |
| NL28 | AGTATAGGAACTTCTGGCCTGAGTGGCCATGTCCAGGGCAACATTC | Amplification of the *UMAG_05819* right border |
| NL29 | AGGAGATCTTCTAGAAAGATAATATTCCTGCATTCGCCTTTGTC | Amplification of the *UMAG_05819* right border |
| NL57 | GAGCAGCTGAAGCTTGCATGCTGTGGCGGGCTTAGCGCC | Amplification of the *stp2* promoter |
| NL58 | ACGATCTGCAGCCGGGCGGCCGCCGAAGCCAGGAGATCAAG | Amplification of *stp2* |
| NL65 | GAGCAGCTGAAGCTTGCATGCGGCCTTTCCAGGACTCAA | Amplification of the *stp3* promoter |
| NL66 | ACGATCTGCAGCCGGGCGGCCGCAAGGCTTTTTTGCGCCTT | Amplification of *stp3* |
| SW64 | GAGCTCGGTACCACAGCGTTGACGATATGG | Amplification of the *stp4* promoter |
| SW65 | AGCCGGGCGGCCGCTGGCGAATGCCAAGAAGG | Amplification of *stp4* |
| NL74 | TCGGGCACGTCGTAGGGGTATCTAGAGACGTGTGCAACATTGCC | Amplification of *stp2* with an overhang to *HA* |
| NL72 | TCGGGCACGTCGTAGGGGTATCTAGAAGCAGAAGTGCTGTCGAT | Amplification of *stp3* with an overhang to *HA* |
| SW76 | GGGGTATCTAGAGTGGTGTACTTGGGACCAG | Amplification of *stp4* with an overhang to *HA* |
| NL188 | GGGGGCCCGCGCCTAGGGCGGCTAGCATGATGTTGCCCTTCCAA | Amplification of *stp2* with an overhang to Potef |
| NL189 | GGGGGCCCGCGCCTAGGGCGGCTAGCATGCAGCTAAATCGTACC | Amplification of *stp3* with an overhang to Potef |
| NL190 | GGGGGCCCGCGCCTAGGGCGGCTAGCATGCATCGACCAACTAGC | Amplification of *stp4* with an overhang to Potef |
| NL73 | TCCTCGCCCTTGCTCACCATCCATGGGACGTGTGCAACATTGCC | Amplification of *stp2* with an overhang to *mCherry* |
| NL71 | TCCTCGCCCTTGCTCACCATGCTAGCAGCAGAAGTGCTGTCGAT | Amplification of *stp3* with an overhang to *mCherry* |
| SW77 | GGGCCCCCCGGGGTGGTGTACTTGGGACCAG | Amplification of *stp4* with an overhang to *mCherry* |
| NL41 | AATTGTACCCCTACGACGTGCCCGACTATGCCTAGGG | Amplification of HA with an overhang to pLL36 |
| NL42 | CGCGCCCTAGGCATAGTCGGGCACGTCGTAGGGGTAC | Amplification of HA with an overhang to pLL36 |
| NL60 | CTCGAGTTTTTCAGCAAGATAATATTCCTGTCGACTGCTTATGG | Amplification of *stp2* with an overhang to pLL36corr |
| NL61 | AATATCGTTCAGGCCACCGGTGACGTGTGCAACATTGCC | Amplification of *stp2* with an overhang to the $Hyg^R$ |
| NL62 | TGCGGCCGCATTAATAGGCCTATTACTTGATCTCCTGGC | Amplification of 3'UTR of *stp2* with an overhang to the $Hyg^R$ |
| NL63 | AGGAGATCTTCTAGAAAGATAATATTCTCTCGTGTCTGTTACTG | Amplification of 3'UTR of *stp2* with an overhang to pLL36corr |
| NL67 | CTCGAGTTTTTCAGCAAGATAATATTAACGAACTACCGTCCATC | Amplification of *stp3* with an overhang to pLL36corr |
| NL68 | AATATCGTTCAGGCCACCGGTAGCAGAAGTGCTGTCGAT | Amplification of *stp3* with an overhang to the $Hyg^R$ |
| NL69 | GTGCGGCCGCATTAATAGGCCTAAGGCGCAAAAAAGCCTT | Amplification of 3'UTR of *stp3*with an overhang to the $Hyg^R$ |
| NL70 | AGGAGATCTTCTAGAAAGATAATATTCCAACCTGAGGTTCAAAG | Amplification of 3'UTR of *stp3* with an overhang to pLL36corr |
| SW78 | CTCGAGTTTTTCAGCAAGATAATATTGACGAGATGTGCGGTTTC | Amplification of *stp4* with an overhang to pLL36corr |
| SW79 | TCGAAAATATCGTTCAGGCCACCGGTGTGGTGTACTTGGGACCAG | Amplification of *stp4* with an overhang to the $Hyg^R$ |
| SW80 | AGCTGTGCGGCCGCATTAATAGGCCTCCGCTTCCCCCCTCCCGTC | Amplification of 3'UTR of *stp4*with an overhang to the $Hyg^R$ |
| SW81 | AGGAGATCTTCTAGAAAGATAATATTGATCATCGGACGTGAATC | Amplification of 3'UTR of *stp4* with an overhang to pLL36corr |

| Name | Sequence | Application |
|---|---|---|
| NL174 | TGATCTCAGAGGAGGACCTGCATATGAACGGCTCGATCTCGAAC | Amplification of *stp1-SP* with an overhang to pGBKT7 |
| NL175 | CAAGGGGTTATGCTAGTTATGCGGCCGCCTAACGAGAAGGAGGAGG | Amplification of *stp1-SP* with an overhang to pGBKT7 |
| NL176 | TGATCTCAGAGGAGGACCTGCATATGGACAACCCTCAAATCACA | Amplification of *stp3-SP* with an overhang to pGBKT7 |
| NL177 | CAAGGGGTTATGCTAGTTATGCGGCCGCCTAGGCACTTGTCGAATC | Amplification of *stp3-SP* with an overhang to pGBKT7 |
| NL180 | TGATCTCAGAGGAGGACCTGCATATGGATGCTGCGGGTGCGGTA | Amplification of *pep1-SP* with an overhang to pGBKT7 |
| NL181 | CAAGGGGTTATGCTAGTTATGCGGCCGCTTACATGCCAAACATGCT | Amplification of *pep1-SP* with an overhang to pGBKT7 |
| NL184 | ACGACGTACCAGATTACGCTCATATGGACAACCCTCAAATCACA | Amplification of *stp3-SP* with an overhang to pGADT7 |
| NL185 | GGGTGGAATTCACTGGCCTCCATGGCCTAGGCACTTGTCGAATC | Amplification of *stp3-SP* with an overhang to pGADT7 |
| NL143 | TACCAGATTACGCTCATATGGCGACGCAGAGGGTCGGG | Amplification of *stp4-SP* with an overhang to pGADT7 |
| NL144 | AATTCACTGGCCTCCATGGCTTAGTGGTGTACTTGGGA | Amplification of *stp4-SP* with an overhang to pGADT7 |
| NL145 | TACCAGATTACGCTCATATGGATGCTGCGGGTGCGGTA | Amplification of *pep1-SP* with an overhang to pGADT7 |
| NL146 | AATTCACTGGCCTCCATGGCTTACATGCCAAACATGCT | Amplification of *pep1-SP* with an overhang to pGADT7 |
| NL122 | GAAAGGTGGAGCTCCCCGGGGCCGCCATCATGGAGGAGCAGAAG<br>CTGATCTCAGAGGAGGACCTGCATATGGATGCTGCGGGTGCGGTA | Amplification of *pep1-SP* with an overhang to pYEA |
| NL94 | GACATGGGAGATCCGAATTCTTACATGCCAAACATGCT | Amplification of *pep1-SP* with an overhang to pYEA |
| NL178 | TGATCTCAGAGGAGGACCTGCATATGGACAACCCTCAAATCACA | Amplification of *stp4-SP* with an overhang to pYEA |
| NL172 | GACATGGGAGATCCGAATTCTTAGTGGTGTACTTGGGA | Amplification of *stp4-SP* with an overhang to pYEA |
| NL165 | AACAAATATAAAACAAGATCGTCGACGGTGGAGGTGG<br>GTCTGGTGGAGGTGGCTCAATGGACAACCCTCAAATC | Amplification of *stp3-SP* with an overhang to pYEA |
| NL166 | CATGGGAGATCCGAATTCCTACAGGTCCTCCTCTGAGAT<br>CAGCTTCTGCTCCTCGAATTCGGCACTTGTCGAATCAAT | Amplification of *stp3-SP* with an overhang to pYEA |

### 4.3.5 Plasmids

Plasmids used and created in this work are described here. Plasmids were verified via enzymatic restriction and nucleotide sequences were analyzed by sequencing (Eurofins Genomics). pGBKT7 and its derivatives confer kanamycin resistance while all other plasmids confer ampicillin resistance.

#### Plasmids for the generation of stable *U. maydis* mutants

- pJET1-stuffer: Plasmid derived from pJet1 (Fermentas, St. Leon-Rot, Germany). Contains a 0.6 kb stuffer sequence flanked by EcoRV sites to allow amplification in DH5$\alpha$ and Top10. Kindly provided by K. Schink und M. Bölker.
- pHwtFRT (Khrunyk *et al.*, 2010): Plasmid containing the hygromycin resistance cassette ($Hyg^R$).
- pNL1 (pJETΔUMAG_10030): pJET-derived plasmid containing the *UMAG_10030* deletion construct which consists of a hygromycin resistance cassette flanked by the left and right border of the *UMAG_10030* gene. The left border and right border of *UMAG_10030* were PCR amplified from SG200 gDNA with primers NL2/NL3 and NL4/NL5. The hygromycin resistance cassette was obtained from SfiI digest of pHwtFRT. The three fragments were integrated into the EcoRV linearized pJET backbone via Gibson assembly.
- pNL2 (pJETΔstp3): pJET-derived plasmid containing the *stp3* (*UMAG_00715*) deletion construct which consists of a hygromycin resistance cassette flanked by the left and right border of the *stp3* gene. The left border and right border of *stp3* were PCR amplified from SG200 gDNA with primers NL10/NL11 and NL12/NL13. The hygromycin resistance cassette was obtained from SfiI digest of pHwtFRT. The three fragments were integrated into the EcoRV linearized pJET backbone via Gibson assembly.
- pNL3 (pJETΔstp2): pJET-derived plasmid containing the *stp2* (*UMAG_10067*) deletion construct which consists of a hygromycin resistance cassette flanked by the left and right border of the *stp2* gene. The left border and right border of *stp2* were PCR amplified from SG200 gDNA with primers NL18/NL19 and NL20/NL21. The hygromycin resistance cassette was obtained from SfiI digest of pHwtFRT. The three fragments were integrated into the EcoRV linearized pJET backbone via Gibson assembly.
- pSW16 (pJETΔstp4): pJET-derived plasmid containing the *stp4* (*UMAG_12197*) deletion construct which consists of a hygromycin resistance cassette flanked by the

left and right border of the *stp4* gene. The left border and right border of *stp4* were PCR amplified from SG200 gDNA with primers SW37/SW38 and SW39/SW40. The hygromycin resistance cassette was obtained from SfiI digest of pHwtFRT. The three fragments were integrated into the EcoRV linearized pJET backbone via Gibson assembly. Kindly provided by Sarah Winterberg.

- pNL4 (pJETΔUMAG_05819): pJET-derived plasmid containing the *UMAG_05819* deletion construct which consists of a hygromycin resistance cassette flanked by the left and right border of the *UMAG_05819* gene. The left border and right border of *UMAG_05819* were PCR amplified from SG200 gDNA with primers NL26/NL27 and NL28/NL29. The hygromycin resistance cassette was obtained from SfiI digest of pHwtFRT. The three fragments were integrated into the EcoRV linearized pJET backbone via Gibson assembly.

- p123 (Aichinger *et al.*, 2003): Contains the *gfp* gene under control of the *otef*-promoter and *nos* terminator as well as the *U. maydis* carboxin resistant *ip* allele ($ip^R$). p123 served as backbone to insert constructs ectopically into the *U. maydis ip* locus.

- pNL7 (p123-Pstp2-stp2): This p123-derived plasmid contains the *stp2* gene under control of the *stp2* promoter and the *nos* terminator. The promoter and gene sequence of *stp2* were PCR amplified from SG200 gDNA with primers NL57/NL58. The resulting PCR product was integrated into the p123 SphI/NotI backbone via Gibson assembly.

- pNL8 (p123-Pstp3-stp3): This p123-derived plasmid contains the *stp3* gene under control of the *stp3* promoter and the *nos* terminator. The promoter and gene sequence of *stp3* were PCR amplified from SG200 gDNA with primers NL65/NL66. The resulting PCR product was integrated into the p123 SphI/NotI backbone via Gibson assembly.

- pSW20 (p123-Pstp4-stp4): This p123-derived plasmid contains the *stp4* gene under control of the *stp4* promoter and the *nos* terminator. The promoter and gene sequence of *stp4* were PCR amplified from SG200 gDNA with primers SW64/SW65. The resulting PCR product was integrated into the p123 KpnI/NotI backbone. Kindly provided by Sarah Winterberg.

- p123-mCherry-HA (T. Brefort, unpublished): The p123 derivative allows the expression of *mCherry* with a C-terminal HA affinity tag under the control of the *otef* promoter and the *nos* terminator. For stable integration, the plasmid was cut using SspI or Age1 and integrated into the *U. maydis ip* locus.

- pNL12 (p123-Pstp2-stp2-HA): p123-mCherry-HA-derived plasmid for the expression of *stp2–HA* under control of the *stp2* promoter and the *nos* terminator. The promoter and gene sequence of *stp2* were PCR amplified from SG200 gDNA with primers NL57/NL74. The resulting PCR product was integrated into the p123-mCherry-HA SphI/XbaI backbone via Gibson assembly.

- pNL14 (p123-Pstp3-stp3-HA): p123-mCherry-HA-derived plasmid for the expression of *stp3–HA* under control of the *stp3* promoter and the *nos* terminator. The promoter and gene sequence of *stp3* were PCR amplified from SG200 gDNA with primers NL65/NL72. The resulting PCR product was integrated into the p123-mCherry-HA backbone SphI/XbaI via Gibson assembly.

- pSW23 (p123-Pstp4-stp4-HA): p123-mCherry-HA-derived plasmid for the expression of *stp4–HA* under control of the *stp4* promoter and the *nos* terminator. The promoter and gene sequence of *stp4* were PCR amplified from SG200 gDNA with primers SW64/SW76. The resulting PCR product was integrated into the p123-mCherry-HA KpnI/XbaI backbone. Kindly provided by Sarah Winterberg.

- pNL27 (p123-Potef-stp2-HA): p123-mCherry-HA-derived plasmid for the expression of *stp2–HA* under control of the *otef* promoter and the *nos* terminator. The promoter and gene sequence of *stp2* were PCR amplified from SG200 gDNA with primers NL188/NL74. The resulting PCR product was integrated into the p123-mCherry-HA Nhe1/XbaI backbone via Gibson assembly.

- pNL28 (p123-Potef-stp3-HA): p123-mCherry-HA-derived plasmid for the expression of *stp3–HA* under control of the *otef* promoter and the *nos* terminator. The promoter and gene sequence of *stp3* were PCR amplified from SG200 gDNA with primers NL189/NL72. The resulting PCR product was integrated into the p123-mCherry-HA backbone NheI/XbaI via Gibson assembly.

- pNL29 (p123-Potef-stp4-HA): p123-mCherry-HA-derived plasmid for the expression of *stp4–HA* under control of the *otef* promoter and the *nos* terminator. The promoter and gene sequence of stp4 were PCR amplified from SG200 gDNA with primers NL190/NL191. The resulting PCR product was integrated into the p123-mCherry-HA NheI/XbaI backbone.

- pNL13 (p123-Pstp2-stp2-mCherry-HA): p123-mCherry-HA-derived plasmid for the expression of *stp2–mCherry-HA* under control of the *stp2* promoter and the *nos* terminator. The promoter and gene sequence of *stp2* were PCR amplified from SG200 gDNA with primers NL57/NL73. The resulting PCR product was integrated into the p123-mCherry-HA BmtI/XmaI backbone via Gibson assembly.

- pNL15 (p123-Pstp3-stp3-mCherry-HA): p123-mCherry-HA-derived plasmid for the expression of *stp3–mCherry-HA* under control of the *stp3* promoter and the *nos* terminator. The promoter and gene sequence of *stp3* were PCR amplified from SG200 gDNA with primers NL65/NL71. The resulting PCR product was integrated into the p123-mCherry-HA BmtI/XmaI backbone via Gibson assembly.

- pSW24 (p123-Pstp4-stp4-mCherry-HA): p123-mCherry-HA-derived plasmid for the expression of *stp4–mCherry-HA* under control of the *stp4* promoter and the *nos* terminator. The promoter and gene sequence of *stp4* were PCR amplified from SG200 gDNA with primers SW64/SW77. The resulting PCR product was integrated into the p123-mCherry-HA KpnI/XmaI backbone. Kindly provided by Sarah Winterberg.

- pLL36 (Lo Presti *et al.*, 2016): Plasmid containing Avitag-3HA fused to a hygromycin resistance cassette for tagging effectors endogenously with AvitagHA.

- pLL36corr (HA corrected): pLL36-derived plasmid was generated to replace the 3HA in pLL36 with HA. HA was PCR amplified from pLL36 with primers NL41/NL42. The resulting PCR product was integrated into pLL36 AscI/MfeI via Gibson assembly.

- pNL9 (pJET-stp2-Avitag-HA): The pJet-derived plasmid was generated to create a strain expressing Avi-HA-tagged Stp2. The ORF of *stp2* was PCR amplified from SG200 gDNA with primers NL60/NL61 and downstream of the stop codon of the *stp2* gene (3'UTR) was amplified with primers NL62/63. The Avitag-HA-Hygromycin fragment was obtained from AgeI/StuI digest of pLL36corr. The three fragments were integrated into the EcoRV linearized pJET backbone via Gibson assembly.

- pNL10 (pJET-stp3-Avitag-HA): pJet-derived plasmid was generated to create a strain expressing Avi-HA-tagged Stp3. The ORF of *stp3* was PCR amplified from SG200 gDNA with primers NL67/NL68 and downstream of the stop codon of the *stp3* gene (3'UTR) was amplified with primers NL69/70. The Avitag-HA-Hygromycin fragment was obtained from AgeI/StuI digest of pLL36corr. The three fragments were integrated into the EcoRV linearized pJET backbone via Gibson assembly.

- pSW25 (pJET-stp4-Avitag-HA): pJet-derived plasmid was generated to create a strain expressing Avi-HA-tagged Stp4. The ORF of *stp4* was PCR amplified from SG200 gDNA with primers SW78/SW79 and downstream of the stop codon of

the *stp4* gene (3'UTR) was amplified with primers SW80/SW81. The Avitag-HA-Hygromycin fragment was obtained from AgeI/StuI digest of pLL36corr. The three fragments were integrated into the EcoRV linearized pJET backbone via Gibson assembly.

### Plasmids for the transformation of *S. cerevisiae*

- pGBKT7 (Clontech): The pGBKT7 vector expresses proteins fused to the GAL4 DNA binding domain (DNA-BD). pGBKT7 also contains the T7 promoter, a c-Myc epitope tag, and a MCS. The vector carries a Kanamycin resistance gene ($Kan^r$) for selection in *E. coli* and the *TRP1* nutritional marker for selection in yeast.

- pGBKT7-stp1:pGBKT7-derived plasmid contains *stp1* without secretion signal that was amplified from SG200 gDNA using the primers NL174/NL175. The resulting PCR product was integrated into the empty pGBKT7 NdeI/NotI vector.

- pGBKT7-stp3: pGBKT7-derived plasmid contains *stp3* without secretion signal that was amplified from SG200 gDNA using the primers NL176/NL177. The resulting PCR product was integrated into the empty pGBKT7 NdeI/NotI vector.

- pGBKT7-pep1: This pGBKT7-derived plasmid contains *pep1* without secretion signal that was amplified from SG200 gDNA using the primers NL180/NL181. The resulting PCR product was integrated into the empty pGBKT7 NdeI and NotI vector.

- pGADT7 (Clontech): The pGADT7 vector expresses proteins fused to a GAL4 activation domain (AD). The GAL4 AD fusion contains an N-terminal nuclear localization signal that targets the protein to the yeast nucleus, and a HA Tag, located between the GAL4 AD and the protein of interest. The vector carries an ampicillin resistance gene ($Amp^r$) for selection in *E. coli* and a *LEU2* nutritional marker for selection in yeast.

- pGAD-stp3: This pGADT7-derived plasmid contains a codon optimized version of *stp3* without secretion signal that was PCR amplified using the primers NL184/NL185. The resulting PCR product was integrated into the empty pGADT7 NdeI vector.

- pGAD-stp4: This pGADT7-derived plasmid contains *stp4* without secretion signal that was PCR amplified from SG200 cDNA using the primers NL143/NL144. The resulting PCR product was integrated into the empty pGADT7 NdeI vector.

- pGAD-pep1: This pGADT7-derived plasmid contains *pep1* without secretion signal that was PCR amplified from SG200 gDNA using the primers NL145/NL146. The resulting PCR product was integrated into the empty pGADT7 NdeI vector.

- pYEA (Sandrock and Egly, 2001): The pYEA vector expresses proteins under the control of the phosphoglycerate kinase promoter. The vector carries an ampicillin resistance gene ($Amp^r$) for selection in *E. coli* and a *ADE2* nutritional marker for selection in yeast.

- pYEA-myc-pep1: pYEA-derived plasmid for the expression of *myc-pep1*. *myc-pep1* was PCR amplified from SG200 gDNA with primers NL122/NL94. The *myc* sequence was part of the NL122 primer. The resulting PCR product was integrated into the pYEA XmaI vector.

- pYEA-myc-stp4: pYEA-derived plasmid for the expression of *myc-stp4*. *myc-stp4* was PCR amplified from SG200 cDNA with primers NL178/NL172. The resulting PCR product was integrated into the pYEA-myc-pep1 NdeI/EcoRI vector.

- pYEA-stp3-myc: pYEA-derived plasmid for the expression of *stp3-myc*. *stp3-myc* was PCR amplified from pGAD-stp3 with primers NL165/NL166. The *myc* sequence was part of the NL166 primer. The resulting PCR product was integrated into the pYEA SalI vector.

- pYEA-myc-pep1 myc-stp3: pYEA-myc-pep1-derived plasmid for the expression of *myc-stp3*. *myc-stp3* was PCR amplified from pGBKT7-stp3 with primers NL176/NL177. The resulting PCR product was integrated into the pYEA-myc-pep1 AgeI vector.

## 4.4 Microbiological methods

### 4.4.1 Competent cell preparation and transformation of *E. coli*

The preparation of competent *E. coli* cells and their chemical transformation were modified from Cohen *et al.* (1972). To obtain chemo-competent bacterial cells, 1 ml of an overnight culture was diluted in 100 ml dYT medium supplemented with 10 mM $MgCl_2$ and 10 mM $MgSO_4$. Cultures were incubated at 37°C at 200 rpm until the $OD_{600}$ value reached 0.5-0.6. After incubating on ice for 30 minutes, the cells were pelleted by centrifugation at 3,000 rpm for 8 minutes at 4°C and resuspended in 33 ml of ice-cold RF1-solution. After incubating again for 30 minutes on ice, the cells were pelleted by centrifugation at 300 rpm for 8 minutes at 4°C. The cell pellet was resuspended in 5 ml ice-cold RF2 solution and incubated for 30 minutes on ice. 50 $\mu$l aliquots of competent cell suspension were shock-frozen in 1.5 ml microcentrifuge tubes and subsequently stored at -80°C.

| Solution | Composition | Notes |
|---|---|---|
| RF1-solution | 100 mM Rubidium chloride<br>50 mM Manganese(II) chloride × 4 $H_2O$<br>30 mM Potassium acetate<br>10 mM Calcium chloride × 2 $H_2O$<br>15% (w/v) Glycerol | pH was adjusted to 5.8 (glacial acetic acid)<br>and sterile filtered (store at 4°C) |
| RF2-solution | 10 mM MOPS<br>10 mM Rubidium chloride<br>10 mM Calcium chloride × 2 $H_2O$<br>15% (w/v) Glycerol | pH was adjusted to 5.8 (NaOH)<br>and sterile filtered (store at 4°C) |

For the transformation, 50 $\mu$l aliquots of competent *E. coli* cells were thawed on ice and subsequently 1-5 ng plasmid DNA or 2 $\mu$l ligation mixture were added. The samples were gently mixed and incubated on ice for 20 minutes. The mixture was then heat-shocked at 42°C for 30 seconds and immediately cooled on ice. 200 $\mu$l of dYT medium were added and cells were incubated at 37°C and 900 rpm for 30 minutes (ampicillin resistance) or 1 hour (kanamycin resistance). Finally, the transformation mixture was plated on YT agar plates containing the antibiotic used for selection and incubated overnight at 37°C.

### 4.4.2 Protoplast preparation and transformation of *U. maydis*

Protoplast preparation and transformation of *U. maydis* strains was performed as described in Schulz *et al.* (1990). *U. maydis* cells were grown overnight in $YEPS_{Light}$ medium at 28°C and 200 rpm. In the morning, cell cultures were diluted to a cell density of $OD_{600}$ 0.1-0.2 and grown to an $OD_{600}$ of 0.8-1.0. Cells were harvested by centrifugation at 4°C for 5 minutes at 3,000 rpm, washed in 25 ml SCS and resuspended

in 2 ml SCS containing 3.5 mg/ml Novozyme. Cells were pelleted by centrifugation at 4°C for 5 minutes at 3,000 rpm, washed in 25 ml SCS buffer and resuspended in 2 ml SCS buffer containing 3.5 mg/ml Novozyme. To digest the cell wall, cells were incubated for approximately 5-10 minutes at room temperature, which was monitored under the microscope. When approximately 30-50% of the cells lost the cigar-shape and rounded up, the reaction was stopped and the cells were washed three times with 10 ml ice cold SCS. Subsequently, the protoplasts were centrifuged at 2,400 rpm at 4°C for 5 minutes. Following, protoplasts were washed with ice cold STC buffer and again centrifuged at 2,400 rpm at 4°C for 5 minutes. Finally, the resulting protoplast pellet was carefully resuspended in 0.5 ml of ice-cold STC buffer and 60 $\mu$l protoplast aliquots were filled into pre-cooled 1.5 ml microcentrifuge tubes and stored at -80°C.

For the transformation of *U. maydis*, the protoplast aliquot was thawed on ice and 1$\mu$l heparin (stock solution 15 mg/ml) and up to 10 $\mu$l of DNA (3-5 $\mu$g) were added. The mixture was gently flicked and incubated for 10 minutes on ice. Afterwards, 500 $\mu$l STC/PEG were added and after gently mixing, the protoplasts were incubated for another 15 minutes on ice. The transformation mixture was carefully plated on a freshly prepared regeneration agar plate consisting of a 10 ml bottom layer containing 2× selection antibiotic and a 10 ml top layer without selection antibiotic. Plates were incubated at 28°C for 4-7 days until colonies appeared. These were singled and grown on PD agar plates containing the respective antibiotic. From there, single colonies were picked, saved on PD-plates and used for DNA extraction.

| Solution | Composition | Notes |
|---|---|---|
| SCS solution 1 | 0.6% (w/v) Sodium citrate × $H_2O_2$ (f.c. 20 mM)<br>18.2% (w/v) Sorbitol (f.c. 1 M) | Dissolve each in $H_2O_{bid}$<br>Add enough solution 2 |
| SCS solution 2 | 0.4% (w/v) Citric acid × $H_2O$ (f.c. 20 mM)<br>18.2% (w/v) Sorbitol (f.c. 1 M) | to solution 1 to reach pH 5.8<br>and autoclave |
| STC solution | 10 mM Tris-Cl, pH 7.5<br>100 mM CaCl2<br>1 M Sorbitol | Dissolve in $H_2O_{bid}$<br>and sterile filtrate |
| STC/PEG solution | 60.0% (v/v) STC-buffer<br>40.0% (w/v) PEG | Mix and sterile filtrate |
| Regeneration agar | 1.0% (w/v) Yeast-Extract<br>0.4% (w/v) Peptone<br>0.4% (w/v) Sucrose<br>18.2% (w/v) Sorbitol (f.c. 1 M)<br>1.5% (w/v) Agar | Dissolve in $H_2O_{bid}$<br>and autoclave |

### 4.4.3 Transformation of *S. cerevisiae*

Yeast strains were grown overnight in YEPD at 28°C. At the next day the culture was diluted into 3 ml fresh medium per transformed sample and incubated until reaching an $OD_{600}$ of 0.8. After mixing and centrifuging for 5 minutes at 4,000 g the supernatant was removed and the pellet was resuspended in 50 $\mu$l yeast transformation buffer.1,5$\mu$g plasmid DNA was added to the prepared yeast cells and gently mixed before being incubated at 42°C for 1 hour. 50 $\mu$l of YEPD were added to the cell solution before spreading everything on the according selection medium.

| Solution | Composition |
|---|---|
| Yeast transformation solution | 60% PEG<br>4 M LiAC<br>1 M DTT<br>$H_2O_{bid}$ |

## 4.5 Molecular biological methods

### 4.5.1 *In vitro* modification of nucleic acids

The concentration of nucleic acids was determined by photometry. Photometric measurements were performed using a NanoDrop 2000 spectrophotometer (Life Technologies GmbH, Darmstadt, Germany).

#### 4.5.1.1 Restriction of DNA

The restriction of DNA fragments was performed with type II restriction endonucleases (NEB) for 2-16 hours at enzyme-specific temperatures. The amount of digested DNA ranged from 0.5 $\mu$g to 5 $\mu$g. A common digestion reaction was composed as follows:

| |
|---|
| 0.5 - 5 $\mu$g Plasmid DNA |
| 2 $\mu$l Enzyme-specific 10× NEB buffer (1-4) |
| 2 $\mu$l 10× BSA |
| 0.5 U (units) Restriction enzyme |
| Add $H_2O_{bid}$ to 20 $\mu$l |

#### 4.5.1.2 Gibson assembly

Cloning of plasmids was done as described in Gibson *et al.* (2009) using 2× Gibson Assembly Master Mix (NEB). For the Gibson assembly, 10 $\mu$l of 2× Gibson Assembly

Master Mix were incubated together with 50-100 ng linearized plasmid backbone and two to three times the amount of the DNA fragments and $H_2O_{bid}$ in a final volume of 20 $\mu$l. The mixture was incubated at 50°C for 15 to 60 minutes, depending on number of fragments being assembled. Subsequently, 2 $\mu$l of the generated product were directly transformed into competent *E. coli* cells.

#### 4.5.1.3 Polymerase chain reaction

For the amplification of DNA fragments via polymerase chain reaction (PCR) (Mullis *et al.*, 1986). The Phusion Hot Start High Fidelity DNA-Polymerase (Thermo Fisher Scientific) was used. The PCR reactions were usually set up to a 50 $\mu$l reaction volume.

| PCR approach with Phusion DNA polymerase |
|---|
| 50 ng Template DNA |
| 250 $\mu$M dNTPS (1:1:1:1 ratio) |
| 1 $\mu$M Primer 1 (binds on 5' Strand) |
| 1 $\mu$M Primer 2 (binds on 3' Strand) |
| 0.5 U Phusion DNA polymerase |
| 1× Concentrated HF buffer (Thermo Fisher Scientific) |

The respective PCR program used is represented by the following scheme: Initial denaturation - [denaturation - annealing - elongation]×number of cycles - final elongation. A common program was: 98°C/1 minute - [98°C/10 seconds - 55-74°C/20 seconds - 72°C/20 seconds/kb]×35 cycles - 72°C/7 minutes. The elongation time was chosen based on the expected fragment size and rate of synthesis by the polymerase used. The annealing and melting temperatures of the oligonucleotides were calculated using the Clone Manager 9.0 software (Sci-Ed-Software, Denver, CO, US) *in silico*. All PCR reactions were performed in a TProfessional Standard Gradient Thermocycler (Biometra, Göttingen, Germany).

#### 4.5.1.4 Sequencing of nucleic acids

Sequencing of plasmids and PCR products was carried out by Eurofins MWG Synthesis (Eurofins Genomics). DNA sequencing results were analyzed using Clone Manager 9.0 software (Sci-Ed-Software).

## 4.5.2 Isolation of nucleic acids

### 4.5.2.1 Isolation of plasmid DNA from *E. coli*

For plasmid DNA isolation from *E. coli*, the Qiagen QIAprep Spin Miniprep Kit was used according to the manufacturer's protocol.

### 4.5.2.2 Isolation of genomic DNA from *U. maydis*

For the isolation of genomic DNA (gDNA) from *U. maydis*, 2 ml of a thickly grown *U. maydis* overnight culture were transferred in a 2 ml microcentrifuge tube from where 6 $\mu$l were dropped on a PD plate to preserve the according clone. Subsequently, the culture was pelleted at 13,000 rpm for 1 minute. After discarding the supernatant, 300 mg of glass beads, 400 $\mu$l *Ustilago*-lysis buffer and 500 $\mu$l of TE-phenol/chloroform were added to the cell pellet. The cells were then lysed on a Vibrax-VXR shaker (IKA, Staufen, Germany) at 2,500 rpm for 20 minutes. This was followed by 15 minutes of centrifugation at 13,000 rpm, during which the phases separated. The upper aqueous phase, containing the extracted DNA, was transferred to a fresh 1.5 ml microcentrifuge tube and precipitated by adding 1 ml of ethanol. After inverting the tube several times, the mixture was centrifuged for 5 minutes at 13,000 rpm. The resulting DNA pellet was washed with 75% ethanol and centrifuged again for 5 minutes at 13,000 rpm. After the supernatant was discarded, the resulting pellet was dried at room temperature and finally dissolved in 50 $\mu$l Tris-EDTA (TE) buffer containing 50 $\mu$g/ml RNaseA by incubation in a Thermomixer (Eppendorf, Hamburg, Germany) at 55°C and 1,200 rpm for 15 minutes. The extracted DNA was stored at 4°C.

| Solution | Composition | Notes |
|---|---|---|
| *Ustilago*-lysis buffer | 2% (v/v) Triton X-100<br>1% (w/v) SDS 100 mM NaCl<br>10 mM Tris-Cl, pH 8.0<br>1 mM EDTA | Dissolve in $H_2O_{bid}$ |
| TE-phenol/chloroform | Mixture of phenol (in TE-buffer)<br>and chloroform in a 1:1 ratio | |

### 4.5.2.3 RNA extraction

For the isolation of total RNA from infected maize tissue, pooled plant material of each sample was ground to a fine powder in liquid nitrogen using a Retsch CryoMill (Retsch GmbH, Haan, Germany) with a 50 ml grinding beaker and a 20 mm grinding ball. For each sample, the machine was precooled for 30 seconds followed by 60 seconds of grinding

at 20 Hz. The plant powder was kept at -80°C. To extract the RNA approximately 500 mg of powder was resuspended in 1 ml TRIzol reagent (Life Technologies GmbH). After centrifugation of the samples at 13,300 rpm for 10 minutes, the supernatant was transferred to a fresh reaction tube and 200 $\mu$l of chloroform were added. The samples were shortly vortexed and incubated for 10 minutes at room temperature. After a centrifugation step at 13,300 rpm for 10 minutes, the upper aqueous phase was transferred to a fresh 1.5 ml reaction tube containing 500 $\mu$l isopropanol. The samples were incubated at room temperature for 10 to 30 minutes. For precipitation of the RNA, the tube was centrifuged at 13,300 rpm for 15 minutes and the supernatant was discarded. After a washing step with 1 ml 75% ethanol and centrifugation at 13,300 rpm for 10 minutes, the supernatant was discarded and the pellet was dissolved in 89 $\mu$l of RNase free $H_2O$ at 55°C for 10 minutes. To eliminate genomic DNA contamination, the Ambion Turbo DNA-free Kit (Life Technologies GmbH) was used according to the manufacturers' protocol. The total RNA was further purified using the RNeasy Mini Kit (Qiagen) and subjected to quality control with an Agilent 2100 Bioanalyzer (Agilent, Santa Clara, CA, USA) according to the instructions of the Agilent RNA 6000 Nano Assay Protocol. Sequencing for the RNAseq dataset was done at the Cologne Center for Genomics, Cologne, Germany.

## 4.5.3 Separation and detection of nucleic acids

### 4.5.3.1 Agarose gel electrophoresis

Agarose gel electrophoresis was performed for a size-specific separation of nucleic acids. Depending on the on the size of the fragments to be separated agarose gels of 0.8-2.0% agarose concentration were prepared. The respective amount of agarose was dissolved in 1× TAE buffer by boiling in a microwave. After cooling down to ~60°C, ethidium bromide (f.c. 0.25 $\mu$g/ml) was added and the gel was poured into an appropriate gel casting tray. After the gel solidified, it was transferred into a running gel chamber and covered with 1× TAE buffer. Samples were mixed with non-denaturing loading dye, loaded on the gel and separated by applying a constant voltage of 90-120 V. DNA was visualized by UV irradiation at 254 nm on a UV table (2UV Transilluminator, UVP, Upland, CA, USA) and documented using the UV solo TS Imaging system (Biometra GmbH, Göttingen, Germany).

| Solution | Composition | Notes |
|---|---|---|
| 50× TAE buffer | 2 M Tris base<br>2 M Acetic acid<br>50 mM EDTA, pH 8.0 | Dissolve in $H_2O_{bid}$ |

#### 4.5.3.2 DNA blotting and hybridization (Southern analysis)

For Southern analysis (Southern, 1975), 10 $\mu$l of genomic DNA, isolated as described in chapter 4.5.2.2, was treated with the respective restriction enzyme over night. The restriction enzyme was selected in order to yield fragment sizes of the locus that define a distinguishable size difference between transformed locus of interests and corresponding wild type locus. Digestions were separated on a 1x TAE 0.8% agarose gel for ~3 hours at 90 V. Depurination of large fragments was done by incubating the gel in 0.25 N HCl for 15 minutes and subsequently neutralizing it in 0.4 M NaOH for 15 minutes to facilitate the transfer of big DNA fragments during the blotting process. Subsequently, the DNA was transferred from the gel to a nylon membrane (Hybond-N+, GE Healthcare). The transfer was facilitated by a capillary blot with 0.4 M NaOH as transfer solution. Afterwards, the membrane was placed into a hybridization tube, in which the subsequent steps were carried out. The membrane was pre-hybridized with 20 ml Southern hybridization buffer in a hybridization oven (HB-1000 Hybridizer, VWR Darmstadt, Germany) at 68°C for 30 minutes. Immobilized DNA was detected by DIG-labeled probes. Probes were generated by labeling DNA fragments with PCR-based DIG-High Prime labeling mix (Roche) according to the manufacturers' protocol. Probes were denatured at 95°C for 10 minutes and added to 20 ml pre-warmed Southern hybridization buffer (68°C). After prehybridization of the membrane with Southern hybridization buffer for 30 minutes, the buffer was removed and the prepared probe solution was added. Hybridization was performed at 68°C for at least 6 hours. Afterwards, the membrane was washed twice with Southern wash buffer at 68°C for 15 minutes. The subsequent steps were performed at room temperature. The membrane was washed once with DIG wash buffer for 5 minutes followed by a 30 minutes blocking step with DIG2 buffer. After blocking, 20 ml of the DIG antibody solution was added. Membrane and antibody solution were incubated for at least 30 minutes followed by three 15 minutes washing steps in DIG wash buffer to remove residual antibody. The membrane was equilibrated for 5 minutes in DIG3 buffer, followed by a 5 minutes incubation in CDP star solution. In the next step, the membrane was incubated for 15 minutes at 37°C to activate the light emitting reaction. Finally the DNA fragments were visualized using X-ray films (CEA, Hamburg, Germany) and the Agfa CP 1000 film processor (AGFA HealthCare, Mortsel, Belgium).

| Buffer | Composition | Notes |
|---|---|---|
| Southern hybridization buffer | 50% (v/v) Na-phosphate buffer, pH 7.0<br>35% (v/v) 20% SDS | Dissolve in $H_2O_{bid}$ |
| Southern wash buffer<br>5.0% (v/v) 20% SDS (f.c. 1.0%) | 10.0% (v/v) 1 M Na-phosphate buffer, pH 7.0 | Dissolve in $H_2O_{bid}$ |
| 1 M Na-phosphate buffer | Solution 1: 1 M $Na_2HPO_4$<br>Solution 2: 1 M $NaH_2PO_4 \times H_2O$ | Add Solution 2 to Solution 1<br>until pH reaches 7.0 in $H_2O_{bid}$ |
| DIG wash buffer | 0.3% (v/v) Tween-20 in DIG1 | |
| Anti-DIG antibody solution | Anti-DIG AB 1:10,000 in DIG2 | |
| DIG1 (1×) | 0.1 M Maleic acid 0.15 M NaCl | Dissolve in $H_2O_{bid}$<br>and adjust pH to 7.5 (NaOH) |
| DIG2 (1×) | 1% (w/v) Milk powder in DIG1 | |
| DIG3 (1×) | 0.1 M Tris-HCl<br>0.1 M NaCl<br>50.0 mM $MgCl_2$ | Dissolve in $H_2O_{bid}$,<br>adjust pH to 9.5 (Tris-HCl)<br>and sterile filtrate |
| CDP-Star Solution | CDP-Star (Roche) 1:100 in 10 ml DIG3 | |

## 4.6 Protein and biochemical methods

### 4.6.1 Protein extraction and immunoprecipitation from infected plant material

Plant samples were harvested by cutting and collecting the infected plant parts and storing them immediately in liquid nitrogen. Frozen plant material was ground to a fine powder using a prechilled mortar and pestle or the Retsch CryoMill. Resulting plant powder was stored in liquid nitrogen or at -80°C. For protein extraction a fresh prechilled mortar was placed on ice and filled with ice-cold extraction buffer and approximately 100 $\mu$l of fine glass beads or silica spheres were added. The ratio of sample to buffer was 1:4 (1 ml of powder to 4 ml of buffer). Subsequently frozen plant material was transferred to the extraction buffer and quickly regrinded in the buffer with a chilled pestle. The samples were then transferred to a fresh 5 ml tubes and incubated on ice for 30 minutes. Afterwards the samples were centrifuges at 4°C for 15 minutes at 20,000 g and the resulting supernatant was transferred into a fresh tube. 12 $\mu$l of magnetic beads (Pierce Anti-HA magnetic beads, Thermo Fisher Scientific) were added and the sampels were incubate at 4°C with rotation for 1 hour. The magentic beads were separated on a magnetic separator and washed 5 times in extraction buffer. Finally, the beads were resuspendendin 1x SDS-PAGE loading buffer and boiled at 95° for 5 minutes to elute the proteins. After a brief centrifugation, the supernatant was analyzed by SDS PAGE and western blot.

| Solution | Composition | Notes |
|---|---|---|
| HNN lysis buffer stock | 50 mM HEPES<br>150 mM NaCl<br>5 mM EDTA | Steril filter the stock solution |
| Added to HNN Buffer | Protease inhibitor cocktail tablet (Roche)<br>0.1% NP 40<br>1.0% Polyvinylpyrrolidon (PVPP) | Let PVPP dissolve for at least 30 minutes before adding NP40 and the inhibitor tablet |

### 4.6.2 Sample preparation for mass spectrometry

Plant lysate samples were prepared and proteins were immunoprecipitated with 12 $\mu$l of magnetic beads as described in the previous section. After separating the beads on a magnetic separator, they were washed three times with 700 $\mu$l of 100 mM Ammoniumbicabonate (ABC). In the next step beads were resuspended in 240 $\mu$l of 100 mM ABC from which 40 $\mu$l (40/240 $\mu$l equals 2/12 $\mu$l starting volume of beads) were taken as a control to be analyzed by western blot. To the remaining sample 100 $\mu$l of elution buffer 1 were added, the sample was vortexed and incubated for 30 minutes on a thermomixer at 27° Cat 1200 rpm. During this, proteins are released from the beads due to the trypsin digest. Therefore, the beads were separated and the supernatant was transfered to a fresh 2 ml tube. The beads were resuspended in 40$\mu$l elution buffer 2 and separated on a magnetic separator. The collected supernatant was combined with the first eluate in the fresh tube. After repeating this one more time, the tube was vortexed and left over night at room temperature.

At the next day, 40 $\mu$l of iodoacetamid (5mg/ml) were added, the sample was vortexed and incubated for 30 minutes in the dark. The sample was acidified to a pH $< 2$ by adding 100 $\mu$l of 5% trifluoroacetic acid (TFA), which was subsequently ensured via an pH stripe.

This was followed by a C18 Microspincolumn purification. For the subsequent C18 Microspincolumn purification, C18 Micro SpinColumns (The Nest Group, Southborough, USA) were assembled with 2 ml conical microcentrifuge tubes and conditioned with 150 $\mu$l buffer 1. After centrifuging for 30 seconds at 1,600 rpm, this was repeat a second time. Next, the columns were equilibrated three times with 150 $\mu$l of buffer 2 with centrifuging at 2,400 rpm for 30 seconds in between. The column was transferred to a fresh conical tube and loaded with the protein sample. After centrifuging at 1,800 rpm for 2 minutes, the flow-through was reloaded and centrifuged again. The column was washed three times with 150 $\mu$l of buffer 3 with centrifugations at 2,400 rpm for 30 seconds in between. After that the column was transferred to a new 2 ml tube and the bound peptides were eluted by loading three time 100 $\mu$l of buffer 4 with centrifugations at 1,600 rpm for 30 seconds in between. The eluted peptides were subsequently concentrated using the Savant

SPD131DDA SpeedVac (Thermo Fisher Scientific) at high pressure and 45°C for 2 hours. Peptides were resuspendend in 25 $\mu$l of buffer 5, vortexed for 10 sec and treated with 20 pulses of ultrasonication using the UP200St (Hielscher Ultrasonics, Teltow, Germany) with an amplitude of 20% and a pulse rate of 0.5 seconds. After vortexing again the sample was transferred to a chromatography vial (J.G. Finneran, Vineland, NJ, USA) and analyzed by LC-MS/MS (done by T. Glatter from the core facility for mass spectrometry and proteomics, Max Planck Institute for Terrestrial Microbiology, Marburg, Germany).

| Buffer for protein digestion | Composition |
|---|---|
| 1 M Ammoniumbicarbonate | |
| 8 M urea in 100 mM Ammoniumbicarbonate | |
| Elution buffer 1 | 1.6 M Urea<br>100 mM Ammoniumbicabonate<br>10 $\mu$g/ml Trypsin |
| Elution buffer 2 | 1.6 M urea<br>100 mM Ammoniumbicabonate<br>1 mM TCEP (stock is 0.2 M) |
| 27 mM Iodacetamide | |

| Buffer for C18 purification | Composition |
|---|---|
| Buffer 1 | Acetonitrile |
| Buffer 2 | 0.1% TFA |
| Buffer 3 | 5.0% Acetonitrile<br>95.0% Water (v/v)<br>0.1% TFA |
| Buffer 4 | 50.0% Acetonitrile<br>50.0% Water (v/v)<br>0.1% TFA |
| Buffer 5 | 0.15% Formic acid<br>2.00% Acetonitrile |

### 4.6.3 Deglycosylation

The respective fusion proteins were immunoprecipitated from soluble protein extracts from infected maize tissue as described in chapter 4.6.1. After washing the beads, they were suspended in 40$\mu$l of $H_2O_{bid}$ and subsequently treated with either the protein deglycosylation mix or water according to the manufacturers protocol (Protein Deglycosylation Mix II, P6044, NEB) and finally analyzed via western blot.

### 4.6.4 Translocation assay

The assay utilizes transgenic maize lines that express the bacterial biotin ligase BirA in their cytoplasm. BirA has the ability to biotinylate any protein that has a short peptide termed the Avitag. Effectors tagged with an Avitag are biotinylated in case of translocation into the cytoplasm and can then be immunoprecipitated from infected leaves of the BirA plants using streptavidin beads. The assay was conducted as described in Lo Presti *et al.* (2016). The protein extraction and immunoprecipitation from infected plant material was done as described in chapter 4.6.1.

### 4.6.5 Protein extraction from *S. cerevisiae*

In order to check for protein expression of the *S. cerevisiae* strains used the yeast based interaction studies, western blot analysis was performed. For that *S. cerevisiae* was grown in the according selection medium overnight, diluted in the morning in 5 ml and grown to an $OD_{600}$ of 1.0. Cells were pelleted by centriguation at 13,000 rpm for 5 minutes at room temperature and the pellet was immediately resuspendend in 1 ml 1× PBS with 1 mM PMSF. After that the cultures were again centrifuged at 13,000 rpm for 5 minutes at room temperature. The resulting pellets were resuspendend in 30 $\mu$l ESB Buffer and incubated for 3 minutes at 95°C. The cell pellet was disrupted adding 0.3 g glass beads and subsequently shaken for 5 minutes on a Vibrax shaker (IKA, Staufen, Germany) at 1200rpm. Finally, 70 $\mu$l of ESB Buffer were added and samples were incubated for 1 minute at 95°C. The supernatanat was used for western blot analysis.

| Solution | Composition |
|---|---|
| ESB-Buffer | 2.0% (w/v) SDS<br>80 mM Tris/HCl, pH 8.0<br>10.0% (v/v) Glycerol<br>1.5% (w/v) DTTred<br>0.1 mg/ml Bromophenol blue |

### 4.6.6 Secretion assay

For the induction of *b*-filaments in AB33 derivatives the strains were cultivated to an $OD_{600}$ of 0.6 in 100 ml AM (2% glucose) and harvested by centrifugation at 3000 rpm for 5 minutes at room temperature. Subsequently, the cells were washed twice with pre-warmed (28°C) $H_2O_{bid}$ to remove residual medium. The cell pellet was dissolved in 100 ml pre-warmed (28°C) NM (2% glucose) and incubated for approximately 6 hours at 28°C. The formation of *b*-filaments was observed microscopically. After the respective

time, the samples were centriguged at 3,000 rpm for 10 minutes at 4°C. The cell pellets were kept at -20°C and the cell-free supernatant was precipitated with trichloroacetic acid (TCA). For this 20 ml of TCA (100%) were added to 80 ml of supernatant. The samples were kept over night at 4°C. The next day samples were centrifuged at 8,000 g for 2 hours at 4°C. The supernatant was carefully discarded and the samples were washed in 2 ml ice-cold acetone and transferred to a 5 ml microcentrifuge tube. Afterwards they were washed three-times with 5 ml of ice-cold acetone, with centrifugation steps (13,000g, 30 minutes at 4°C) in between. Finally, the pellets were dried at 60°C and subjected to immunoblotting.

### 4.6.7 Co-immunoprecipitation of proteins from *S. cerevisiae*

For the co-immunoprecipitation of the yeast strain with all four complex members the protocol was modified after Gerace and Moazed (2014). *S. cerevisiae* strains were grown overnight SD selection medium medium, diluted in the morning in 250 ml and grown to an $OD_{600}$ of 1.0-2.0. Cells were pelleted by centrifugation at 3,500 g for 5 minutes at 4°C. Afterwards, cells were wash once with 1×TBS. For each strain approximately, 0.5 g cells were transferred to 2ml screw-capped tubes and flash frozen in liquid nitrogen. Transferred cell pellets were weighed just prior to freezing and the weight of each pellet noted. Tubes were stored at -80°C. For the CO-IP, 0.1 ml of ice-cold, freshly prepared 1×Lysis Buffer for each 0.1 g of cells were added to the frozen samples. The cells were thawed by gently flicking and inverting the tubes. Once completely thawed the tubes were kept on ice and 0.3 g of glass beads were added. Using a bead beating instrument the tubes were pulsed for 45 seconds at homogenizing intensity. Afterwards, tubes were placed on ice for 5 minutes before a second 45 second pulse, which was followed by centrifuging the samples at 20,000 g for 5 minutes at 4°C. The resulting supernatant was transferred to a fresh microcentrifuge tube and 25 $\mu$l of Ha-coated magnetic beads were added. Samples were incubated on an end-over-end rotator at 4°C for 2 hours. The following sample preparation for mass spectrometry was done as described in chapter 4.6.2.

| Buffer | Composition |
|---|---|
| 2× Lysis buffer | 100 mM Na-HEPES, pH 7.5<br>400 mM NaOAc, pH 7.5<br>2 mM EDTA<br>2 mM EGTA<br>10 mM MgOAc<br>10% Glycerol |
| 1× Lysis buffer | 1× (2× Lysis Buffer)<br>0.25% NP-40<br>3 mM DTT<br>1 mM PMSF<br>1 Protease inhibitor cocktail tablet |

### 4.6.8 SDS polyacrylamide gel electrophoresis

Protein separation was performed according to Laemmli (1970) by Sodium dodecyl sulfate polyacrylamide gel electrophoresis (SDS-PAGE). Utilizing an electric field denatured proteins get separated according to their size during the SDS-PAGE. For that, protein samples were completely denatured by adding 1× SDS loading dye and incubating for 10 minutes at 95°C. Hereby, the proteins get negatively charged which correlates with the molecular mass of each protein. SDS polyacrylamide gel were composed of a stacking and separation gel (Mini Protean System, Bio-Rad, Munich). In the stacking gel proteins concentrate before entering the separation gel. There, the proteins are separated according to their molecular weight, smaller proteins migrate faster through the gel than larger proteins. The higher the concentration of acrylamide, the higher is the density of the meshed molecular network. Gels with high acrylamide concentrations are used for separation of small proteins, whereas low percentage gels are for separating large proteins. Samples were loaded on the gel into gel pockets. The separation of proteins was performed with a current of 20 mA until proteins were concentrated in the stacking gel followed by 25 mA for separation. As reference for the molecular weight of the separated proteins the PageRuler Prestained Protein ladder (Thermo Fisher Scientific) was used.

| SDS gel | Composition |
|---|---|
| Stacking gel | 5.00% (v/v) Polyacrylamide<br>0.10 % (w/v) SDS<br>in 125 mM Tris-HCl, pH 6.8<br>0.10 % (w/v) Ammonium persulfate (APS)<br>0.05 % (v/v) Tetramethylethylenediamine (TEMED) |
| Separating gel | 12-15 % (v/v) Polyacrylamide<br>0.10% (w/v) SDS<br>in 375 mM Tris-HCl, pH 8.8<br>0.10% (w/v) Ammonium persulphate<br>0.05% (v/v) TEMED |

| Buffer | Composition | Notes |
|---|---|---|
| 4× SDS-gel loading buffer | 10 ml 1.5 M Tris-HCl pH 6.8<br>30 ml Glycerin<br>6 ml 20% SDS<br>5 mg Bromophenol blue<br>3 g DTT (f.c. 400 mM) | Fill up to<br>50 ml with $H_2O_{bid}$ |
| SDS running buffer | 25 mM Tris-HCl, pH 8.0<br>192 mM glycin<br>4 mM SDS | |

### 4.6.9 Immunological protein detection by chemiluminescence (Western blot)

The semi-dry Trans-Blot Turbo Transfer System (BioRad, Munich, Germany) was used to transfer proteins separated by SDS-PAGE to a PVDF nitrocellulose membrane. The blotting procedure was performed according to the manufacturers' protocol using the Trans-Blot Turbo blotting apparatus as well as the membranes and protein blotting consumables provided for the system. The transfer was performed at 1.3 A and up to 25 V for one mini format gel or at 2.5 A and up to 25 V for two mini format gels. For this the Bio-Rad preprogrammed protocol "Mixed MW (Turbo)" was used by default. The protocol lasts seven minutes and is for proteins with a molecular weight ranging from 5-150 kDa. After the transfer, the membrane was incubated in blocking solution for 1 hour at room temperature. Afterwards the blocking solution was replaced with an antibody solution containing the primary antibody. The membrane was incubated over night at 4°C. The next day the membrane was washed three times for 10 minutes with TBS-T buffer followed by an 1 hour incubation at room temperature in TBS-T buffer containing the secondary antibody. The antibodies used in this study are listed in

Table 4.3. The membrane was washed for three more times with TBS-T buffer for 10 minutes each and then incubated for 5 minutes with ECL chemiluminescent detection reagent (GE Healthcare). The membrane was sealed in a plastic bag and western blots were developed using X-ray films (CEA, Hamburg, Germany) and the Agfa CP 1000 film processor (AGFA HealthCare, Mortsel, Belgium). Depending on the intensity of the signal observed the exposure time ranged from 1-120 minutes.

| Solution | Composition |
|---|---|
| TBS-T | 50 mM Tris-HCl, pH 7.5<br>150 mM NaCl<br>0.1% (v/v) Tween 20 |
| Blocking solution | 5% (w/v) Milk powder in TBS-T |
| Antibody solution | Antibody diluted in 2.5% (w/v) milk powder in TBS-T |

### 4.6.10 Antibodies

Table 4.3 describes the antibodies used in this study.

**Table 4.3:** Antibodies used in this study.

| Antibody | Usage | Manufacturer |
|---|---|---|
| Rabbit anti-HA | Monoclonal primarily antibody from rabbit for HA-protein fusion detection (1:10,000) | Sigma-Aldrich |
| Mouse anti-HA | Monoclonal primarily antibody from mouse for HA-protein fusion detection (1:5,000) | Sigma-Aldrich |
| Mouse anti-myc | Monoclonal primarily antibody from mouse for myc-protein fusion detection (1:10,000) | Sigma-Aldrich |
| Mouse anti-$\alpha$-tubulin | Monoclonal primary antibody from mouse for cell lysis detection (1:2,000) | Sigma-Aldrich |
| Anti-rabbit | Monoclonal secondary antibody from horse for rabbit anti-HA detection (1:10,000) | Cell Signaling Technology |
| Anti-mouse | Monoclonal secondary antibody from horse for mouse anti-HA detection (1:10,000) | Cell Signaling Technology |

## 4.7 Plant methods

### 4.7.1 Cultivation of *Z. mays*

For the conducted infection assays of this thesis the maize variant Early Golden Bantam (EGB) (UrbanFarmers, New York City, NY, USA) was used. ZmPIN1a-YFP were used

for indicated microscopy. Maize lines ZmPIN1a-YFP were provided from Cold Spring Harbor Laboratory.

All corn plants were cultivated in a temperature controlled greenhouse with a light-dark cycle of 28°C for 14 hours and 20°C for 10 hours. During the day phase, the illumination intensity was at least 25 kLux-30 kLux (with additional sunlight up to 90 kLux). For RNAseq experiments, maize plants were grown in a phytochamber (Vötsch Industrietechnik GmbH, Balingen-Frommern, Germany) with the same conditions as described above. In addition, phytochamber daytime phases included a one hour simulation of sunrise (13 hours + 1 hour sunrise) and nighttime phases one hour for the simulation of the sunset (9 hours + 1 hour sunset) (ramping). During daytime phases the humidity was set to 60% and during nighttime phases to 40% . Per pot four corn grains were sowed. Maize plants were grown in Fruhstorfer soil type "T" and watered once a day.

### 4.7.2 Pathogenicity assay

For maize infections, *U. maydis* strains were grown overnight (28°C, 200 rpm) in $YEPS_{Light}$ liquid medium, diluted in the morning and grown to an $OD_{600}$ of 0.8-1.0. Cells were pelleted by centriguation at 3,500 g for 5 minutes at room temperature. Afterwards the $OD_{600}$ was adjusted with sterile $H_2O$ to $OD_{600}$ of 1.

Seven-day-old maize seedlings were infected by injecting the inoculum with a syringe at the base of the plant. Plants used for microscopy were injected approximately 2 cm above the soil. 12 days after plant infection the disease symptoms were scored according to Kämper *et al.* (2006) (Table 4.4).

**Table 4.4:** Classification of symptoms of infected maize seedlings.

| Symptoms | Description |
|---|---|
| Without symptoms | No infection symptoms are visible |
| Chlorosis | The plant displays yellowish discoloration on infected leaves |
| Ligula swelling | The plant displays a slight swelling of the ligula |
| Small tumors | Only few and/or little tumors ($< 1$ mm) are visible |
| Normal tumors | The biggest tumors visible are $> 1$ mm |
| Heavy tumors | The plant displays a change of growth axis as a result of tumor formation |
| Dead plants | The plant died due to the infection with *U. maydis* |

## 4.8 Staining and microscopy

### 4.8.1 Staining methods

#### 4.8.1.1 Sample preparation

Plant samples were harvested at the indicated time points and a small piece of leaf tissue was cut from about 1-2 cm below the infection mark. Tissue pieces were placed directly or following the respective staining method on a glass-slide and covered with $H_2O_{bid}$. They were than analyzed by confocal microscopy.

#### 4.8.1.2 WGA-AF488 and propidium iodide co-staining

To co-stain the fungal hyphae and the plant cell wall in contrasting shades, fungal hyphae were stained with Alexafluor 488, WGA (Invitrogen) and plant cell walls using Propidium Iodide (Sigma-Aldrich). Infected leaf tissue was harvested at 3 dpi and placed into 100% ethanol to remove the chlorophyll. Samples were bleached overnight or until the entire chlorophyll was removed. Next, the ethanol was replaced by 10% KOH and samples were incubated at 85°C for 3-4 hours. The leaves were subsequently washed twice with 1 ml 1× PBS (pH 7.4). The WGA/PI stainingsolution was added and the fully covered samples were incubated for 30 minutes. During the incubation the leaves were vacuum infiltrated 3 times for 2 minutes. Leaf samples were washed twice in 1× PBS, then transferred to fresh 1× PBS and stored at 4°C in the dark until being analyzed by confocal microscopy.

| Solution | Composition | Notes |
|---|---|---|
| Propidium iodide stock solution | 10 mg/ml PI in 1× PBS | Store at 4°C |
| WGA-AF488 stock solution | 1 mg/ml in $H_2O_{bid}$ | Store at 4°C in the dark |
| WGA/PI staining solution | 20 $\mu$g/ml Propidium iodide<br>10 $\mu$g/ml WGA-AF488<br>0.02% Tween20 in PBS (pH 7.4) | Store at 4°C in the dark |

#### 4.8.1.3 Calcofluor white staining

Calcofluor white (Sigma-Aldrich) was used to stain fungal hyphae on the leaf surface as it binds to chitin, but is unable to penetrate the plant cuticle. For these leaves, samples were incubated in calcofluor staining solution for 30 sec and subsequently rinsed with $H_2O_{bid}$.

| Solution | Composition | Notes |
|---|---|---|
| Calcofluor stock solution | 10 mg/ml in DMSO | Store at -20°C, protect from light |
| Calcofluor staining solution | Calcofluor stock solution was diluted 1:1,000 in $H_2O_{bid}$ | |

#### 4.8.1.4 Aniline blue staining

For staining, plant-derived callose depostions, infected leaf material harvested at 1-2 dpi were rinsed twice with 50% ethanol and once with 0.1 M $Na_2HPO_4$ at room temperature. Afterwards, the samples were incubated for 30 minutes in 0.1 M $Na_2HPO_4$ at room temperature. Samples were then placed in freshly prepared 0.05% aniline blue (w/v in 0.1 M $Na_2HPO_4$ ) and incubated for 30-60 minutes in the dark.

#### 4.8.1.5 FM4-64 staining

To stain the plant plasma membrane, infected leaf material was harvested at 1-2 dpi and stained with FM4-64 . An aliquot of stock solution (10 $\mu$ of 1.6 mM FM4-64 in DMSO) was resuspended in 1 ml $H_2O_{bid}$. The plant sample was placed within and it was ensured that it is fully covered with the staining solution. Samples were incubated in the dark for 1-2 hours at room temperature.

### 4.8.2 Microscopy methods

#### 4.8.2.1 Confocal microscopy

Confocal microscopy was performed using a Leica TCS SP8x/WLL (White Light Laser) or a TCS SP5II confocal laser-scanning microscope (Leica, Wetzlar, Germany). The laser channels used for confocal microscopic analysis are listed in Table 4.5. Image data was processed using the Leica Application Suite X, version 3.1.5.

**Table 4.5:** Laser with their respective excitation and detection wavelength.

| Laser | Excitation wavelength | Detection wavelength | Purpose |
|---|---|---|---|
| WLL/Argon | 488 nm | 506-536 nm | AF488 |
| WLL/DPSS | 561 nm | 640-725 nm | PI |
| WLL/Argon | 488 nm | 495-530 nm | GFP |
| 405 diode | 405 nm | 400-550 nm | Autofluorescence |
| 405 diode | 405 nm | 630-655 nm | Aniline blue |
| WLL | 561 nm | 569-665 nm | RFP |
| WLL/DPSS | 514/561 nm | 623-700 nm | FM4-64 |
| 405 diode | 405 nm | 430-550 nm | Calcofluor white |
| WLL | 585 nm | 597-635 nm | mCherry |
| 405 diode | 405 nm | 416-477 nm | Cell wall autofluorescence |
| WLL | 514 nm | 520-550 nm | YFP |

#### 4.8.2.2 mCherry microscopy

The visualization of the mCherry fusion proteins via live cell microscopy was exclusively done with with the Leica TCS SP8×/WLL confocal microscope. Detection was achieved with HyD detector where the detection time was gated (between 0.3 and 6.0 nanoseconds) after the excitation laser pulse. For image deconvolution the HyVolution software package (Leica and Scientific Volume Imaging B.V., Hilversum, Netherlands) was used on highest resolution settings.

#### 4.8.2.3 Plasmolysis of infected plant material

For plasmolysis experiments, infected leaf material was harvested at 2-4 dpi and incubated in a 1 M NaCl or 1 M sorbitol solution for 5-30 minutes. The samples were subsequently analyzed by confocal microscopy.

#### 4.8.2.4 Immuno-transmission electron microscopy

The immuno-transmission electron microscopy (Immuno-TEM) approach where the HA-specific immunostain was performed prior to embedding the SG200stp3-HA infected leaf discs was conducted by K. Snetselaar. For detailed information concerning this method please refer to Professor Karen Snetselaar, Saint Joseph's University, PA, USA.

## 4.9 Bioinformatic methods

### 4.9.1 RNAseq analysis

The RNAseq raw data was provided by the Cologne Center for Genomics, Cologne, Germany. The read mapping, normalization and statistical analysis of differential gene expression was done as described in Lanver *et al.* (2018). Initially, the obtained reads were quality-filtered and mapped against the annotated maize genome using the CLC genomics workbench (Qiagen), version 9.5.3. Afterwards, the data was normalized using the DESeq2 package, version 1.10 (Love *et al.*, 2014) in R, version 3.4.4. Differentially expressed genes, defined as a a doubling or halving of the gene count at an adjusted significance level of $p<0.01$, were identified. They were qualitatively analyzed and displayed as a Venn diagram using the web-based tool InteractiVenn (Heberle *et al.*, 2015). Additionally, differentially expressed genes were submitted to AgriGO, version 2.0, for gene ontology analysis (Tian *et al.*, 2017). Enriched GO terms were selected using Singular Enrichment Analysis (SEA) with the maize genome as background.

### 4.9.2 Miscellaneous software tools and databases

Additional software and databases used during this study included:

- The MIPS PEDANT 3 database to derive *U. maydis* gene and protein sequences, molecular weights and predicted signal peptide length (Mewes *et al.*, 2002).
- Clone Manager (Sci-Ed-Software), version 9.0, was used for planning of cloning strategies as well as amino acid and nucleotide sequence comparisons.
- CLC Main Workbench, version 7.6.4, was utilized to compare amino acid sequence alignments and the orthologs of different smut fungi.
- ApoplastP was used to predict the apoplastic localization of the effector proteins (Sperschneider *et al.*, 2018).
- The SMART (Simple Modular Architecture Research Tool) online tool was deployed to analyze protein domains (Letunic and Bork, 2017).

# References


Ahuja, I., R. Kissen and A. M. Bones (2012). "Phytoalexins in defense against pathogens". *Trends in Plant Science* 17 (2), pp. 73–90.

Aichinger, C., K. Hansson, H. Eichhorn, F. Lessing, G. Mannhaupt, W. Mewes and R. Kahmann (2003). "Identification of plant-regulated genes in *Ustilago maydis* by enhancer-trapping mutagenesis". *Molecular Genetics and Genomics* 270 (4), pp. 303–14.

Andersen, E. J., S. Ali, E. Byamukama, Y. Yen and M. P. Nepal (2018). "Disease resistance mechanisms in plants". *Genes* 9 (7).

Anderson, R. G., D. Deb, K. Fedkenheuer and J. M. McDowell (2015). "Recent progress in RXLR effector research". *Molecular Plant-Microbe Interactions* 28 (10), pp. 1063–72.

Ausubel, F. M., R. Brent, R. E. Kingston, D. D. Moore, J. G. Seidman, J. A. Smith and K. Struhl (1987). *Current protocols in molecular biology*. NY: Wiley.

Ausubel, F. M. (2002). *Short protocols in molecular biology: a compendium of methods from current protocols in molecular biology*.

Banuett, F. and I. Herskowitz (1996). "Discrete developmental stages during teliospore formation in the corn smut fungus, *Ustilago maydis*". *Development* 122 (10), pp. 2965–76.

Banuett, F. and I. Herskowitz (1994). "Morphological transitions in the life cycle of *Ustilago maydis* and their genetic control by the a and b loci". *Experimental Mycology* 18 (3), pp. 247–66.

Barnett, H. L. and F. L. Binder (1973). "The fungal host-parasite relationship". *Annual Review of Phytopathology* 11 (1), pp. 273–92.

Basse, C. W. and G. Steinberg (2004). "*Ustilago maydis*, model system for analysis of the molecular basis of fungal pathogenicity". *Molecular Plant Patholgy* 5 (2), pp. 83–92.

Bellincampi, D., F. Cervone and V. Lionetti (2014). "Plant cell wall dynamics and wall-related susceptibility in plant–pathogen interactions". *Frontiers in Plant Science* 5, p. 228.

Berens, M. L., H. M. Berry, A. Mine, C. T. Argueso and K. Tsuda (2017). "Evolution of hormone signaling networks in plant defense". *Annual Review of Phytopathology* 55 (1), pp. 401–25.

Böhm, H., I. Albert, L. Fan, A. Reinhard and T. Nürnberger (2014). "Immune receptor complexes at the plant cell surface". *Current Opinion in Plant Biology* 20, pp. 47–54.

Bigeard, J., J. Colcombet and H. Hirt (2015). "Signaling mechanisms in pattern-triggered immunity (PTI)". *Molecular Plant* 8 (4), pp. 521–39.

Bölker, M., M. Urban and R. Kahmann (1992). "The a mating type locus of *U. maydis* specifies cell signaling components". *Cell* 68 (3), pp. 441–50.

Boller, T. and G. Felix (2009). "A renaissance of elicitors: perception of microbe-associated molecular patterns and danger signals by pattern-recognition receptors". *Annual Review of Plant Biology* 60 (1), pp. 379–406.

Boudsocq, M. and J. Sheen (2013). "CDPKs in immune and stress signaling". *Trends in Plant Science* 18 (1), pp. 30–40.

Brachmann, A., G. Weinzierl, J. Kamper and R. Kahmann (2001). "Identification of genes in the bW/bE regulatory cascade in *Ustilago maydis*". *Molecular Microbiology* 42 (4), pp. 1047–63.

Brachmann, A, J König, C Julius and M Feldbrügge (2004). "A reverse genetic approach for generating gene replacement mutants in *Ustilago maydis*". *Molecular Genetics and Genomics* 272 (2), pp. 216–26.

Brefort, T., G. Doehlemann, A. Mendoza-Mendoza, S. Reissmann, A. Djamei and R. Kahmann (2009). "*Ustilago maydis* as a pathogen". *Annual Review of Phytophatology* 47, pp. 423–45.

Broomfield, P. L. and J. A. Hargreaves (1992). "A single amino-acid change in the iron-sulphur protein subunit of succinate dehydrogenase confers resistance to carboxin in *Ustilago maydis*". *Current Genetics* 22 (2), pp. 117–21.

Burg, H. A. van den, S. J. Harrison, M. H. Joosten, J. Vervoort and P. J. de Wit (2006). "*Cladosporium fulvum* Avr4 protects fungal cell walls against hydrolysis by plant chitinases accumulating during infection". *Molecular Plant-Microbe Interactions* 19 (12), pp. 1420–30.

Caillaud, M. C., L. Wirthmueller, J. Sklenar, K. Findlay, S. J. Piquerez, A. M. Jones, S. Robatzek, J. D. Jones and C. Faulkner (2014). "The plasmodesmal protein PDLP1 localises to haustoria-associated membranes during downy mildew infection and regulates callose deposition". *PLoS Pathogens* 10 (10), e1004496.

Cao, Y., Y. Liang, K. Tanaka, C. T. Nguyen, R. P. Jedrzejczak, A. Joachimiak and G. Stacey (2014). "The kinase LYK5 is a major chitin receptor in *Arabidopsis* and forms a chitin-induced complex with related kinase CERK1". *eLife* 3.

Castanheira, S. and J. Perez-Martin (2015). "Appressorium formation in the corn smut fungus *Ustilago maydis* requires a G2 cell cycle arrest". *Plant Signaling & Behavior* 10 (4), e1001227.

Cesari, S. (2018). "Multiple strategies for pathogen perception by plant immune receptors". *New Phytologist* 219 (1), pp. 17–24.

Chang, H.-X., L. A. Miller and G. L. Hartman (2014). "Melanin-independent accumulation of turgor pressure in appressoria of *Phakopsora pachyrhizi*". *Phytopathology* 104 (9), pp. 977–84.

Chen, J., R. Shrestha, J. Ding, H. Zheng, C. Mu, J. Wu and G. Mahuku (2016). "Genome-wide association study and QTL mapping reveal genomic loci associated with *Fusarium* ear rot resistance in tropical maize germplasm". *G3: Genes/Genomes/Genetics* 6 (12), pp. 3803–15.

Christensen, J. J. (1963). "Corn smut caused by *Ustilago maydis*". *Monographs. American Phytopathology Society* 2.

Cohen, S. N., A. C. Chang and L. Hsu (1972). "Nonchromosomal antibiotic resistance in bacteria: genetic transformation of *Escherichia coli* by R-factor DNA". *Proceedings of the National Academy of Sciences of the United States of America* 69 (8), pp. 2110–14.

Counihan, N. A., S. A. Chisholm, H. E. Bullen, A. Srivastava, P. R. Sanders, T. K. Jonsdottir, G. E. Weiss, S. Ghosh, B. S. Crabb, D. J. Creek, P. R. Gilson and T. F. de Koning-Ward (2017). "*Plasmodium falciparum* parasites deploy RhopH2 into the host erythrocyte to obtain nutrients, grow and replicate". *eLife* 6, e23217.

Couto, D. and C. Zipfel (2016). "Regulation of pattern recognition receptor signalling in plants". *Nature Reviews Immunology* 16, p. 537.

Cross, T. G., D. Scheel-Toellner, N. V. Henriquez, E. Deacon, M. Salmon and J. M. Lord (2000). "Serine/threonine protein kinases and apoptosis". *Exp Cell Res* 256 (1), pp. 34–41.

Cui, H., K. Tsuda and J. E. Parker (2015). "Effector-triggered immunity: from pathogen perception to robust defense". *Annual Review of Plant Biology* 66, pp. 487–511.

Dean, R., J. A. Van Kan, Z. A. Pretorius, K. E. Hammond-Kosack, A. Di Pietro, P. D. Spanu, J. J. Rudd, M. Dickman, R. Kahmann, J. Ellis and G. D. Foster (2012). "The Top 10 fungal pathogens in molecular plant pathology". *Molecular Plant Patholgy* 13 (4), pp. 414–30.

Djamei, A., K. Schipper, F. Rabe, A. Ghosh, V. Vincon, J. Kahnt, S. Osorio, T. Tohge, A. R. Fernie, I. Feussner, K. Feussner, P. Meinicke, *et al.* (2011). "Metabolic priming by a secreted fungal effector". *Nature* 478 (7369), pp. 395–8.

Djamei, A. and R. Kahmann (2012). "*Ustilago maydis*: dissecting the molecular interface between pathogen and plant". *PLoS Pathogens* 8 (11), e1002955.

Dobon, A., D. C. E. Bunting, L. E. Cabrera-Quio, C. Uauy and D. G. O. Saunders (2016). "The host-pathogen interaction between wheat and yellow rust induces temporally coordinated waves of gene expression". *BMC Genomics* 17 (1), p. 380.

Dodds, P. N. and J. P. Rathjen (2010). "Plant immunity: towards an integrated view of plant–pathogen interactions". *Nature Reviews Genetics* 11, p. 539.

Doehlemann, G., R. Wahl, M. Vranes, R. P. de Vries, J. Kämper and R. Kahmann (2008). "Establishment of compatibility in the *Ustilago maydis*/maize pathosystem". *Journal of Plant Physiology* 165 (1), pp. 29–40.

Doehlemann, G., K. van der Linde, D. Assmann, D. Schwammbach, A. Hof, A. Mohanty, D. Jackson and R. Kahmann (2009). "Pep1, a secreted effector protein of *Ustilago maydis*, is required for successful invasion of plant cells". *PLoS Pathogens* 5 (2), e1000290.

Doehlemann, G., S. Reissmann, D. Assmann, M. Fleckenstein and R. Kahmann (2011). "Two linked genes encoding a secreted effector and a membrane protein are essential for *Ustilago maydis*-induced tumour formation". *Molecular Microbiology* 81 (3), pp. 751–66.

Does, H. C. van der and M. Rep (2017). "Adaptation to the host environment by plant-pathogenic fungi". *Annual Review of Phytophatology* 55, pp. 427–50.

Doidy, J., E. Grace, C. Kühn, F. Simon-Plas, L. Casieri and D. Wipf (2012). "Sugar transporters in plants and in their interactions with fungi". *Trends in Plant Science* 17 (7), pp. 413–22.

Ehness, R., M. Ecker, D. E. Godt and T. Roitsch (1997). "Glucose and stress independently regulate source and sink metabolism and defense mechanisms via signal transduction pathways involving protein phosphorylation". *The Plant Cell* 9 (10), pp. 1825–41.

Elsworth, B., K. Matthews, C. Q. Nie, M. Kalanon, S. C. Charnaud, P. R. Sanders, S. A. Chisholm, N. A. Counihan, P. J. Shaw, P. Pino, J. A. Chan, M. F. Azevedo, *et al.* (2014). "PTEX is an essential nexus for protein export in malaria parasites". *Nature* 511 (7511), pp. 587–91.

Ensminger, A. W. (2016). "*Legionella pneumophila*, armed to the hilt: justifying the largest arsenal of effectors in the bacterial world". *Current Opinion in Microbiology* 29, pp. 74–80.

Foster, A. J., L. S. Ryder, M. J. Kershaw and N. J. Talbot (2017). "The role of glycerol in the pathogenic lifestyle of the rice blast fungus *Magnaporthe oryzae*". *Environmental Microbiology* 19 (3), pp. 1008–16.

Fu, Z. Q. and X. Dong (2013). "Systemic acquired resistance: turning local infection into global defense". *Annual Review of Plant Biology* 64 (1), pp. 839–63.

Galan, J. E., M. Lara-Tejero, T. C. Marlovits and S. Wagner (2014). "Bacterial type III secretion systems: specialized nanomachines for protein delivery into target cells". *Annual Review of Microbiology* 68, pp. 415–38.

Gallavotti, A., Y. Yang, R. J. Schmidt and D. Jackson (2008). "The relationship between auxin transport and maize branching". *Plant Physiology* 147 (4), pp. 1913–23.

Garcia-Muse, T., G. Steinberg and J. Perez-Martin (2003). "Pheromone-induced G2 arrest in the phytopathogenic fungus *Ustilago maydis*". *Eukaryot Cell* 2 (3), pp. 494–500.

Gerace, E. and D. Moazed (2014). "Coimmunoprecipitation of proteins from yeast". *Methods in Enzymology*. Vol. 541. Elsevier, pp. 13–26.

Gervais, J., C. Plissonneau, J. Linglin, M. Meyer, K. Labadie, C. Cruaud, I. Fudal, T. Rouxel and M. H. Balesdent (2017). "Different waves of effector genes with contrasted genomic location are expressed by *Leptosphaeria maculans* during cotyledon and stem colonization of oilseed rape". *Molecular Plant Patholgy* 18 (8), pp. 1113–26.

Gibson, D. G., L. Young, R.-Y. Chuang, J. C. Venter, C. A. Hutchison III and H. O. Smith (2009). "Enzymatic assembly of DNA molecules up to several hundred kilobases". *Nature Methods* 6 (5), p. 343.

Giraldo, M. C., Y. F. Dagdas, Y. K. Gupta, T. A. Mentlak, M. Yi, A. L. Martinez-Rocha, H. Saitoh, R. Terauchi, N. J. Talbot and B. Valent (2013). "Two distinct secretion systems facilitate tissue invasion by the rice blast fungus *Magnaporthe oryzae*". *Nature Communications* 4, p. 1996.

Giraldo, M. C. and B. Valent (2013). "Filamentous plant pathogen effectors in action". *Nature Reviews Microbiology* 11, p. 800.

Glazebrook, J. (2005). "Contrasting mechanisms of defense against biotrophic and necrotrophic pathogens". *Annual Review of Phytopathology* 43, pp. 205–27.

Gómez-Gómez, L. and T. Boller (2000). "FLS2: An LRR receptor–like kinase involved in the perception of the bacterial elicitor flagellin in *Arabidopsis*". *Molecular Cell* 5 (6), pp. 1003–11.

Goverse, A. and G. Smant (2014). "The activation and suppression of plant innate immunity by parasitic nematodes". *Annual Review of Phytopathology* 52 (1), pp. 243–65.

Gupta, P., I. Ravi and V. Sharma (2013). "Induction of $\beta$-1,3-glucanase and chitinase activity in the defense response of *Eruca sativa* plants against the fungal pathogen *Alternaria brassicicola*". *Journal of Plant Interactions* 8 (2), pp. 155–61.

Hacquard, S., B. Kracher, T. Maekawa, S. Vernaldi, P. Schulze-Lefert and E. Ver Loren van Themaat (2013). "Mosaic genome structure of the barley powdery mildew pathogen and conservation of transcriptional programs in divergent hosts". *Proceedings of the National Academy of Sciences of the United States of America* 110 (24), E2219–28.

Heberle, H., G. V. Meirelles, F. R. da Silva, G. P. Telles and R. Minghim (2015). "InteractiVenn: a web-based tool for the analysis of sets through Venn diagrams". *BMC Bioinformatics* 16 (1), p. 169.

Hemetsberger, C., C. Herrberger, B. Zechmann, M. Hillmer and G. Doehlemann (2012). "The *Ustilago maydis* effector Pep1 suppresses plant immunity by inhibition of host peroxidase activity". *PLoS Pathogens* 8 (5), e1002684.

Hemetsberger, C., A. N. Mueller, A. Matei, C. Herrberger, G. Hensel, J. Kumlehn, B. Mishra, R. Sharma, M. Thines, R. Huckelhoven and G. Doehlemann (2015). "The

fungal core effector Pep1 is conserved across smuts of dicots and monocots". *New Phytologist* 206 (3), pp. 1116–26.

Ho, C.-M., J. R. Beck, M. Lai, Y. Cui, D. E. Goldberg, P. F. Egea and Z. H. Zhou (2018). "Malaria parasite translocon structure and mechanism of effector export". *Nature* 561 (7721), pp. 70–5.

Holliday, R. (1974). "*Ustilago maydis*". *Bacteria, Bacteriophages, and Fungi*. Springer, pp. 575–95.

Horbach, R., A. R. Navarro-Quesada, W. Knogge and H. B. Deising (2011). "When and how to kill a plant cell: infection strategies of plant pathogenic fungi". *Journal of Plant Physiology* 168 (1), pp. 51–62.

Huett, A. (2017). "Combinatorial actions of bacterial effectors revealed by exploiting genetic tools in yeast". *Molecular Systems Biology* 13 (1), p. 911.

Irieda, H., H. Maeda, K. Akiyama, A. Hagiwara, H. Saitoh, A. Uemura, R. Terauchi and Y. Takano (2014). "*Colletotrichum orbiculare* secretes virulence effectors to a biotrophic interface at the primary hyphal neck via exocytosis coupled with SEC22-mediated traffic". *The Plant Cell* 26 (5), pp. 2265–81.

Irieda, H., S. Ogawa and Y. Takano (2016). "Focal effector accumulation in a biotrophic interface at the primary invasion sites of *Colletotrichum orbiculare* in multiple susceptible plants". *Plant Signaling & Behavior* 11 (2), e1137407.

Ito, D., M. A. Schureck and S. A. Desai (2017). "An essential dual-function complex mediates erythrocyte invasion and channel-mediated nutrient uptake in malaria parasites". *eLife* 6, e23485.

James, P., J. Halladay and E. A. Craig (1996). "Genomic libraries and a host strain designed for highly efficient two-hybrid selection in yeast". *Genetics* 144 (4), pp. 1425–36.

Jones, J. D. and J. L. Dangl (2006). "The plant immune system". *Nature* 444 (7117), pp. 323–9.

Jong, J. C. de, B. J. McCormack, N. Smirnoff and N. J. Talbot (1997). "Glycerol generates turgor in rice blast". *Nature* 389, p. 244.

Jonge, R. de, H. P. van Esse, A. Kombrink, T. Shinya, Y. Desaki, R. Bours, S. van der Krol, N. Shibuya, M. H. Joosten and B. P. Thomma (2010). "Conserved fungal LysM effector Ecp6 prevents chitin-triggered immunity in plants". *Science* 329 (5994), pp. 953–5.

Jung, P. P., N. Christian, D. P. Kay, A. Skupin and C. L. Linster (2015). "Protocols and programs for high-throughput growth and aging phenotyping in yeast". *PLoS One* 10 (3), e0119807.

Jupe, J., R. Stam, A. J. Howden, J. A. Morris, R. Zhang, P. E. Hedley and E. Huitema (2013). "*Phytophthora capsici*-tomato interaction features dramatic shifts in gene expression associated with a hemi-biotrophic lifestyle". *Genome Biology* 14 (6), R63.

Kahmann, R., G. Steinberg, C. Basse, M. Feldbrügge and J. Kämper (2000). "*Ustilago maydis*, the causative agent of corn smut disease". *Fungal pathology*. Springer, pp. 347–71.

Kemen, E., A. Gardiner, T. Schultz-Larsen, A. C. Kemen, A. L. Balmuth, A. Robert-Seilaniantz, K. Bailey, E. Holub, D. J. Studholme, D. MacLean and J. D. G. Jones (2011). "Gene gain and loss during evolution of obligate parasitism in the white rust pathogen of *Arabidopsis thaliana*". *PLoS Biology* 9 (7), e1001094.

Khang, C. H., R. Berruyer, M. C. Giraldo, P. Kankanala, S.-Y. Park, K. Czymmek, S. Kang and B. Valent (2010). "Translocation of *Magnaporthe oryzae* effectors into rice cells and their subsequent cell-to-cell movement". *The Plant Cell*, tpc–109.

Khrunyk, Y., K. Münch, K. Schipper, A. N. Lupas and R. Kahmann (2010). "The use of FLP-mediated recombination for the functional analysis of an effector gene family in the biotrophic smut fungus *Ustilago maydis*". *New phytologist* 187 (4), pp. 957–68.

Kleemann, J., L. J. Rincon-Rivera, H. Takahara, U. Neumann, E. V. L. van Themaat, H. C. van der Does, S. Hacquard, K. Stüber, I. Will, W. Schmalenbach, E. Schmelzer and R. J. O'Connell (2012). "Sequential delivery of host-induced virulence effectors by appressoria and intracellular hyphae of the phytopathogen *Colletotrichum higginsianum*". *PLoS Pathogens* 8 (4), e1002643.

Kämper, J. (2004). "A PCR-based system for highly efficient generation of gene replacement mutants in *Ustilago maydis*". *Molecular Genetics and Genomics* 271 (1), pp. 103–10.

Kämper, J., R. Kahmann, M. Bölker, L. J. Ma, T. Brefort, B. J. Saville, F. Banuett, J. W. Kronstad, S. E. Gold, O. Muller, M. H. Perlin, H. A. Wosten, *et al.* (2006). "Insights from the genome of the biotrophic fungal plant pathogen *Ustilago maydis*". *Nature* 444 (7115), pp. 97–101.

Kämper, J., M. Reichmann, T. Romeis, M. Bölker and R. Kahmann (1995). "Multiallelic recognition: nonself-dependent dimerization of the bE and bW homeodomain proteins in *Ustilago maydis*". *Cell* 81 (1), pp. 73–83.

Koh, S., A. André, H. Edwards, D. Ehrhardt and S. Somerville (2005). "*Arabidopsis thaliana* subcellular responses to compatible *Erysiphe cichoracearum* infections". *The Plant Journal* 44 (3), pp. 516–29.

Kolattukudy, P. E., R. Mohan, M. A. Bajar and B. A. Sherf (1992). "Plant peroxidase gene expression and function". *Biochemical Society Transactions* 20 (2), pp. 333–7.

Laemmli, U. K. (1970). "Cleavage of structural proteins during the assembly of the head of bacteriophage T4". *Nature* 227 (5259), p. 680.

Lanver, D., P. Berndt, M. Tollot, V. Naik, M. Vranes, T. Warmann, K. Munch, N. Rossel and R. Kahmann (2014). "Plant surface cues prime *Ustilago maydis* for biotrophic development". *PLoS Pathogens* 10 (7), e1004272.

Lanver, D., A. N. Muller, P. Happel, G. Schweizer, F. B. Haas, M. Franitza, C. Pellegrin, S. Reissmann, J. Altmuller, S. A. Rensing and R. Kahmann (2018). "The biotrophic development of *Ustilago maydis* studied by RNA-seq analysis". *The Plant Cell* 30 (2), pp. 300–23.

Lanver, D., M. Tollot, G. Schweizer, L. L. Presti, S. Reissmann, L.-S. Ma, M. Schuster, S. Tanaka, L. Liang, N. Ludwig, *et al.* (2017). "*Ustilago maydis* effectors and their impact on virulence". *Nature Reviews Microbiology* 15 (7), p. 409.

Lemoine, R., S. La Camera, R. Atanassova, F. Dédaldéchamp, T. Allario, N. Pourtau, J.-L. Bonnemain, M. Laloi, P. Coutos-Thévenot and L. Maurousset (2013). "Source-to-sink transport of sugar and regulation by environmental factors". *Frontiers in Plant Science* 4, p. 272.

Letunic, I. and P. Bork (2017). "20 years of the SMART protein domain annotation resource". *Nucleic Acids Research* 46 (D1), pp. D493–6.

Liang, L. (2012). "The role of Stp1, a secreted effector, in the biotrophic interaction of Ustilago maydis and its host plant maize". PhD thesis. Philipps-Universität Marburg.

Lisk, G. and S. A. Desai (2005). "The plasmodial surface anion channel is functionally conserved in divergent malaria parasites". *Eukaryotic Cell* 4 (12), pp. 2153–59.

Liu, B., J. F. Li, Y. Ao, J. Qu, Z. Li, J. Su, Y. Zhang, J. Liu, D. Feng, K. Qi, Y. He, J. Wang, *et al.* (2012). "Lysin motif-containing proteins LYP4 and LYP6 play dual roles in peptidoglycan and chitin perception in rice innate immunity". *The Plant Cell* 24 (8), pp. 3406–19.

Liu, T., T. Song, X. Zhang, H. Yuan, L. Su, W. Li, J. Xu, S. Liu, L. Chen, T. Chen, M. Zhang, L. Gu, *et al.* (2014). "Unconventionally secreted effectors of two filamentous pathogens target plant salicylate biosynthesis". *Nature Communications* 5, p. 4686.

Lo Presti, L., D. Lanver, G. Schweizer, S. Tanaka, L. Liang, M. Tollot, A. Zuccaro, S. Reissmann and R. Kahmann (2015). "Fungal effectors and plant susceptibility". *Annual Review of Plant Biology* 66, pp. 513–45.

Lo Presti, L., B. Zechmann, J. Kumlehn, L. Liang, D. Lanver, S. Tanaka, R. Bock and R. Kahmann (2016). "An assay for entry of secreted fungal effectors into plant cells". *New Phytologist* 213 (2), pp. 956–64.

Loon, L. C. van, M. Rep and C. M. Pieterse (2006). "Significance of inducible defense-related proteins in infected plants". *Annual Review of Phytophatology* 44, pp. 135–62.

Love, M. I., W. Huber and S. Anders (2014). "Moderated estimation of fold change and dispersion for RNA-seq data with DESeq2". *Genome biology* 15 (12), p. 550.

Ma, L. S., L. Wang, C. Trippel, A. Mendoza-Mendoza, S. Ullmann, M. Moretti, A. Carsten, J. Kahnt, S. Reissmann, B. Zechmann, G. Bange and R. Kahmann (2018). "The *Ustilago maydis* repetitive effector Rsp3 blocks the antifungal activity of mannose-binding maize proteins". *Nature Communications* 9 (1), p. 1711.

Martinez-Espinoza, A. D., M. D. Garcia-Pedrajas and S. E. Gold (2002). "The Ustilaginales as plant pests and model systems". *Fungal Genetics and Biology* 35 (1), pp. 1–20.

Maruta, N., Y. Trusov and J. R. Botella (2016). "Yeast three-hybrid system for the detection of protein-protein interactions". *Methods in Molecular Biology* 1363, pp. 145–54.

Mendgen, K., M. Hahn and H. Deising (1996). "Morphogenesis and mechanisms of penetration by plant pathogenic fungi". *Annual Review of Phytophatology* 34, pp. 367–86.

Mendoza-Mendoza, A., P. Berndt, A. Djamei, C. Weise, U. Linne, M. Marahiel, M. Vranes, J. Kämper and R. Kahmann (2009). "Physical-chemical plant-derived signals induce differentiation in *Ustilago maydis*". *Molecular Microbiology* 71 (4), pp. 895–911.

Meng, X. and S. Zhang (2013). "MAPK cascades in plant disease resistance signaling". *Annual Review of Phytopathology* 51, pp. 245–66.

Mentlak, T. A., A. Kombrink, T. Shinya, L. S. Ryder, I. Otomo, H. Saitoh, R. Terauchi, Y. Nishizawa, N. Shibuya, B. P. Thomma and N. J. Talbot (2012). "Effector-mediated suppression of chitin-triggered immunity by ı*Magnaporthe oryzae* is necessary for rice blast disease". *Plant Cell* 24 (1), pp. 322–35.

Mewes, H.-W., D. Frishman, U. Güldener, G. Mannhaupt, K. Mayer, M. Mokrejs, B. Morgenstern, M. Münsterkötter, S. Rudd and B Weil (2002). "MIPS: a database for genomes and protein sequences". *Nucleic Acids Research* 30 (1), pp. 31–4.

Micali, C. O., U. Neumann, D. Grunewald, R. Panstruga and R. O'Connell (2011). "Biogenesis of a specialized plant-fungal interface during host cell internalization of *Golovinomyces orontii* haustoria". *Cell Microbiology* 13 (2), pp. 210–26.

Miya, A., P. Albert, T. Shinya, Y. Desaki, K. Ichimura, K. Shirasu, Y. Narusaka, N. Kawakami, H. Kaku and N. Shibuya (2007). "CERK1, a LysM receptor kinase, is essential for chitin elicitor signaling in *Arabidopsis*". *Proceedings of the National Academy of Sciences of the United States of America* 104 (49), pp. 19613–8.

Möller, M. and E. H. Stukenbrock (2017). "Evolution and genome architecture in fungal plant pathogens". *Nature Reviews Microbiology* 15 (12), pp. 756–71.

Monteiro, F. and M. T. Nishimura (2018). "Structural, functional, and genomic diversity of plant NLR proteins: an evolved resource for rational engineering of plant immunity". *Annual Review of Phytophatology*.

Mueller, A. N., S. Ziemann, S. Treitschke, D. Aßmann and G. Doehlemann (2013). "Compatibility in the *Ustilago maydis*-maize interaction requires inhibition of host cysteine proteases by the fungal effector Pit2". *PLoS Pathogens* 9 (2), e1003177.

Mullis, K., F. Faloona, S. Scharf, R. Saiki, G. Horn and H Erlich (1986). "Specific enzymatic amplification of DNA in vitro: the polymerase chain reaction". *Cold Spring Harbor symposia on quantitative biology*. Vol. 51. Cold Spring Harbor Laboratory Press, pp. 263–273.

Mur, L. A. J., P. Kenton, A. J. Lloyd, H. Ougham and E. Prats (2008). "The hypersensitive response; the centenary is upon us but how much do we know?" *Journal of Experimental Botany* 59 (3), pp. 501–20.

O'Connell, R. J., M. R. Thon, S. Hacquard, S. G. Amyotte, J. Kleemann, M. F. Torres, U. Damm, E. A. Buiate, L. Epstein, N. Alkan, J. Altmüller, L. Alvarado-Balderrama, *et al.* (2012). "Lifestyle transitions in plant pathogenic *Colletotrichum fungi* deciphered by genome and transcriptome analyses". *Nature Genetics* 44, p. 1060.

Oliveira-Garcia, E. and B. Valent (2015). "How eukaryotic filamentous pathogens evade plant recognition". *Current Opinion in Microbiology* 26, pp. 92–101.

Pandey, S. P. and I. E. Somssich (2009). "The role of WRKY transcription factors in plant immunity". *Plant Physiology* 150 (4), p. 1648.

Petre, B. and S. Kamoun (2014). "How do filamentous pathogens deliver effector proteins into plant cells?" *PLoS Biology* 12 (2), e1001801.

Pieterse, C. M., D. V. d. Does, C. Zamioudis, A. Leon-Reyes and S. C. V. Wees (2012). "Hormonal modulation of plant immunity". *Annual Review of Cell and Developmental Biology* 28 (1), pp. 489–521.

Pillai, A. D., W. Nguitragool, B. Lyko, K. Dolinta, M. M. Butler, S. T. Nguyen, N. P. Peet, T. L. Bowlin and S. A. Desai (2012). "Solute restriction reveals an essential role for clag3-associated channels in malaria parasite nutrient acquisition". *Molecular Pharmacology*, mol–112.

Pryce-Jones, E., T. Carver and S. J. Gurr (1999). "The roles of cellulase enzymes and mechanical force in host penetration by *Erysiphe graminis* f. sp. *hordei*". *Physiological and Molecular Plant Pathology* 55 (3), pp. 175–82.

Qin, J., K. Wang, L. Sun, H. Xing, S. Wang, L. Li, S. Chen, H.-S. Guo and J. Zhang (2018). "The plant-specific transcription factors CBP60g and SARD1 are targeted by a Verticillium secretory protein VdSCP41 to modulate immunity". *eLife* 7, e34902.

Rabe, F., J. Bosch, A. Stirnberg, T. Guse, L. Bauer, D. Seitner, F. A. Rabanal, A. Czedik-Eysenberg, S. Uhse, J. Bindics, B. Genenncher, F. Navarrete, *et al.* (2016). "A complete toolset for the study of *Ustilago bromivora* and *Brachypodium sp.* as a fungal-temperate grass pathosystem". *eLife* 5.

Rao, V. S., K. Srinivas, G. N. Sujini and G. N. Kumar (2014). "Protein-protein interaction detection: methods and analysis". *International Journal of Proteomics* 2014, p. 147648.

Redkar, A., R. Hoser, L. Schilling, B. Zechmann, M. Krzymowska, V. Walbot and G. Doehlemann (2015a). "A secreted effector protein of *Ustilago maydis* guides maize leaf cells to form tumors". *The Plant Cell* 27 (4), pp. 1332–51.

Redkar, A., M. Villajuana-Bonequi and G. Doehlemann (2015b). "Conservation of the *Ustilago maydis* effector See1 in related smuts". *Plant Signaling & Behavior* 10 (12), e1086855.

Rehmany, A. P., A. Gordon, L. E. Rose, R. L. Allen, M. R. Armstrong, S. C. Whisson, S. Kamoun, B. M. Tyler, P. R. Birch and J. L. Beynon (2005). "Differential recognition of highly divergent downy mildew avirulence gene alleles by RPP1 resistance genes from two *Arabidopsis* lines". *The Plant Cell* 17 (6), pp. 1839–50.

Rodriguez-Moreno, L., M. K. Ebert, M. D. Bolton and B. Thomma (2018). "Tools of the crook- infection strategies of fungal plant pathogens". *The Plant Journal* 93 (4), pp. 664–74.

Rooney, H. C., J. W. Van't Klooster, R. A. van der Hoorn, M. H. Joosten, J. D. Jones and P. J. de Wit (2005). "Cladosporium Avr2 inhibits tomato Rcr3 protease required for Cf-2-dependent disease resistance". *Science* 308 (5729), pp. 1783–6.

Sambrook, J., E. F. Fritsch, T. Maniatis, *et al.* (1989). *Molecular cloning: a laboratory manual*. Ed. 2. Cold spring harbor laboratory press.

Sanchez-Vallet, A., R. Saleem-Batcha, A. Kombrink, G. Hansen, D. J. Valkenburg, B. P. Thomma and J. R. Mesters (2013). "Fungal effector Ecp6 outcompetes host immune receptor for chitin binding through intrachain LysM dimerization". *eLife* 2, e00790.

Sandrock, B., F. Tirode and J.-M. Egly (2001). "Three-Hybrid Screens". *Two-Hybrid Systems*. Springer, pp. 271–289.

Sandrock, B. and J.-M. Egly (2001). "A yeast four-hybrid system identifies CAK as a regulator of the XPD helicase, a subunit of TFIIH". *Journal of Biological Chemistry*.

Scherer, M., K. Heimel, V. Starke and J. Kämper (2006). "The Clp1 protein is required for clamp formation and pathogenic development of *Ustilago maydis*". *The Plant Cell* 18 (9), pp. 2388–401.

Schilling, L., A. Matei, A. Redkar, V. Walbot and G. Doehlemann (2014). "Virulence of the maize smut *Ustilago maydis* is shaped by organ-specific effectors". *Molecular Plant Pathology* 15 (8), pp. 780–89.

Schipper, K. (2009). "Charakterisierung eines *Ustilago maydis* Genclusters, das für drei neuartige sekretierte Effektoren kodiert". PhD thesis. Philipps-Universität Marburg.

Schirawski, J., G. Mannhaupt, K. Münch, T. Brefort, K. Schipper, G. Doehlemann, M. Di Stasio, N. Rössel, A. Mendoza-Mendoza and D. Pester (2010). "Pathogenicity

determinants in smut fungi revealed by genome comparison". *Science* 330 (6010), pp. 1546–8.

Schmoll, M., C. Dattenbock, N. Carreras-Villasenor, A. Mendoza-Mendoza, D. Tisch, M. I. Aleman, S. E. Baker, C. Brown, M. G. Cervantes-Badillo, J. Cetz-Chel, G. R. Cristobal-Mondragon, L. Delaye, *et al.* (2016). "The genomes of three uneven siblings: footprints of the lifestyles of three trichoderma species". *Microbiology and Molecular Biology Reviews* 80 (1), pp. 205–327.

Schornack, S., M. van Damme, T. O. Bozkurt, L. M. Cano, M. Smoker, M. Thines, E. Gaulin, S. Kamoun and E. Huitema (2010). "Ancient class of translocated oomycete effectors targets the host nucleus". *Proceedings of the National Academy of Sciences of the United States of America* 107 (40), pp. 17421–6.

Schuler, D., R. Wahl, K. Wippel, M. Vranes, M. Münsterkötter, N. Sauer and J. Kämper (2015). "Hxt1, a monosaccharide transporter and sensor required for virulence of the maize pathogen *Ustilago maydis*". *New Phytologist* 206 (3), pp. 1086–100.

Schulz, B., F. Banuett, M. Dahl, R. Schlesinger, W. Schäfer, T. Martin, I. Herskowitz and R. Kahmann (1990). "The b alleles of *U. maydis*, whose combinations program pathogenic development, code for polypeptides containing a homeodomain-related motif". *Cell* 60 (2), pp. 295–306.

Schuster, M., G. Schweizer, S. Reissmann and R. Kahmann (2016). "Genome editing in *Ustilago maydis* using the CRISPR-Cas system". *Fungal Genetics and Biology* 89, pp. 3–9.

Schuster, M., G. Schweizer and R. Kahmann (2018). "Comparative analyses of secreted proteins in plant pathogenic smut fungi and related basidiomycetes". *Fungal Genetics and Biology* 112, pp. 21–30.

Scott, M. P. and M. Emery (2016). "Maize: overview". *Reference Module in Food Science*. Elsevier.

Seitner, D., S. Uhse, M. Gallei and A. Djamei (2018). "The core effector Cce1 is required for early infection of maize by *Ustilago maydis*". *Molecular Plant Pathology* 19 (10), pp. 2277–87.

Sekhwal, M. K., P. Li, I. Lam, X. Wang, S. Cloutier and F. M. You (2015). "Disease resistance gene analogs (RGAs) in plants". *International Journal of Molecular Sciences* 16 (8), pp. 19248–90.

Selin, C., T. R. de Kievit, M. F. Belmonte and W. G. Fernando (2016). "Elucidating the role of effectors in plant-fungal interactions: progress and challenges". *Frontiers in Microbiology* 7, p. 600.

Shen, Q., Y. Liu and N. I. Naqvi (2018). "Fungal effectors at the crossroads of phytohormone signaling". *Current Opinion in Microbiology* 46, pp. 1–6.

Sherling, E. S., E. Knuepfer, J. A. Brzostowski, L. H. Miller, M. J. Blackman and C. v. Ooij (2017). "The *Plasmodium falciparum* rhoptry protein RhopH3 plays essential roles in host cell invasion and nutrient uptake". *eLife* 6, e23239.

Shipman, E. N., K. Jones, C. B. Jenkinson, D. W. Kim, J. Zhu and C. H. Khang (2017). "Nuclear and structural dynamics during the establishment of a specialized effector-secreting cell by *Magnaporthe oryzae* in living rice cells". *BMC Cell Biology* 18 (1), p. 11.

Snetselaar, K. M. and C. W. Mims (1992). "Sporidial fusion and infection of maize seedlings by the smut fungus *Ustilago maydis*". *Mycologia*, pp. 193–203.

Snetselaar, K. M. and C. W. Mims (1994). "Light and electron microscopy of *Ustilago maydis* hyphae in maize". *Mycological Research* 98 (3), pp. 347–55.

Snetselaar, K. M., M. Bölker and R. Kahmann (1996). "*Ustilago maydis*: mating hyphae orient their growth toward pheromone sources". *Fungal Genetics and Biology* 20 (4), pp. 299–312.

Southern, E. M. *et al.* (1975). "Detection of specific sequences among DNA fragments separated by gel electrophoresis". *Journal of Molecular Biology* 98 (3), pp. 503–17.

Sperschneider, J., P. N. Dodds, K. B. Singh and J. M. Taylor (2018). "ApoplastP: prediction of effectors and plant proteins in the apoplast using machine learning". *New Phytologist* 217 (4), pp. 1764–78.

Stefanini, I., C. De Filippo and D. Cavalieri (2013). "Yeast as a model in High-throughput screening of small-molecule libraries". *Diversity-Oriented Synthesis: Basics and Applications in Organic Synthesis, Drug Discovery, and Chemical Biology*, pp. 455–82.

Steinberg, G., M. Schliwa, C. Lehmler, M. Bölker, R. Kahmann and J. R. McIntosh (1998). "Kinesin from the plant pathogenic fungus *Ustilago maydis* is involved in vacuole formation and cytoplasmic migration". *Journal of Cell Science* 111 (Pt 15), pp. 2235–46.

Steinberg, G. and J. Perez-Martin (2008). "*Ustilago maydis*, a new fungal model system for cell biology". *Trends in Cell Biology* 18 (2), pp. 61–7.

Stirnberg, A. and A. Djamei (2016). "Characterization of ApB73, a virulence factor important for colonization of *Zea mays* by the smut *Ustilago maydis*". *Molecular Plant Patholgy* 17 (9), pp. 1467–79.

Strange, R. N. and P. R. Scott (2005). "Plant disease: a threat to global food security". *Annual Review of Phytopathology* 43 (1), pp. 83–116.

Tanaka, S., T. Brefort, N. Neidig, A. Djamei, J. Kahnt, W. Vermerris, S. Koenig, K. Feussner, I. Feussner and R. Kahmann (2014). "A secreted *Ustilago maydis* effector promotes virulence by targeting anthocyanin biosynthesis in maize". *eLife* 3, e01355.

Tanaka, S., X. Han and R. Kahmann (2015). "Microbial effectors target multiple steps in the salicylic acid production and signaling pathway". *Frontiers in Plant Science* 6, p. 349.

Teh, O.-K. and D. Hofius (2014). "Membrane trafficking and autophagy in pathogen-triggered cell death and immunity". *Journal of experimental botany* 65 (5), pp. 1297–312.

Thomma, B. P.H. J., T. Nürnberger and M. H.A. J. Joosten (2011). "Of PAMPs and effectors: the blurred PTI-ETI dichotomy". *The Plant Cell* 23 (1), p. 4.

Tian, T., Y. Liu, H. Yan, Q. You, X. Yi, Z. Du, W. Xu and Z. Su (2017). "agriGO v2.0: a GO analysis toolkit for the agricultural community, 2017 update". *Nucleic Acids Research* 45 (W1), W122–29.

Tollot, M., D. Assmann, C. Becker, J. Altmüller, J. Y. Dutheil, C.-E. Wegner and R. Kahmann (2016). "The WOPR protein Ros1 is a master regulator of sporogenesis and late effector gene expression in the maize pathogen *Ustilago maydis*". *PLoS Pathogens* 12 (6), e1005697.

Torto, T. A., S. Li, A. Styer, E. Huitema, A. Testa, N. A. Gow, P. van West and S. Kamoun (2003). "EST mining and functional expression assays identify extracellular effector proteins from the plant pathogen *Phytophthora*". *Genome Research* 13 (7), pp. 1675–85.

Toruno, T. Y., I. Stergiopoulos and G. Coaker (2016). "Plant-pathogen effectors: cellular probes interfering with plant defenses in spatial and temporal manners". *Annual Review of Phytophatology* 54, pp. 419–41.

Tyler, B. M., S. D. Kale, Q. Wang, K. Tao, H. R. Clark, K. Drews, V. Antignani, A. Rumore, T. Hayes, J. M. Plett, I. Fudal, B. Gu, *et al.* (2013). "Microbe-independent entry of oomycete RxLR effectors and fungal RxLR-like effectors into plant and animal cells is specific and reproducible". *Molecular Plant-Microbe Interactions* 26 (6), pp. 611–6.

Urbanus, M. L., A. T. Quaile, P. J. Stogios, M. Morar, C. Rao, R. Di Leo, E. Evdokimova, M. Lam, C. Oatway, M. E. Cuff, J. Osipiuk, K. Michalska, *et al.* (2016). "Diverse mechanisms of metaeffector activity in an intracellular bacterial pathogen, *Legionella pneumophila*". *Molecular Systems Biology* 12 (12), p. 893.

Van Esse, H. P., J. W. van't Klooster, M. D. Bolton, K. A. Yadeta, P. van Baarlen, S. Boeren, J. Vervoort, P. J.G. M. de Wit and B. P.H. J. Thomma (2008). "The *Cladosporium fulvum* virulence protein Avr2 inhibits host proteases required for basal defense". *The Plant Cell* 20 (7), pp. 1948–63.

Varden, F. A., J. C. De la Concepcion, J. H. Maidment and M. J. Banfield (2017). "Taking the stage: effectors in the spotlight". *Current Opinion in Plant Biology* 38, pp. 25–33.

Viotti, C. (2016). "ER to golgi-dependent protein secretion: The conventional pathway". *Unconventional Protein Secretion*. Springer, pp. 3–29.

Voegele, R. T. and K. W. Mendgen (2011). "Nutrient uptake in rust fungi: how sweet is parasitic life?" *Euphytica* 179 (1), pp. 41–55.

Voigt, C. A. (2014). "Callose-mediated resistance to pathogenic intruders in plant defense-related papillae". *Frontiers in Plant Science* 5, p. 168.

Vranes, M. (2006). "Transkriptom-Analyse der frühen Infektionsphase von *Ustilago maydis*: Identifikation neuer pathogenitätsrelevanter Gene". PhD thesis.

Wagner, S., I. Grin, S. Malmsheimer, N. Singh, C. E. Torres-Vargas and S. Westerhausen (2018). "Bacterial type III secretion systems: a complex device for the delivery of bacterial effector proteins into eukaryotic host cells". *FEMS Microbiology Letters* 365 (19), fny201.

Wahl, R., K. Wippel, S. Goos, J. Kämper and N. Sauer (2010). "A novel high-affinity sucrose transporter is required for virulence of the plant pathogen *Ustilago maydis*". *PLoS Biology* 8 (2), e1000303.

Wawra, S., R. Belmonte, L. Lobach, M. Saraiva, A. Willems and P. van West (2012). "Secretion, delivery and function of oomycete effector proteins". *Current Opinion in Microbiology* 15 (6), pp. 685–91.

Wawra, S., A. Djamei, I. Albert, T. Nurnberger, R. Kahmann and P. van West (2013). "In vitro translocation experiments with RxLR-reporter fusion proteins of Avr1b from *Phytophthora sojae* and AVR3a from *Phytophthora infestans* fail to demonstrate specific autonomous uptake in plant and animal cells". *Molecular Plant-Microbe Interactions* 26 (5), pp. 528–36.

Wawra, S., F. Trusch, A. Matena, K. Apostolakis, U. Linne, I. Zhukov, J. Stanek, W. Kozminski, I. Davidson, C. J. Secombes, P. Bayer and P. van West (2017). "The RxLR Motif of the host targeting effector AVR3a of *Phytophthora infestans* is cleaved before secretion". *The Plant Cell* 29 (6), pp. 1184–95.

Whisson, S. C., P. C. Boevink, L. Moleleki, A. O. Avrova, J. G. Morales, E. M. Gilroy, M. R. Armstrong, S. Grouffaud, P. van West, S. Chapman, I. Hein, I. K. Toth, *et al.* (2007). "A translocation signal for delivery of oomycete effector proteins into host plant cells". *Nature* 450 (7166), pp. 115–8.

Willmann, R., H. M. Lajunen, G. Erbs, M. A. Newman, D. Kolb, K. Tsuda, F. Katagiri, J. Fliegmann, J. J. Bono, J. V. Cullimore, A. K. Jehle, F. Gotz, *et al.* (2011). "*Arabidopsis* lysin-motif proteins LYM1 LYM3 CERK1 mediate bacterial peptidoglycan sensing and immunity to bacterial infection". *Proceedings of the National Academy of Sciences of the United States of America* 108 (49), pp. 19824–9.

Wittek, A., I. Dreyer, K. A. S. Al-Rasheid, N. Sauer, R. Hedrich and D. Geiger (2017). "The fungal UmSrt1 and maize ZmSUT1 sucrose transporters battle for plant sugar resources". *Journal of Integrative Plant Biology* 59 (6), pp. 422–435.

Wong, J. H., M. Alfatah, M. F. Sin, H. M. Sim, C. S. Verma, D. P. Lane and P. Arumugam (2017). "A yeast two-hybrid system for the screening and characterization of small-molecule inhibitors of protein–protein interactions identifies a novel putative Mdm2-binding site in p53". *BMC Biology* 15, p. 108.

Xing, S., N. Wallmeroth, K. W. Berendzen and C. Grefen (2016). "Techniques for the analysis of protein-protein interactions in vivo". *Plant Physiology* 171 (2), pp. 727–58.

Yi, M. and B. Valent (2013). "Communication between filamentous pathogens and plants at the biotrophic interface". *Annual Review of Phytophatology* 51, pp. 587–611.

Yu, X., B. Feng, P. He and L. Shan (2017). "From chaos to harmony: responses and signaling upon microbial pattern recognition". *Annual Review of Phytophatology* 55, pp. 109–37.

Yuan, P., E. Jauregui, L. Du, K. Tanaka and B. W. Poovaiah (2017). "Calcium signatures and signaling events orchestrate plant-microbe interactions". *Current Opinion in Plant Biology* 38, pp. 173–83.

Zeng, F.-S., F. Menardo, M.-F. Xue, X.-J. Zhang, S.-J. Gong, L.-J. Yang, W.-Q. Shi and D.-Z. Yu (2017). "Transcriptome analyses shed new insights into primary metabolism and regulation of *Blumeria graminis* f. sp. *tritici* during conidiation". *Frontiers in Plant Science* 8, p. 1146.

Zhang, S. and J.-R. Xu (2014). "Effectors and effector delivery in *Magnaporthe oryzae*". *PLoS Pathogens* 10 (1), e1003826.

Zimmermann, A., S. Hofer, T. Pendl, K. Kainz, F. Madeo and D. Carmona-Gutierrez (2018). "Yeast as a tool to identify anti-aging compounds". *FEMS Yeast Research* 18 (6), foy020.

Zipfel, C. (2014). "Plant pattern-recognition receptors". *Trends in Immunology* 35 (7), pp. 345–51.

Zipfel, C., G. Kunze, D. Chinchilla, A. Caniard, J. D. Jones, T. Boller and G. Felix (2006). "Perception of the bacterial PAMP EF-Tu by the receptor EFR restricts Agrobacterium-mediated transformation". *Cell* 125 (4), pp. 749–60.

vanEsse, H. P., M. D. Bolton, I. Stergiopoulos, P. J. de Wit and B. P. Thomma (2007). "The chitin-binding *Cladosporium fulvum* effector protein Avr4 is a virulence factor". *Molecular Plant-Microbe Interactions* 20 (9), pp. 1092–101.

# Supplemental material

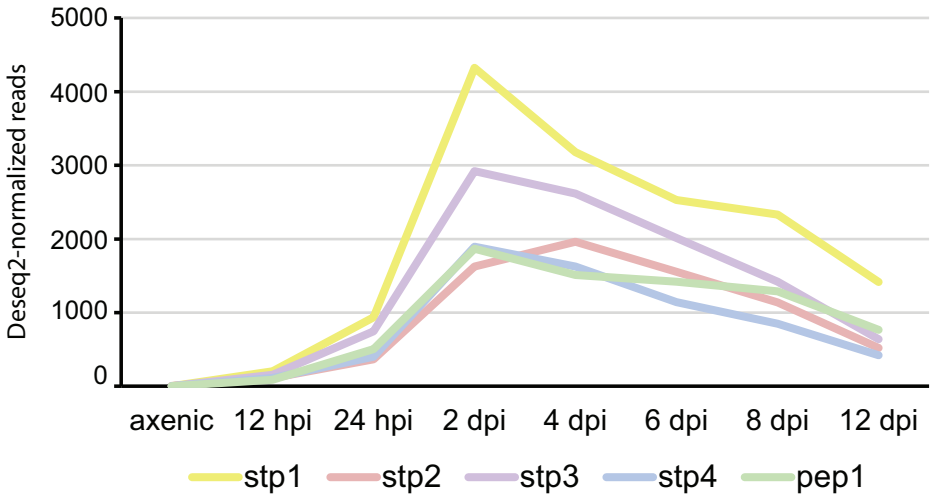


**Figure S1: Expression of essential effector genes of the magenta module during biotrophic development.** RNAseq data are from Lanver *et al.* (2018), in which plants were infected with with FB1 and FB2. Samples were collected at the indicated time points. Axenic refers to expression in axenic culture. Read counts were normalized using DEseq2.

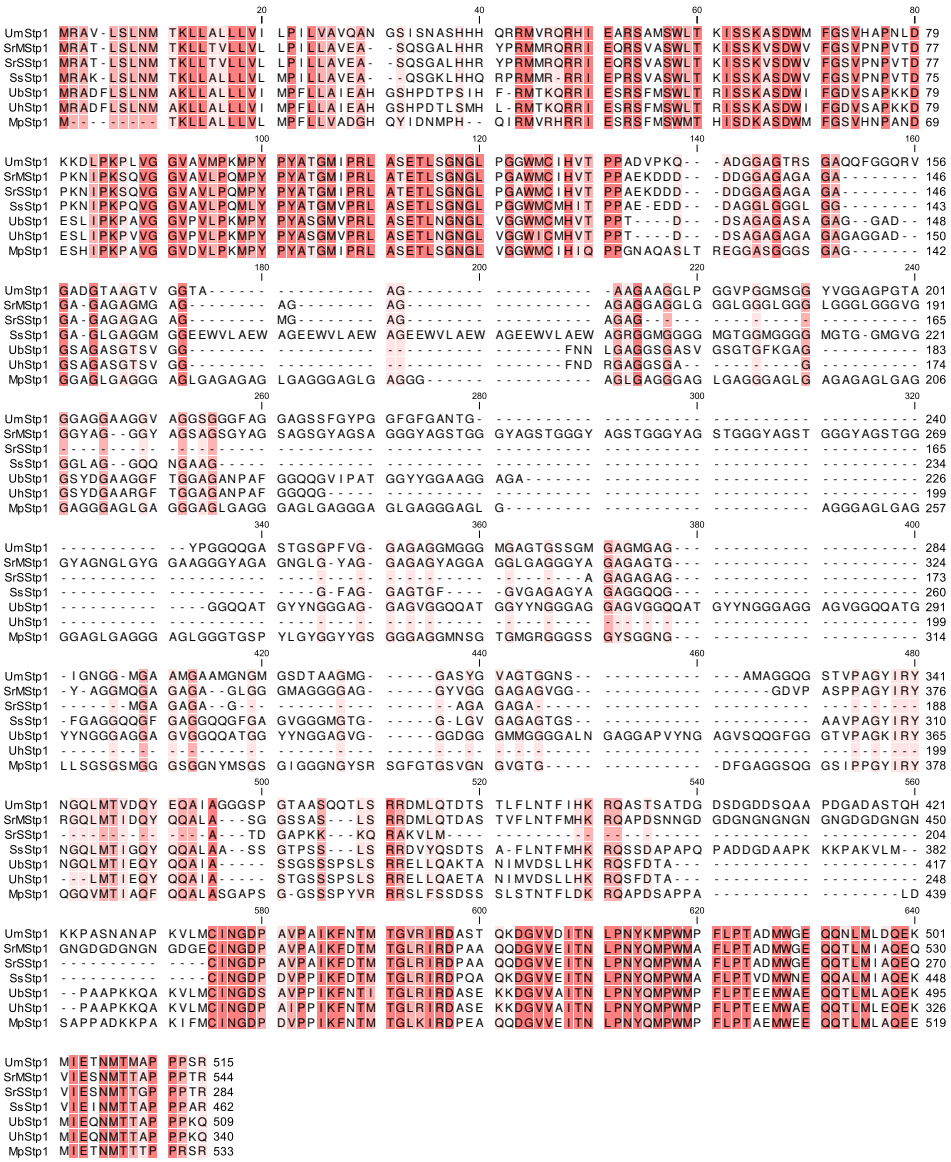

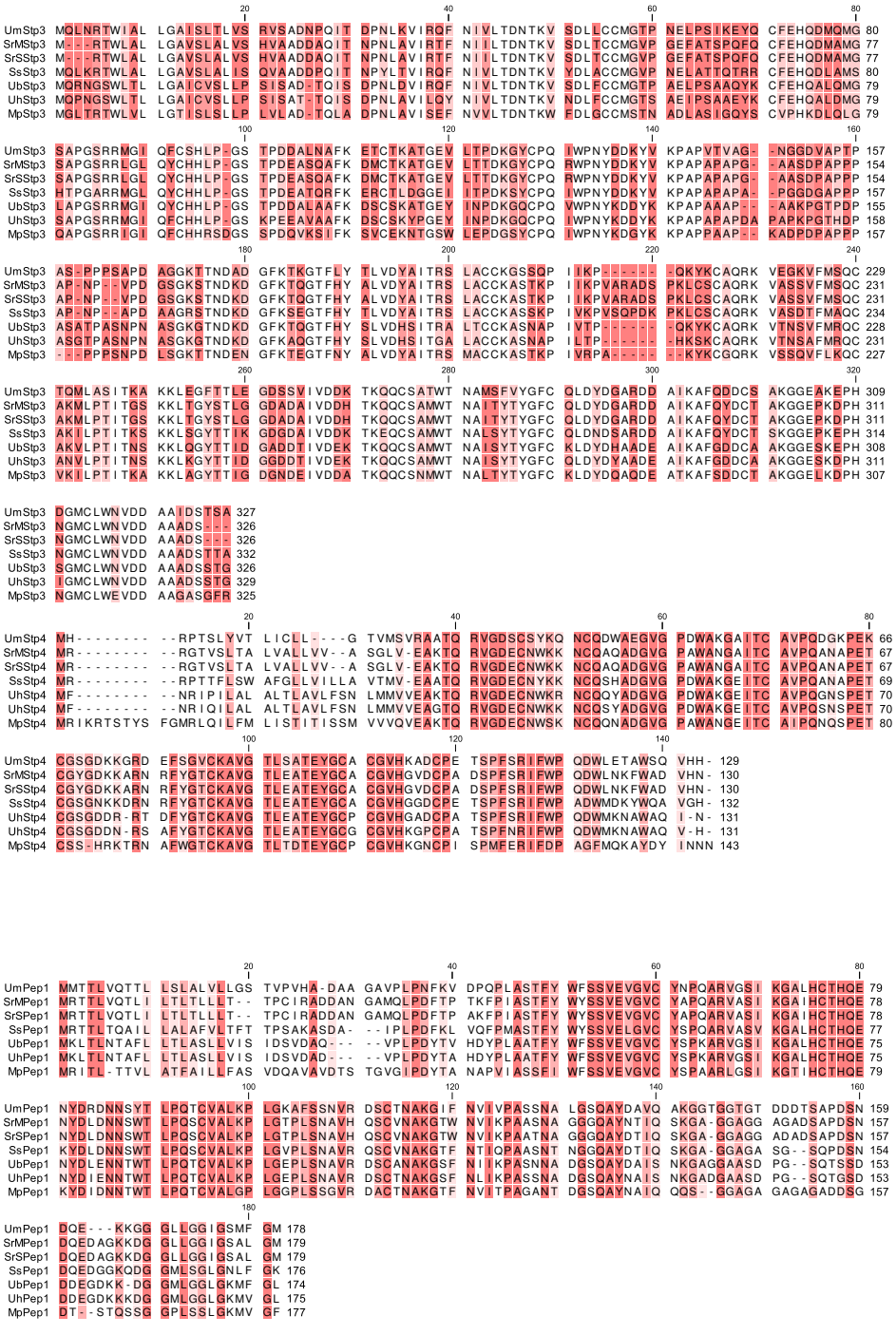

**Figure S2: Conservation between the essential effectors of *U. maydis* and their orthologs from plant pathogenic smut fungi.** Amino acid sequence alignments of *U. maydis* (Um) essential effectors with their orthologs from *Sporisorium reilianum* f. sp. *zeae* (SrM), *S. reilianum* f. sp. *sorghi* (SrS), *Sporisorium scitamieum* (Ss), *Ustilago bromivora* (Ub), *Ustilago hordei* (Uh) and *Melanopsichium pennsylvanicum* (Mp). The alignment was generated using the CLC Genomics Workbench 8.

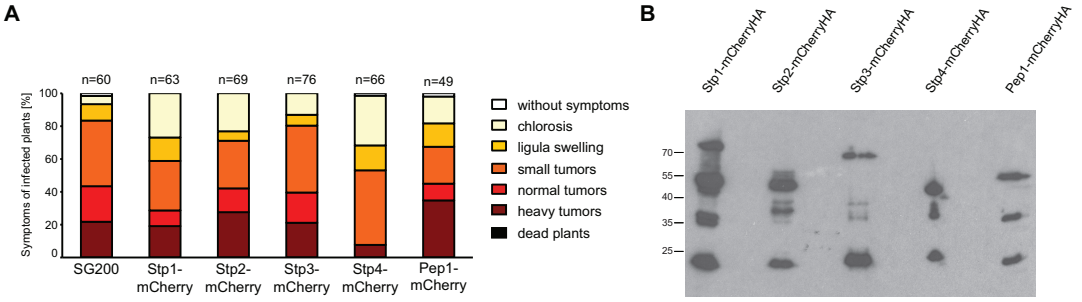


**Figure S3: Virulence of SG200 strains expressing mCherry-HA-tagged proteins.** (A) Plants were infected with the indicated *U. maydis* strains and assessed for disease symptoms at 12 dpi. Depending on their strongest symptom they were assigned to a disease category. The color code for the symptom categories is given on the right. The infections were conducted in three biological replicates and average values are expressed as percentage of the total number of infected plants (n), shown above each column. (B) Fusion proteins were immunoprecipitated from maize tissue infected with *U. maydis* strains described in A. Infected maize tissue was harvested at 3 dpi. Anti-Ha western blot analysis shows that the highest bands are the expected sizes for the full-length fusion proteins. In addition, two smaller fragment were detected, which are most likely cleaved mCherry and its degraded form. Numbers on the left indicate the size in kDa.

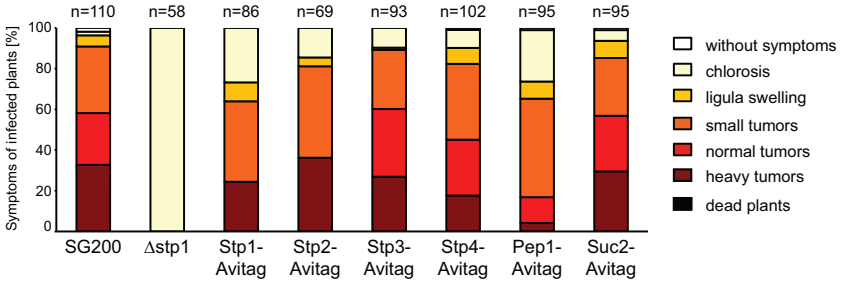


**Figure S4: Virulence of SG200 strains expressing Avi-HA-tagged proteins.** Plants were infected with the indicated *U. maydis* strains and assessed for disease symptoms at 12 dpi. Depending on their strongest symptom they were assigned to a disease category. The color code for the symptom categories is given on the right. The infections were conducted in three biological replicates and average values are expressed as percentage of the total number of infected plants (n), shown above each column.

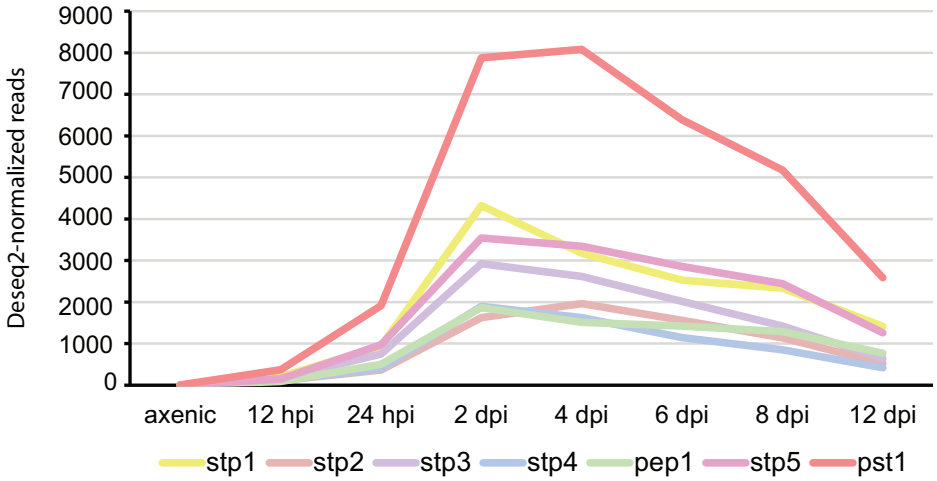


**Figure S5: Expression of essential effector genes of the magenta module during biotrophic development.** RNAseq data are from Lanver *et al.* (2018), in which plants were infected with with FB1 and FB2. Samples were collected at the indicated time points. Axenic refers to expression in axenic culture. Read counts were normalized using DEseq2.

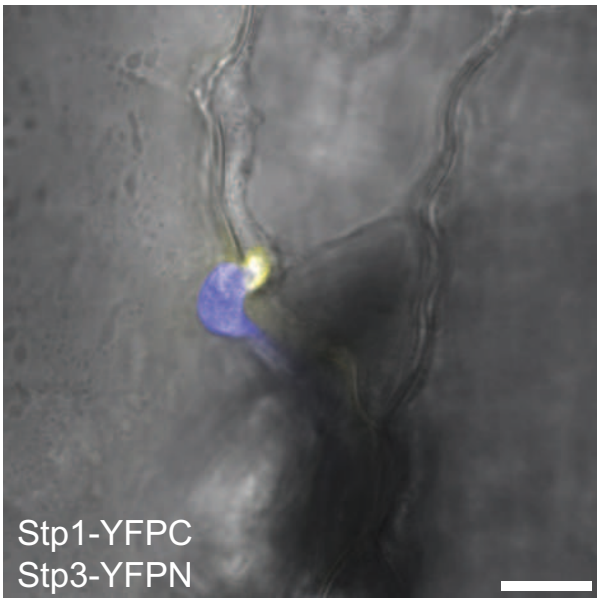


**Figure S6: Microscopy of a strain expressing effector complex members with large tags.** Maize seedlings infected with the strain SG200stp1-YFPC stp3-YFPN were observed at 2 dpi by confocal microscopy. The confocal picture shows an overlay of UV induced autofluorescence (yellow) and bright field projection (grey). Pictures are maximum projections of confocal z-stacks. The scale bar represents 10 $\mu$m.

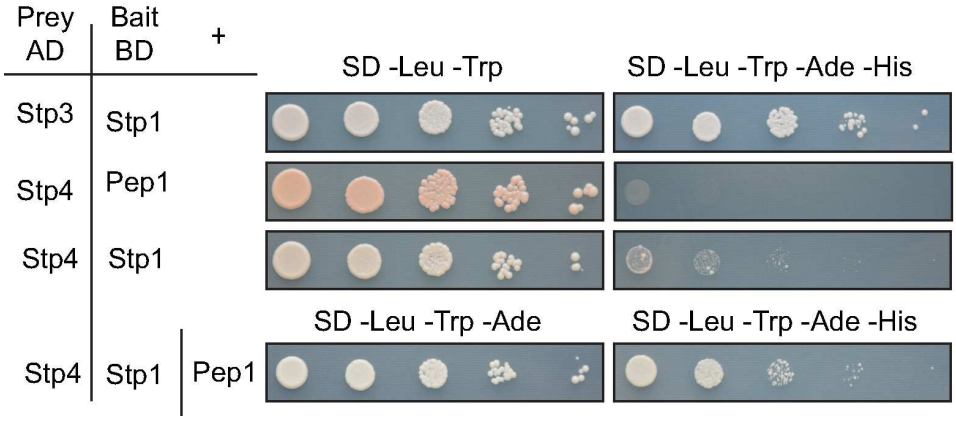


**Figure S7: Yeast Two-/ Three-Hybrid analysis of complex member interactions.** To prove that ABC9Δ behaves like its progenitor strain AH109 when it comes to expressing the complex members, several representative Y2H and an Y3H interaction were tested in the ABC9Δ background. Assays as described in Figures 2.21 and 2.22.

**Table S6:** Total spectrum counts of unique peptides for respective proteins are shown for three biological replicates (I, II, III). Secreted mCherry-HA served as negative control. Proteins with confirmed interactions are indicated by colored background.

| Protein / Peptides | Stp1-HA multiple | | | Stp2-HA multiple | | | Stp3-HA multiple | | | mCherry-HA | | |
|---|---|---|---|---|---|---|---|---|---|---|---|---|
| | I | II | III | I | II | III | I | II | III | I | II | III |
| Stp1 | N/A | N/A | 64 | 0 | 0 | 0 | 26 | 14 | 50 | 0 | 0 | 0 |
| Stp2 | N/A | N/A | 0 | 10 | 7 | 13 | 0 | 0 | 0 | 0 | 0 | 0 |
| Stp3 | N/A | N/A | 34 | 0 | 0 | 0 | 14 | 12 | 22 | 0 | 0 | 0 |
| Stp4 | N/A | N/A | 16 | 0 | 0 | 0 | 9 | 6 | 18 | 0 | 0 | 0 |
| Pep1 | N/A | N/A | 47 | 0 | 0 | 0 | 8 | 6 | 38 | 1 | 0 | 0 |
| mCherry | N/A | N/A | 0 | 0 | 0 | 0 | 0 | 0 | 2 | 31 | 22 | 54 |

# Acknowledgments

I would like to express my gratitude to my supervisor Prof. Dr. Regine Kahmann for giving me the chance to work and complete this thesis in her group over the last four years. I am especially grateful for all her advice as well as the many opportunities to conduct exciting experiments and present the results at conferences.

I would like to thank Prof. Dr. Rensing for functioning as my second supervisor and the members of my examination committee, Prof. Dr. Kahmann, Prof. Dr. Rensing, Prof. Dr. Bölker and Prof. Dr. Batschauer. Furthermore, I appreciate the mentorship of Prof. Dr. Rensing, Prof. Dr. Bölker, Prof. Dr. Bange and Dr. Glatter as members of my "Thesis Advisory Committee".

I am very grateful to Dr. Stefanie Reißmann for her excellent day-to-day supervision and all her advice, support and encouragement. I would like to thank Dr. Timo Glatter for his collaboration and support regarding the mass spectrometry experiments. Furthermore, I would like to thank Prof. Dr. Karen Snetselaar for providing us with great immuno-TEM pictures. I would like to acknowledge the IMPRS graduate school for their financial support as well as for the opportunity to learn about the research conducted in other groups.

I am especially thankful for the numerous strains created by Sarah, Karin and Daniela. I am particularly indebted to Daniela for her countless contributions to this project. I would also like to thank our gardeners, Stefan and Regina, as well as our kitchen support staff, Ria and Anita, for maintaining an excellent laboratory environment. I very much enjoyed working with all my current and former colleagues and would like to thank them for all the helpful advice, fruitful discussions and many tremendously fun lunches, coffee breaks and bar visits.

I will cherish all the friends I have won over the years at the MPI, making my time in Marburg truly special. I would especially like to thank Mariana, who was always there for me on the other side of the wall. Finally, I would like to express my gratitude to my family and my boyfriend Martin for the many years of support and encouragement.